Single Spin Switching in Open Quantum Systems

Dissertation
zur Erlangung des Doktorgrades
des Fachbereichs Physik
der Universität Hamburg

von
Christoph Hübner
aus Henstedt-Ulzburg

Hamburg 2015

Gutachter/in der Dissertation:	Prof. Dr. Daniela Pfannkuche
	Prof. Dr. Viðar Guðmundsson
Gutachter/in der Disputation:	Prof. Dr. Daniela Pfannkuche
	Porf. Dr. Roland Wiesendanger
Datum der Disputation:	23.10.15
Vorsitzender des Prüfungsausschusses	Prof. Dr. Michael Thorwart
Vorsitzender des Promotionsausschusses:	Prof. Dr. Jan Louis
Dekan der MIN Fakultät:	Prof. Dr. Heinrich Graener

In Erinnerung und gewidmet meinem Cousin Felix Mücke.

Abstract

In this thesis, quantum many body effects between a localized magnetic moment and itinerant electrons of the supporting substrate are studied. The description begins with coherent spin dynamics of a single electron passing a localized quantum spin. Subsequently the complexity of the system is further increased by considering electron reservoirs and additional electric and magnetic fields. Finally, magnetization dynamics in the classical limit is investigated by considering a vanishing level spacing between the energy eigenstates of the localized spin system.

In the first part of this thesis, the spin exchange between a single itinerant electron and a localized spin-1/2 impurity is considered to occur within a finite region. The exact time evolution of a Gaussian wave packet, representing the spatial distribution of the itinerant electron, shows coherent spin dynamics, while both spins are within interaction range. This leads to a dependence of the spin dynamics on the momentum of the itinerant electron and motivates the development of a spin scattering formalism. A numerical exact solution of the Lippmann-Schwinger equation, including the spin degree of freedom, is presented in terms of the T-matrix. For comparison, the spin scattering solution is analytically derived for the contact form of the mutual spin interaction. With the assumption of an exchange interaction within a certain range, a higher probability for coherent magnetization reversal of both spins can be observed, compared to the contact form of the interaction. Additionally, in a certain parameter range, the probability of spin reversal appears to be independent of the electron's momentum.

In the second part, the localized spin is assumed to result from a single magnetic adatom placed on a substrate. The crystal field thus creates an anisotropic potential for the single spin, that separates the two ground states with opposite magnetic orientation by an energy barrier. In systems consisting of single or a few magnetic atoms a direct transition between the ground states due to spin exchange with a single conduction electron has been observed. In this work, the electron induced magnetization reversal over and through the barrier is described with a non-equilibrium master equation from which the switching rate is determined. The impact of crystal field symmetry onto the switching rate is investigates in detail. In the presence of inelastic spin excitations, that can be controlled in a scanning tunneling microscope setup, crystal symmetry leads to short cuts through the barrier. These give rise to an increased switching rate, similar to quantum tunneling of magnetization, which is shown in presence of a magnetic field. In the absence of spin excitations, the symmetry of the system can lead to a protection of the ground states against single electron induced switching. Two protection mechanisms are

elaborated, that differ in their dependence on a magnetic field. While one relies on time reversal symmetry, the other one is robust against magnetic fields. In a systematic analysis, spin and rotation symmetry combinations are proposed that provide a protection against single electron induced ground state switching.

Finally, the master equation approach is compared with a semiclassical description for magnetization reversal. The temperature induced reversal shows in both approaches an Arrhenius law, that allows to determine the barrier height. It is reduced in the presence of strong transversal anisotropy, since saddle points in the anisotropy potential occur. It is shown that a classical Fokker-Planck equation can be derived from the quantum master equation in the classical limit. The classical limit is determined by small level spacing between spin states, with respect to all other energy scales.

In summary this thesis provides an insight into electron induced magnetization dynamics of a single spin in presence of electric and magnetic fields and ranges from the quantum to the classical regime.

Kurzfassung

In der vorliegenden Doktorarbeit werden Quanten-Vielteilchen-Effekte untersucht die zwischen lokalisierten magnetischen Momenten und aus einem Trägermaterial stammenden beweglichen Elektronen auftreten. Zunächst beginnt die Betrachtung mit der kohärenter Dynamik eines lokalisierten Spins der mit dem Spin eines einzelnen sich bewegenden Elektrons wechselwirkt. Darauf folgend werden komplexere Systeme untersucht, in denen sowohl Streuung an mehreren aufeinander folgenden Elektronen als auch die Anwesenheit von elektrischen und magnetischen Feldern berücksichtigt wird. Zuletzt wird die Magnetisierungsdynamik im klassischen Limes betrachtet, was bedeutet, dass der energetische Abstand zwischen Eigenzuständen des lokalisierten Spins verschwindet.

In dem ersten Teil der Arbeit wird der Spin-Austausch zwischen einem lokalen Spin-1/2-Teilchen und einem einzelnen freien Elektron als ortsabhängig angesehen. Die exakte Zeitentwicklung weist kohärente Spin-Dynamik auf, während das freie Elektron, welches als Gaußsches Wellpanket modelliert ist, und der lokale Spin in Wechselwirkungsreichweite sind. Dies führt zu einer Abhängigkeit der Spin-Dynamik von dem Impuls des freien Elektrons und motiviert die Entwicklung des folgenden spinabhängigen Streuformalismus. Dieser stellt eine numerisch exakte Lösung der spinabhängigen Lippmann-Schwinger Gleichung dar, in Form der so genannten T-Matrix. Zum Vergleich wird eine analytische Lösung für das Problem einer kontaktartigen Austauschwechselwirkung präsentiert. Es wird gezeigt, dass die kohärente Magnetisierungsumkehr der jeweiligen Spins mit einer höheren Wahrscheinlichkeit auftritt, falls die gegenseitige Wechselwirkung der Spins innerhalb eines ausgedehnten Raumbereichs geschieht. Zusätzlich ist die Wahrscheinlichkeit für Magnetisierungsumkehr innerhalb eines bestimmten Parameterbereiches unabhängig von dem Impuls des sich bewegenden Elektrons.

In dem zweiten Teil wird angenommen, dass das lokale magnetische Moment von einem einzelnen magnetischen Atom auf einer Oberfläche stammt. Das Kristallfeld generiert ein anisotropes Potential, welches auf den Gesamtspin des Atoms wirkt. Hierdurch werden zwei Grundzustände mit umgekehrter magnetischer Orientierung durch eine Energiebarriere getrennt. In derartigen Systemen, bestehend aus einzelnen oder wenigen magnetischen Atomen, wurden direkte Übergänge zwischen den Grundzuständen beobachtet, welche auf die Wechselwirkung mit einzelnen Leitungselektronen zurückzuführen sind. In dieser Arbeit wird die Elektronen induzierte Magnetisierungsumkehr über und durch die Energiebarriere mittels einer Mastergleichung beschrieben und die charakteristische Umschaltrate bestimmt. Im Detail wird der Einfluss von Symmetrien im Kristallfeld auf die Umschaltrate untersucht. Symmetriebedingte Abkürzungen

durch die Barriere können beobachtet werden, falls inelastische Spinanregungen auftreten, beispielsweise hervorgerufen in einem Rastertunnelmikroskop. Dies führt zu einer erhöten Umschaltrate, welche mit dem Effekt des Quantentunnelns der Magnetisierung vergleichbar ist und in Anwesenheit von Magnetfeldern auftritt. In Abwesenheit von inelastischen Spinanregungen ist es möglich, dass auch der durch einzelne Elektronen hervorgerufene direkte Übergang zwischen den Grundzuständen verboten ist, was wiederum durch die Symmetrie bedingt ist. Dies führt zu einem Schutz gegen Einzel-Elektronen induziertes Umschalten der Magnetisierung. Zwei dieser Schutzmechanismen werden genauer untersucht und unterscheiden sich in ihrem Verhalten in Anwesenheit eines Magnetfeldes. Während der eine Mechanismus auf Zeit-Inversions-Symmetrie beruht, zeigt der andere eine robuste Beständigkeit gegenüber Magnetfeldern. Eine systematische Analyse erlaubt die Vorhersage des Auftretens eines Schutzmechanismus in Systemen mit bestimmtem Spin- und Rotationssymmetrie.

Zuletzt werden Resultate der Mastergleichung mit denen aus semiklassischen Formalismen zur Beschreibung der Magnetisierungsumkehr verglichen. Das temperaturinduzierte Umschalten folgt in beiden Formalismen einem Arrhenius Gesetz und erlaubt somit die Höhe der Energiebarriere zu bestimmen. Diese wird reduziert durch starke transversale Anisotropie, indem Sattelpunkte in der Potentiallandschaft entstehen. Es wird gezeigt, dass die Mastergleichung im klassischen Limes in eine Fokker-Planck Gleichung übergeht. Der klassische Limes wird erreicht durch verschwindend kleine Energieunterschiede zwischen Spinzuständen im Verhältnis zu allen anderen Energieskalen.

Zusammenfassend verschafft diese Doktorarbeit einen Einblick in die durch Elektronen induzierte Magnetisierungsdynamik eines einzelnen Spins der elektrischen und magnetischen Felder ausgesetzt ist. Dabei wird der thematische Bogen vom quantenmechanischen bis in das klassische Regime gespannt.

Contents

Introduction 1

> "I would like to describe a field, in which little has been done, but in which an enormous amount can be done in principle. This field is not quite the same as the others in that it will not tell us much of fundamental physics (in the sense of, "What are the strange particles?") but it is more like solid-state physics in the sense that it might tell us much of great interest about the strange phenomena that occur in complex situations. Furthermore, a point that is most important is that it would have an enormous number of technical applications.
>
> What I want to talk about is the problem of manipulating and controlling things on a small scale." [Richard P. Feynman (1959)]

1.1 Introduction

Already in the year 1959 famous physicist Richard P. Feynman stated the importance of miniaturizing logic elements of a computer down to the atomic scale. He approximated the size of a single bit, which is the basic information (1 or 0) of a computing unit, to be a cube of $5 \times 5 \times 5$ atoms[55]. This would allow storage capacity to be 10^6 times larger than todays average of approximately 250Gbit/in^2 for a conventional hard drive. Obviously a huge potential for technological application is implied by this extreme miniaturization. Likewise, for the understanding of physical processes in correlated quantum systems it is of great interest to conduct research at the atomic scale. But let us begin with the technological advantages of miniaturization and why

it became important for todays society.

For electronic devices and circuits there has been an ongoing trend of miniaturization. For example in integrated circuits the transistor density approximately doubles every year as described by Moore's law[121]. This miniaturization allows to build smaller devices with faster processing units, larger memory and more capabilities. Building smaller and more powerful devices increases the portability and extends the field of application. It also allows to merge technologies into one device. This happened for example when mobile computers and mobile telephones were merged into smartphones, which started to appear on the consumer market in 2007. Nowadays, according to emarket.com[1], already one quarter of the worldwide population uses a smartphone. This rapid development is an example of the worldwide demand for portable high performance electronic devices with a big amount of capabilities.

But why do we require a large amount of storage capacity? To answer this question we need to examine the amount of data that is consumed by society and look at the sort of data that generates the largest amount in average by each person. Studies have estimated the total amount of information that was processed in 2008 by world's servers to be approximately 9.57 zettabytes[147], which is $9.57 \cdot 10^9$ terrabytes. This is such a huge amount of data that we have to convert this into more conceivable units. An average person processed 12 gigabytes of data at work per day. This would have taken 8 workdays to download in the beginning of the internet during the early 90s. The amount that is actually stored is of course much smaller, since multiple server requests point to the same data. Nevertheless, about 200 exabytes were stored on hard drives during 2008[25;80] with an exponential growth rate.

Also on the consumer side a big amount of data is requested each day. In this case not only server processed information needs to be taken into account but also television, personal computer and other sources of information should be included. In 2008 an average american citizen consumed about 34 gigabytes per day[25] with an annual growth rate of 4.4 percent. Video sources, such as television, streamed videos or video games, dominate the daily consumed bytes with approximately 90 percent. This cannot necessarily be traced back onto an extensive usage of those sources but on the sheer bit rate that is needed to stream videos and implies a large amount of memory to store them. This stands for both real and rendered video sources. Thus, if the consumer request on high quality video material further increases, the amount of data that is processed and stored worldwide will also continue to grow rapidly. This leads to a demand on more efficient and denser memory technology in future, while shortcomings are already noticeable, even today. For example, handheld devices

can easily capture video material with a bit rate of 45 Mbps but the storage units cannot keep up with this in terms of heat production and limiting amount of memory capacity. In conclusion, we can already see a trend for the need of memory devices with much higher density than todays high end products.

Beside technical and manufacturing problems associated with high density memory, there are also open physical questions on length scales at which quantum many body effects become important. The question arises whether a molecule or atom can remain in a specific configuration, if coupled to an electron reservoir that leads to decoherence, relaxation or excitations. But also how the electronic environment is influenced by the atom or molecule. In this thesis we want to focus on the magnetic properties under the influence of a controllable electric environment. Thus we review in the following the main achievements in physics, that have a close connection to this work and lead to magnetic memory at the atomic scale.

Common in all electronic circuits is the conductance manipulation of the charge carriers. For example, a simple switch has two states either conducting or insulating, whose status can be read out from the current in the circuit. But charge carriers such as electrons also have another attribute, which is the spin. Already when the spin was detected by Gerlach and Stern in 1922 [65] they observed an alteration of a silver beam trajectory due to the interaction of the intrinsic spin with an inhomogeneous magnetic field. Even though the concept of the spin did not exist during that time, its influence on transport properties was observed. Later, the theoretical spin concept was proposed by Pauli. However, its origin was not fully understood until Dirac derived it from relativistic quantum mechanics in 1928 [48].

From there on, the spin was an essential quantity in physics. In combination with the Pauli exclusion principle [132] the spin concept allowed to explain things like occupation of electronic shells in atoms [130] or magnetism [79] in solids. Latter is a result of the exchange interaction, a purely quantum mechanical interaction between the unpaired spins in the magnetic material. Beside mutual spin interaction also the effect of electric and magnetic fields were studied. 1930 Kramers [98] stated that a time-reversal symmetry conserving field can only break but double degeneracy, if the spin possesses a half integer of the momentum quantum. Furthermore, 1940 Pauli combined the concept of spin with the statistic properties of particles in equilibrium, the so called spin statistic theorem [131]. And Stevens derived an operator representation of the crystal field acting on the angular momentum of embedded magnetic ions [151]. All those findings point out the importance of considering the electromagnetic environment and correlations with other spin possessing particles,

when investigating the properties of a spin embedded in a host material.

The impact of the spin on the conductance, as mentioned before, was observed in magnetic impurity-doped metals[40;66] but not resolved until 1964 by Kondo[94]. He explained the unexpected increase of resistance[181] with decreasing temperature by the rising amount of scattering processes between conduction electrons and the impurities.

Schrieffer and Wolff[145] demonstrated that Kondos theory was based on the s-d interaction between localized magnetic d-states and s-states of the conduction electrons as described by Anderson[2]. With a different approach Appelbaum derived a Kondo like Hamiltonian from the Anderson model to explain the zero bias anomaly, found in tunnel junctions[104;177]. In contrast to the afore mentioned effect in magnetic impurity-doped metals, the conductance at zero bias increases with temperature. This, so called Kondo resonance, appears when a localized spin forms a bound state with the free electrons of the surrounding material and generates a low resistance channel for the conduction electrons, which is stable below the Kondo temperature. Thus another example was found, in which the electric properties highly depend on the correlations of a spin with the surrounding material. But observation of spin correlations on a single magnetic impurity level was not possible at that time. Thus during the 60s and 70s research on the interaction between conduction electrons and magnetic impurities continued in bulk materials, such as metals[39] or diluted magnetic semiconductors[73]. Latter are still in the focus of research and allow to study magnetism and the influence of charge carries in materials with controllable electronic properties at low concentration of magnetic impurities[47;124;166].

Quantum dots, discovered by Ekimov in 1981[52], present systems with intermediate properties between bulk semiconductors and single molecules. Frequently, they are called artificial atoms due to the discrete quantum degrees of freedom. They can be investigated in a field-effect transistor setup to control the discrete energy levels with a gate[96;150] and study transport via attached electron reservoirs. Quantum dots were used to probe their discrete energy spectrum[97;143;163] by utilizing the conductance for spectroscopy. Further, coherence effects in transport through multi-dot arrangements[19;20;76;120] or charging effects such as the Coulomb blockade[13;59;74] or spin blockade[28;53;171;172] as a result of spin selection rules were investigated. The development of non-equilibrium theories such as the diagrammatic perturbation theory[144] and other techniques[159], which are based on the non-equilibrium Greens function formalism on the Keldysh contour[85;88;112], allowed to go beyond linear response. This allows to investigate transport within the Coulomb blockade,

where sequential electron transport is exponentially suppressed[12;101;116;138]. In this blockade region, where Coulomb repulsion inhibits the charging of the quantum dot, the Anderson model becomes equivalent to the Kondo model as demonstrated by Schrieffer, Wolf and Appelbaum. In this case, transport through the quantum dot appears due to cotunneling, including virtual occupation of quantum dot states, that can lead to an inelastic spin excitation within the quantum dot. In a previous work I[83] studied the effects of cotunneling in a single level quantum dot with a magnetic impurity, which has much in common with the transport through a magnetic atom, subject to this thesis. Further progress in theoretical methods was made to go to arbitrary order in the coupling. Beyond those techniques are the reordering of diagrammatic expressions to control appearing divergencies[93], the iterative summation of path integrals[11], the time convolution less master equation expansion to arbitrary order[160], renormalization group techniques[137] and the non-equilibrium quantum Monte Carlo approach[10;72].

Although quantum dots allowed to study spin transport through nano structures with diameters of a few nanometer, they do not allow to reach the atomic scale. The invention of an important experimental tool, namely the scanning tunneling microscope by Bing and Rohrer in 1983[18], enabled to scan a conducting surface with atomic resolution. But single atom manipulation was not possible in the early years. Meanwhile a milestone in terms of information storage technology was reached, when Fert and Grünberg discovered the giant magnetoresistance in 1988[6;17]. This resistance effect in layered magnetic materials is so large, that the application in a commercial hard drive by IBM was presented only nine years later. The even stronger effect of giant tunnel magnetoresistance, found in magnetic tunnel junctions[119;129], allows for the development of new memory concepts, such as magnetoresistive random access memory. While both effects can be found in todays memory devices they do rely on layer systems. In 1990 two achievements were made in scanning tunneling microscopy technology, namely the single atom manipulation and positioning[146] and the spin polarized scanning tunneling microscope[176]. They, in principle, allow to build structures atom by atom and measure the magnetic moment of a single atom. It was not until 2002 when Bennewitz et al.[14] presented an approach to store information in the presence or absence of a Si adatom in a regular pattern on a Si substrate. The activation energy for removal of an atom was approximately $1eV$ resulting in a life time of a single bit at room temperature between 2 and 3 years. Unfortunately the signal to noise ratio at room temperature slows down the reading process with a scanning tunneling microscope, such that this concept is not

compatible in speed with conventional hard drives.

In order to store information in the magnetic moment of an atom or molecule, at least two magnetic orientations need to be energetically favored and separated by an energy barrier. Magnetic molecules show crystalline magnetic anisotropy [24;62;63] resulting from the ligand field acting on the core magnetic atoms [117;151]. Mannini et al. [111] investigated their potential usability for magnetic memory with time dependent x-ray magnetic circular dichroism and achieved a stable magnetic orientation for 220 seconds at 0.5 Kelvin.

A scanning tunneling microscope allows the detection of inelastic spin excitations to infer magnetic properties of adatoms [77;90;107]. Further, one can observe the influence of substrate electrons, for example manifested in a Kondo resonance [126;157] or electron mediated interaction between neighboring magnetic adatoms [82;113;183]. Additionally, the spin state can be manipulated with inelastic spin excitations, which result from electrons tunneling form a spin polarized tip to the substrate [108]. This offers a way to write information in the magnetic orientation of an adatom. Combining the two concepts of spin polarized [21;175] and time resolved scanning tunneling microscopy [106;164] further enables to examine the dynamics of magnetization reversal. This is crucial for the investigation of the live time of an oriented magnetic moment and the technical application. This life time, or the related switching rate, was studied, in terms of telegraph noise in the tunnel current, for systems with decreasing size [128], beginning with clusters of $200-600$ Fe atoms [22], decreasing to 78 Fe atoms and leading to a single bit stored within just 12 Fe atoms [105]. Up to that point the theoretical description was either based on a classical model, that includes spin-torque in a Fokker-Planck equation [3;23;36;102] or master equation, that allowed to calculate the stationary non-equilibrium probability distribution and current [42;46;54]. In this approach the inelastic spin excitations are equivalent to the cotunnling that is known from the quantum dot description with the Anderson model [43].

As a part of my PhD project, we determined the dynamic properties for a single spin, representing a 5 Fe atom cluster on a Cu substrate, from a master equation approach and demonstrated results in good correspondence to the experimental data [89]. We were able to assign characteristic behavior in the magnetization switching of the cluster to the interaction with tunneling electrons. In the temperature dependence we distinguished between classical switching over the anisotropy barrier and single electron induced switching through the barrier as a result of transversal anisotropy. In this thesis, we focus on a more general discussion and suggest the interested reader to take a look into our publication from 2013, to see the relation to

experimental results.

The master equation approach includes both, classical and quantum effects. In 2014 we compared the semiclassical Fokker-Planck and master equation approach with each other and pointed out similarities and differences[34]. For example the spin quantization, present in a quantum mechanical system, leads to a threshold voltage for current induced magnetization reversal, which is absent in the classical description.

A common strategy to decrease the switching rate was to find substrate and adatom combinations with large magnetic anisotropy[61;81;133;136;179] of usually a few tens meV. A different approach was demonstrated by Miyamachi et al.[118] for a single holmium atom on a Pt(111) substrate. The three fold rotational symmetry of the system results in selection rules for electron induced transitions between spin states of the adatom. In the case of a single holmium adatom with a total spin of $J = 8$,which is currently still discussed[50], a single electron cannot induce a direct transition between the ground states with opposite spin orientations.

We demonstrated in 2014 that the protection mechanism in a three fold symmetric system breaks down, when time reversal symmetry is broken by a magnetic field[84]. Also resonances of the switching rate were proposed, that result from short cuts in the anisotropy barrier similar to quantum tunneling of magnetization[114]. Additionally we demonstrated the appearance of a protection mechanism in a four fold symmetric system, that is robust against magnetic fields and thus promising for a potential technical application.

1.2 Scope of this thesis

In this thesis, we investigate the results of mutual interaction between itinerant conduction electrons and a single localized magnetic moment that is subject to an electrostatic and magnetic environment. We elaborate the exchange of spin leading to dynamics in the orientation of the localized magnetic moment. Likewise, we demonstrate the influence of the exchange interaction onto the spin dependent transport properties of the itinerant electrons with a scattering formalism. Further, the presence of an electrostatic potential and a magnetic field is included, which creates an anisotropic potential for the localized magnetic moment. We demonstrate the relation between symmetries in the electrostatic field and the electron induced magnetization dynamics. The utilized master-equation approach covers both quantum and classical effects, which is highlighted for temperature induced magnetization

reversal. Finally, we derive the classical limit of the master equation in terms of a Fokker-Planck equation.

In chapter 2, we introduce the exchange interaction and present its spatially dependent representation[16] for a localized and an itinerant spin. Latter is represented by a Gaussian wave packet associated with a spin. The exact time evolution of a single itinerant electron passing a localized spin is shown. We assumed a Gaussian like exchange interaction between an itinerant and a localized spin and demonstrate the mutual spin exchange while both are in interaction range.

The results of chapter 2 motivate the introduction of a spin dependent scattering formalism in chapter 3. The T-matrix is introduced on the basis of the Lippmann-Schwinger equation, which allows to relate the scattered with the incoming wave function. We solve the T-matrix equation numerically exact for any shape of spatially extended exchange interaction by introducing a discretization in momentum space that relies on Gaussian quadrature. Then, we relate the solution to the spin dependent transmission and reflection amplitudes. An analytic solution for the contact exchange interaction in form of a delta function is derived for comparison and for determination of finite range effects. Also for comparison, the transmission probability of a delta, a Pöschl-Teller and a Gaussian potential is shown. This helps for the interpretation of the results, when spin exchange is included. Especially in focus is the switching probability of the localized spin with regard to chapter 4. Finally the relation between the T-matrix and the scattered wave function is demonstrated.

In chapter 4, the localized spin is subject to an electrostatic field created by ligands in the crystal structure of a substrate. The Stevens operator representation of the crystal field is introduced and applied in presence of specific rotational symmetries. Effects of the electrostatic and magnetic fields onto the discrete spin states are demonstrated, utilizing the method of exact diagonalization. The interaction with conduction electrons is modeled by an Appelbaum Hamiltonian, while considering a setup that represents a spin polarized scanning tunneling microscope. From a master equation approach a characteristic switching rate is deduced, that describes the electron induced magnetization reversal of the localized magnetic moment. Spin excitations due to inelastic electron scattering and single electron induced magnetization switching is shown for systems with different rotation symmetries. The robustness, with respect to a magnetic field, of a symmetry related protection mechanism against single electron induced switching is shown in a three-fold and four-fold symmetric system. Resonances from quantum tunneling of magnetization and short cut tunneling are explained as results of the rotation symmetry. We also

establish an alternative representation of the spin states, that allows to predict the occurrence of a protection against induced switching from the rotation symmetry and spin quantum number of the local magnetic moment.

The last chapter 5 connects the master equation with the classical description of magnetization reversal. We first visualize the anisotropy potential on which a classical magnetic moment would follow trajectories. Then we compare our findings from the master equation for thermally induced magnetization reversal, also known as superparamagnetic relaxation, with results from a classical Fokker-Planck equation. Finally, we derive from the master equation a Fokker-Planck equation in the classical limit, where the level spacing vanishes.

Two particle spin interaction 2

At the atomic scale, the exchange interaction is the dominating mutual interaction between two magnetic particles, while the magnetic dipole-dipole interaction can be neglected between two quantum mechanical objects. It results from the Coulomb repulsion between them and the Pauli principle[78]. We present in the following a derivation of the exchange interaction between two fermions and further introduce a model with spatial dependence of the exchange interaction.

2.1 Exchange interaction

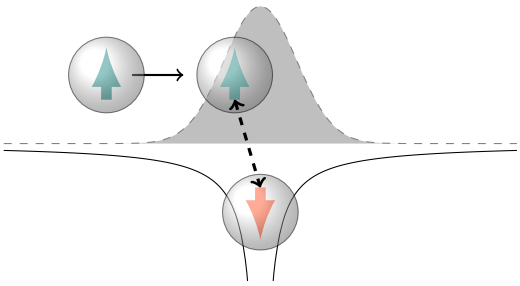

FIGURE 2.1: Schematic representation of spatially extended exchange interaction between an itinerant spin (blue) and a localized spin (red).

A system with two fermions, for example electrons, can be described by the Hamiltonian

$$\hat{H} = \hat{H}_0 + \hat{H}_C \tag{2.1}$$

including the single particle terms $\hat{H}_0 = \hat{H}_c + \hat{H}_l$ labeled with c and l as well as the mutual Coulomb repulsion $\hat{H}_C$. According to Pauli's spin statistic theorem, the many body wave function of two fermions needs to be antisymmetric with respect to a permutation of particles. Hence, if the spacial part $|\Phi\rangle$ of the total wave function is symmetric, the spin part $|\chi\rangle$ needs to be antisymmetric and vice versa. Thus, many body wave functions of two fermions

$$|\Psi_S\rangle = |\Phi_+\rangle|\chi_-\rangle \tag{2.2}$$

$$|\Psi_A\rangle = |\Phi_-\rangle|\chi_+\rangle \tag{2.3}$$

can be constructed, which obey the symmetry of a fermionic state. The superscript $+/-$ illustrates the symmetric/antisymmetric linear combination

$$\langle x_1, x_2|\Phi_\pm\rangle = \frac{1}{\sqrt{2(1+|S|^2)}}\left(\phi_c(x_1)\phi_l(x_2) \pm \phi_l(x_1)\phi_c(x_2)\right) \tag{2.4}$$

$$|\chi_\pm\rangle = \frac{1}{\sqrt{2}}\left(|\uparrow\downarrow\rangle \pm |\downarrow\uparrow\rangle\right) \tag{2.5}$$

of single particle wave function products in real space $\phi_i(x)$ and spin space $|\uparrow / \downarrow\rangle$. In case of electrons, the two possible spin orientations are indicated by the arrows. Inclusion of the overlap integral

$$S = \int dx \phi_c^*(x)\phi_l(x) \tag{2.6}$$

allows to consider nonorthogonal states in real space[5;110]. This is known as the Heitler-London approach[134;182], which assumes all single particle wave functions to be eigenfunctions of the corresponding single particle Hamiltonian without necessarily being orthogonal to each other. Note, an equivalent expressions for the exchange interaction can be derived if using orthogonal Wannier wave functions[149] instead. In first order perturbation theory an energy correction

$$\epsilon \approx \epsilon_0 + \langle\Psi_i|\hat{H}_C|\Psi_i\rangle \tag{2.7}$$

to the eigenvalues ϵ of $\hat{H}_0$ leads to an energy splitting between the symmetric $|\Phi_+\rangle$ and antisymmetric state $|\Phi_-\rangle$ with reference to the spacial part. Explicitly the energies are shifted by $E_\pm^\Phi = \langle\Phi_\pm|\hat{H}_C|\Phi_\pm\rangle = (C \pm A)/(1 \pm |S|^2)$. This expression includes the Coulomb integral

$$C = \frac{e^2}{4\pi\epsilon_0}\int dx_1 \int dx_2 |\phi_c(x_1)|^2 |\phi_l(x_2)|^2 \frac{1}{|x_1 - x_2|} \tag{2.8}$$

and the exchange integral

$$A = \frac{e^2}{4\pi\epsilon_0}\int dx_1 \int dx_2 \phi_l^*(x_1)\phi_c(x_1)\phi_c^*(x_2)\phi_l(x_2)\frac{1}{|x_1 - x_2|}. \tag{2.9}$$

While the Coulomb integral accounts for the classical repulsion of two electrons represented by their probability density, the exchange integral takes into consideration the fact that both electrons are indistinguishable. This gives an energy splitting between the symmetric and antisymmetric spacial part of the wave function. Taking into account only the spin part of the wave function allows to write an effective Hamiltonian for the two particle interaction. Utilizing a vector of Pauli matrices $\vec{\sigma}_{c/l} = 1/2(\hat{\sigma}_x, \hat{\sigma}_y, \hat{\sigma}_z)$ acting on the spin of an electron with label c or l allows to write the effective Hamiltonian in terms of the Coulomb integrals

$$\hat{H}_{\text{eff}} \approx \hat{H}_0 + \frac{1}{4}\left(E_+^\Phi + 3E_-^\Phi - \frac{A - C|S|^2}{1 - |S|^4}\vec{\sigma}_c\vec{\sigma}_l\right). \tag{2.10}$$

This Hamiltonian exactly reproduces the first order energy corrections from the Coulomb repulsion, which can be seen from the expectation value $\langle\Psi_{S/A}|\hat{H}_{\text{eff}}|\Psi_{S/A}\rangle = \epsilon_0 + E_{+/-}^\Phi$. The last term in equation 2.10 describes the exchange interaction and is of quantum mechanical nature. The coefficient $V_{\text{ex}} := \frac{A-C|S|^2}{1-|S|^4}$ is commonly known as exchange constant.

In the following we make use of a model with a spatially dependent exchange

$$V_{\text{ex}}(r - R)\vec{\sigma}_c\vec{\sigma}_l \tag{2.11}$$

where r denotes the position of the itinerant and R of the localized electron. The function $V_{\text{ex}}(r - R)$ incorporates the spatial dependence. This general form of the exchange interaction between itinerant and localized electrons has been used in the description of diluted magnetic semiconductors in terms of the s-d model [60;73]. In this model the itinerant electrons are assumed to occupy states in a s-like conduction band, while the localized electrons are in bands with d character. Interaction with charge carriers in the valence band is described by the p-d model. Similar to the spacial dependence, Schrieffer and Wolff already mentioned a momentum dependence of the exchange interaction within the s-d model [145;148]. A common approximation is the use of the contact form [38;95;135;140]

$$V_0\delta(r - R)\vec{\sigma}_c\vec{\sigma}_l, \tag{2.12}$$

with the delta distribution $\delta(r - R)$ that restricts the exchange to a single point. We will consider this type of interaction in a later chapter. In 1990 Bhattacharjee derived a Gaussian form of the exchange interaction in momentum representation from the interaction between charge carriers in conduction bands and localized magnetic orbitals within diluted magnetic semiconductors [16]. The equivalent Gaussian form in real space was used for the description of Mn doped III-V semiconductors [15;29;139;141;142],

the derivation of Ruderman-Kittel-Kasuya-Yosida interaction [165] in thin films [152;153] and in semiconductor quantum dots with magnetic impurities [35]. In the following we will take the Gaussian form

$$V_0 e^{-4ln(2)(x/\Delta_V)^2} \vec{\sigma}_c \vec{\sigma}_l \tag{2.13}$$

with half width Δ_V at full maximum V_0 to investigate the effects of mutual spin interaction between itinerant and localized electrons. The spatially dependent character has also been experientially observed in quantum wells [109] and quantum dots with a scanning tunneling microscope [123]. We will demonstrate in the following, that a spatially dependent exchange interaction exhibits different characteristics in transport compared to the commonly used contact form.

2.2 Time evolution of Gaussian wave packet

From the perspective of a single itinerant electron, another localized electron creates an effective spin interaction at the origin of our coordinate system, as shown in equation 2.11. We focus on an Gaussian shaped exchange interaction and treat the itinerant electron within the effective mass approximation. This results in the model Hamiltonian

$$\hat{H}(x) = -\frac{\hbar^2}{2m}\frac{d^2}{dx^2} + V_0 e^{-4ln(2)(x/\Delta_V)^2}\vec{\sigma}_c\vec{\sigma}_l \tag{2.14}$$

that is subject to the following discussion. A vector of Pauli matrices $\vec{\sigma}_{c/l} = 1/2(\hat{\sigma}_x, \hat{\sigma}_y, \hat{\sigma}_z)$ is either labeled with c to refer to the itinerant conduction electron spin or with l for the localized spin. Notice, the length scale Δ_V that is deduced from the full width at half maximum of the spatial part $V(x) := V_0 e^{-4ln(2)(x/\Delta_V)^2}$ within the mutual spin interaction term. The question arises how the spin of the localized electron is affected because of the interaction with a passing conduction electron. To answer this, we start by describing the itinerant electron as a Gaussian wave packet that passes the region at which both electrons interact. The initial two particle wave function

$$|\phi(t_0)\rangle = \sqrt{\Delta_c}\int dk \left(\frac{2}{\pi}\right)^{\frac{1}{4}} e^{-((k-k_0)\Delta_c)^2 + ix_0(k_0-k)} |\uparrow_c\downarrow_l\rangle|k\rangle, \tag{2.15}$$

expanded in momentum space k, gives a Gaussian probability distribution around x_0 and variance Δ_c, that is propagating with a mean momentum value k_0. Both spins align antiparallel at initial time t_0 as denoted by the product state $|\uparrow_c\downarrow_l\rangle$. From the initial condition one can determine the state at any time t with the formal solution of the Schrödinger equation

$$|\phi(t)\rangle = e^{-i\hat{H}(t-t_0)/\hbar}|\phi(t_0)\rangle \tag{2.16}$$

by use of the time independent two particle Hamiltonian shown in equation 2.14. We begin our discussion with the dynamics of the itinerant electron. Figure 2.2 shows the time evolution of a propagating electron in form of a wave package that is initiated at $x_0 = -2\Delta_V$ with mean wave vector $k_0 = 100/\Delta_V$. Spins of both electrons are initially aligned antiparallel and the itinerant electron has an initial spin $\uparrow_c$ pointing in positive direction of the quantization axis. On the left hand side of figure 2.2 one can observe the electron entering the interaction region centered at $x = 0$ and exchanging its spin with the localized electron. Since the total spin of both electrons is a conserved quantity $[\hat{H}, \vec{\sigma}_c + \vec{\sigma}_l] = 0$, the spin is transferred to the localized electron which was initially in the $\downarrow_l$ spin state. The amount of spin that

has been transferred reaches its maximum when the electron is in the center of the interaction region.

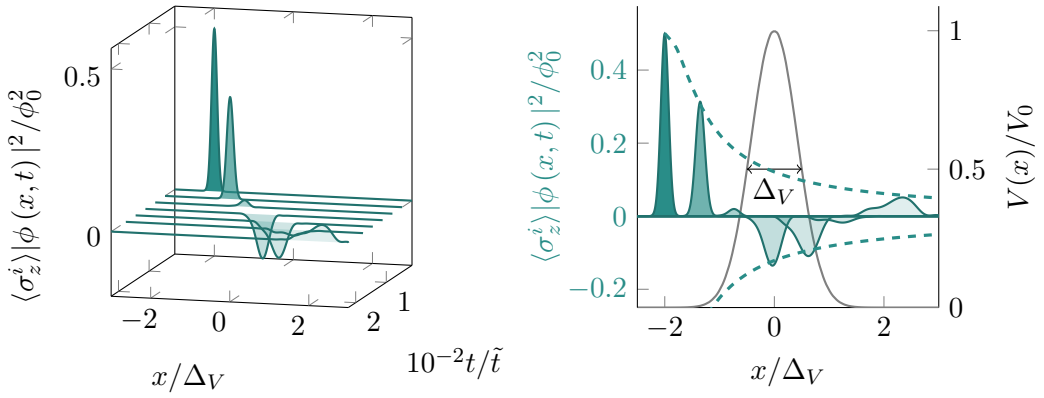

Figure 2.2: Time evolution of a Gaussian wave package, associated with a spin, representing an itinerant electron. (left) time evolution of the spin expectation value at position x and times scaled by the characteristic diffusion time $\tilde{t} = \frac{\hbar}{4m\Delta_V^2}$ of a wave package. (right) Snap shots of the time evolution. Dashed lines indicate the evolution of the maximal absolute expectation for a wave package in the absence of an exchange interaction.

This can be seen even better on the right hand side of figure 2.2, in which snap shots in time are combined into a single picture. As a guidance for the eye a dashed line indicates the expected position for the maximum of the probability distribution if no interaction was present. The deviation from the actual probability distribution of the itinerant electron is owed by dynamics in the spin degree of freedom. While the itinerant electron passes the interaction region, both spins perform a coherent rotation, which ends in a final mixed spin state $a_0|\uparrow_i\downarrow_l\rangle + a_1|\downarrow_i\uparrow_l\rangle$. This becomes even more clear when looking at the z-component of the spin expectation value $\langle\hat{\sigma}_{l,z}\rangle$ for the localized electron. In contrast to the freely moving itinerant electron, the localized electron has only one dynamic attribute, namely its spin degree of freedom. The time evolution of the spin expectation value in figure 2.3 shows oscillations of the localized spin that evolves into a final state. A stronger exchange interaction leads to a more rapid oscillation. The final state is reached, when the itinerant electron passed the interaction region and no spin can be exchanged anymore. Obviously in the limit of no exchange the spins remain in their initial configuration. These results motivate a more precise investigation of the spin scattering with respect to the momentum k_0 of the itinerant electron. Especially the asymptotic limit of the electron far away from the interaction region $x \gg \Delta_V$ is accessible with a scattering

theory.

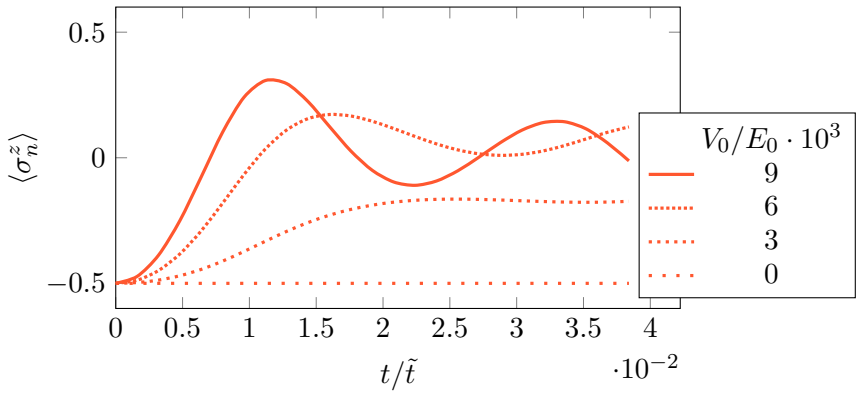

FIGURE 2.3: Time evolution of the localized spin. The frequency of the spin oscillations is increasing with the interaction strength V_0. The number of oscillations is increasing with the range of the interaction. Parameters are the same as in figure 2.2 and energies are given in units of the mean kinetic energy $E_0 = \frac{\hbar^2 k_0^2}{2m}$ of the itinerant electron.

Spin scattering 3

In the following, the mutual spin interaction between a localized and an itinerant spin is investigated. For the description of spin exchange within a finite interaction region, a scattering approach is derived in terms of the T-matrix. With this formalism we go beyond the frequently used contact form of the exchange interaction.

3.1 T-matrix formalism

Preceding results demonstrate an exchange of spin between an itinerant and a localized electron, while the itinerant passes the interaction region, determined by the potential in the Hamiltonian 2.14. As shown in figure 2.3, a stationary spin expectation value for both electrons is reached, when they are out of interaction range. Thus, one needs to perform the time evolution up to the characteristic time scale $\Delta_V m/\hbar k_0$, the itinerant electron needs to pass the interaction region. This becomes a very demanding numerical calculation for electrons with small kinetic energy $\hbar^2 k_0^2/2m$ with respect to the potential height V_0. We therefore proceed with a scattering formalism that is capable of providing simultaneously information about the wave function within and far away from the interaction region. In the following, we will derive a formalism that is based on the Lippmann-Schwinger approach [103] to scattering. Further we make use of a discretization in momentum space, utilized in the group of Vidar Gudmundsson [8;69;71;158;162], to numerically calculate the scattered wave function beyond the first order Born approximation [26;33]. The formalism allows

to solve a time independent Schrödinger equation of the form

$$\left(\hat{H}_0 + \hat{V}\right)|\psi\rangle = E|\psi\rangle, \tag{3.1}$$

with $\hat{H}_0 = \hbar^2\hat{k}^2/2m$ the free particle kinetic energy with eigenfunctions $|k\rangle$ and a scattering potential $\hat{V}$. The scattering potential consists of two components $\hat{V} = \hat{V}_x \otimes \hat{V}_s$ that act on the spacial part $\hat{V}_x$ and the spin part $\hat{V}_s$ of the wave function. Thus we allow for potentials that can be represented by

$$\hat{V} = \sum_{x,S,S'} V_x|x\rangle\langle x|V_{S',S}|S'\rangle\langle S| \tag{3.2}$$

where $|S\rangle$ is a many particle spin state and matrix elements $V_x(V_{S',S})$ resulting form the representation of the potential in real (spin) space. A formal solution to equation 3.1 is given by the the Lippmann-Schwinger equation

$$|\psi\rangle = |\psi_0\rangle + \hat{G}_0\hat{V}\,|\psi\rangle\,, \tag{3.3}$$

with $|\psi_0\rangle = |k_0\rangle|S_0\rangle$ the solution of the free particle Schrödinger equation $\hat{H}_0|\psi_0\rangle = E_0|\psi_0\rangle$ and the free particle Green's function $\hat{G}_0 = \left(E - \hat{H}_0\right)^{-1}$. The complexity of finding a solution is equivalent for the Lippmann-Schwinger and Schrödinger equation. However, a perturbation expansion in $\hat{V}$ naturally arises from the recursive character of equation 3.3, which leads to the Born series

$$|\psi\rangle = \left(1 + \hat{G}_0\hat{V} + \hat{G}_0\hat{V}\hat{G}_0\hat{V} + ...\right)|\psi_0\rangle\,. \tag{3.4}$$

In this series we find the relation between the free wave function $|\psi_0\rangle$ and the solution $|\psi\rangle$ including an additional potential $\hat{V}$. In the Born approximation it is common to use just the first two terms of the Born series to approximate the wave function $|\psi\rangle \approx (1 + \hat{G}_0\hat{V})|\psi_0\rangle$. In fact, we are interested in a solution beyond leading order to allow for non-perturbative potentials. Therefore, by definition of the T-matrix

$$\hat{T} := \hat{V} + \hat{V}\hat{G}_0\hat{T}, \tag{3.5}$$

the Born series can be written in a much shorter form

$$|\psi\rangle = \left(1 + \hat{G}_0\hat{T}\right)|\psi_0\rangle\,. \tag{3.6}$$

Both are the central equations for the following considerations. Truly, the complexity of solving equation 3.5 instead of 3.1 or 3.3 in general remains the same. However, the introduction of a discretization scheme allows to solve equation 3.5 numerically exact, even for potentials with a certain range. In in the following, we present the

discretization scheme, which is based on Gaussian quadrature, that allows to solve equation 3.5 and 3.6 numerically. We will also demonstrate the relation between the T-matrix and properties of a scattering theory such as the transmission amplitude, reflection amplitude and the wave function.

3.2 Discretization with Gaussian quadrature

The main equations 3.5 and 3.6, for the scattering theory, can be solved numerically, when introducing a discretization scheme that is based on the Gaussian quadrature. The appearance of a free particle Green's function in both equations suggests to choose a representation in $\hat{H}_0$ eigenfunctions

$$\langle x|k\rangle = \frac{1}{\sqrt{2\pi}} e^{ikx} \tag{3.7}$$

such that the Green's function $\langle k|\hat{G}_0|k\rangle = 2m/(\hbar^2(k_0^2 - k^2))$ becomes diagonal. Due to the continuous spectrum of $\hat{H}_0$ both equations 3.5 and 3.6 contain an integral of the from

$$\int_{-\infty}^{\infty} \frac{f(k)}{k_E^2 - k^2} dk, \tag{3.8}$$

which we want to make suitable for numerical computation. The first step is to shift the denominator of the Green's function into the complex plane by adding a positive complex number $i\eta$. This gives the so called advanced Green's function, which obeys the causality intrinsic to a scattering theory, namely a propagation from a scattering source[7]. This can be seen at the advanced character of the Green's function

$$\langle x|\hat{G}_0|x'\rangle = -\frac{im}{\hbar^2 k_0} e^{ik_0|x-x'|} \tag{3.9}$$

when written in spacial representation[122]. Substituting this expression in the Born series 3.4 leads to plane waves that propagate from the scattering object represented by $\hat{V}$. A negative η would lead to a retarded Green's function and thus waves propagating to the scatterer.

The integral 3.8 can be transformed by applying the Cauchy principal value $\frac{1}{x \pm i\eta} = \frac{\mathcal{P}}{x} \mp i\pi\delta(x)$, which separates the expression into a principle value integral and one with a simple delta distribution.

$$\begin{aligned} & \int_{-\infty}^{\infty} \frac{f(k)}{k_E^2 - k^2 + i\eta} dk \\ = \; & \mathcal{P} \int_{-\infty}^{\infty} \frac{f(k)}{k_E^2 - k^2} dk - \frac{i\pi}{2|k_0|}(f(k_0) + f(-k_0)) \end{aligned} \tag{3.10}$$

By adding two vanishing terms, since $\int_{-\infty}^{\infty} \frac{1}{k_0^2 - k^2} dk = 0$, we remove the divergency points from the principal value integral.

$$= \int_0^{\infty} \frac{f(k) - f(k_0)}{k_0^2 - k^2} dk + \int_0^{\infty} \frac{f(-k) - f(-k_0)}{k_0^2 - k^2} dk - \frac{i\pi}{2|k_0|}(f(k_0) + f(-k_0)) \tag{3.11}$$

With the application of Gauss-Legendre quadrature[8;173] we can discretize the

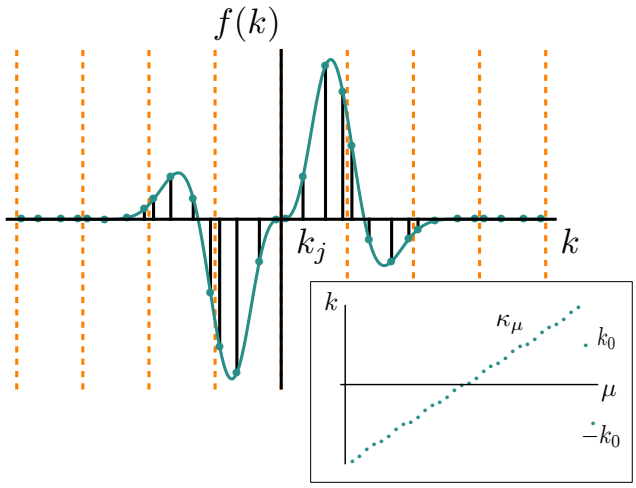

FIGURE 3.1: Visualization of Gauss discretization with momentum mapping $k \to \kappa_\mu$ and weight mapping $\omega_j \to D_\mu$. Vertical lines indicate the grid, in which Gaussian quadrature is applied.

k-space and thus create algebraic expressions for equations 3.5 and 3.6 that include integrals of the form we started with in expression 3.8. One has to assume the function $f(k)$ to vanish for large $|k|$ in order to allow for a truncation of k-space. This gives a restriction on the potentials $\hat{V}$ that can be treated with this formalism. The remaining integrals thus can be solved on a grid by Gaussian quadrature including N_g points k_j as depicted in figure 3.1. The weights ω'_j are calculated such that the integral is equal to the sum

$$= \sum_{j=1}^{N_g} \frac{f(k_j) - f(k_0)}{k_0^2 - k_j^2} \omega'_j + \sum_{j=1}^{N_g} \frac{f(-k_j) - f(-k_0)}{k_0^2 - k_j^2} \omega'_j - \frac{i\pi}{2|k_0|} (f(k_0) + f(-k_0)) \quad (3.12)$$

if the function $f(k)$ can be represented by a polynomial of 7th degree or less, within the $N_g/4$ grid sections. We can further simplify the sum over all $k \in \{-k_{N_g}, \ldots, -k_0, \ldots, k_0, \ldots, k_{N_g}\}$ values by definition of a mapping

$$\kappa_\mu := \begin{cases} -k_{N_g - \mu + 1} & \mu = 1, \ldots, N_g \\ k_{\mu - N_g} & \mu = N_g + 1, \ldots, 2N_g \\ -k_0 & \mu = 2N_g + 1 \\ k_0 & \mu = 2N_g + 2 \end{cases} \quad (3.13)$$

such that only a single sum over the variable μ is left. Additionally the function

$$D_\mu := \begin{cases} \omega'_{N_g-j+1} \frac{1}{k_0^2 - k_{N_g-j+1}^2} & \mu = 1, \ldots, N_g \\ \omega'_{j-N_g} \frac{1}{k_0^2 - k_{j-N_g}^2} & \mu = N_g+1, \ldots, 2N_g \\ -\left(\sum_{j=1}^{N_g} \omega'_j \frac{1}{k_0^2 - k_j^2} + \frac{i\pi}{2|k_0|} \right) & \mu = 2N_g+1, 2N_g+2 \end{cases} \tag{3.14}$$

can be defined, which includes all weights originating from the Gaussian quadrature. An extended derivation of κ_μ and D_μ can be found in the appendix 7.2. We now finally replace the integral we started with

$$\int_{-\infty}^{\infty} \frac{f(k)}{k_0^2 - k^2 + i\eta} dk = \sum_{\mu=1}^{2N_g+2} D_\mu f(\kappa_\mu) \tag{3.15}$$

by a sum which allows to write algebraic expressions for equations 3.5 and 3.6. This discretization scheme allows the application of numerical calculations and the result becomes exact if the function $f(k)$ can be piecewise represented by a polynomial.

3.3 T-matrix main equation

In general a scattering theory deals with the interaction of continuum states with a scattering potential. The lack of boundary conditions for the continuum states leads to the continuous spectrum, which makes the equations unsuitable for numerical calculations. Thus, the elaborated discretization scheme allows to turn the central equation

$$\hat{T} = \hat{V} + \hat{V}\hat{G}_0\hat{T} \tag{3.16}$$

for the T-matrix, into a system of linear equations that can be solved numerically. Utilizing the completeness relation $\mathbb{1} = \sum_S \int dk |S\rangle|k\rangle\langle k|\langle S|$ of the continuum states, including the spin degree of freedom, we can write equation 3.16 in mixed momentum and spin representation

$$\begin{aligned} \langle S_l|\langle k_l|\hat{T}|k_r\rangle|S_r\rangle &= \langle S_l|\langle k_l|\hat{V}|k_r\rangle|S_r\rangle \\ &+ \frac{2m}{\hbar^2}\sum_S \int dk \langle S_l|\langle k_l|\hat{V}|k\rangle|S\rangle \frac{1}{(k_0^2 - k^2)} \langle S|\langle k|\hat{T}|k_r\rangle|S_r\rangle. \end{aligned} \tag{3.17}$$

Since the Green's function $\langle S_l|\langle k_l|\hat{G}_0|k_r\rangle|S_r\rangle = \delta_{S_l,S_r} 2m/(\hbar^2(k_0^2 - k^2))$ is diagonal in spin and momentum space, only a single integral over k remains. The form of the remaining integral is identical to equation 3.8, which allows to apply the discretization scheme. We identify

$$f(k) = \frac{2m}{\hbar^2}\langle S_l|\langle k_l|\hat{V}|k\rangle|S\rangle\langle S|\langle k|\hat{T}|k_r\rangle|S_r\rangle \tag{3.18}$$

and thus replace the integral by a sum

$$\begin{aligned} \langle S_l|\langle k_l|\hat{T}|k_r\rangle|S_r\rangle &= \langle S_l|\langle k_l|\hat{V}|k_r\rangle|S_r\rangle \\ &+ \frac{2m}{\hbar^2}\sum_S \sum_\mu^{2N_g+2} D_\mu \langle S_l|\langle k_l|\hat{V}|\kappa_\mu\rangle|S\rangle\langle S|\langle \kappa_\mu|\hat{T}|k_r\rangle|S_r\rangle. \end{aligned} \tag{3.19}$$

By fixing k_r to a specific value, since it will be later related to the initial momentum of the scattered particle, one can simplify equation 3.19. For $k_l \in \{\kappa_\mu\}$ with $\mu \in \{1, \ldots, 2N_g + 1, 2N_g + 2\}$ all momentum values are included that occur due to the discretization of the continuum. Thus, $\hat{T}$ and $\hat{V}$ can both be represented by vectors. Defining a matrix with elements $\langle S_i|\langle \kappa_i|\mathcal{A}|\kappa_j\rangle|S_j\rangle = \frac{2m}{\hbar^2} D_j \langle S_i|\langle \kappa_i|\hat{V}|\kappa_j\rangle|S_j\rangle$ allows to write equation 3.19 in a simple form

$$\vec{T} = \vec{V} + \mathcal{A}\vec{T} \tag{3.20}$$

that is suitable for numerical computation. Note, if $\hat{V}$ is sparse, $\mathcal{A}$ shows the same sparse pattern. Thus we can use the symmetries that are conserved by the scattering potential to simplify the calculation of the T-matrix.

3.4 Scattering amplitudes including spin

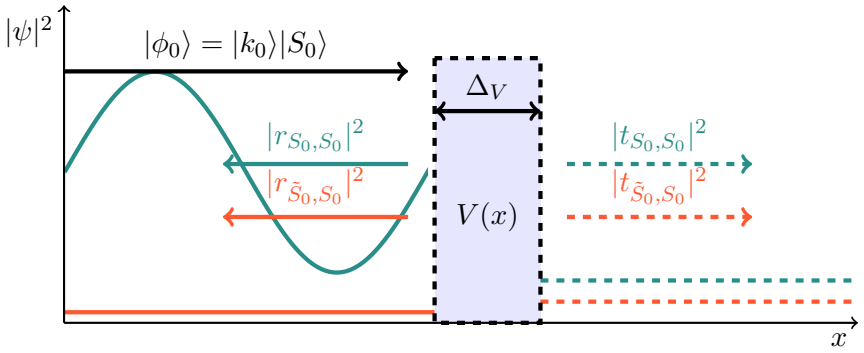

Figure 3.2: Schematics of spin scattering at a potential within the region Δ_V. The spacial representation of the potential is given by $V(x)$. An incoming wave $|\phi_0\rangle$ with initial spin configuration S_0 is either transmitted to the right hand side or reflected to the left hand side of the potential. During the scattering the spin can be exchanged leading to the spin state $\tilde{S}_0$.

Naturally, scattering is used to probe a local interaction between a scatterer and a scattered particle by detecting deviations from its free propagation. When characterizing the interaction region by the length Δ_V as shown in figure 3.2, the scattered wave function in the asymptotic limit needs to be of the form

$$\langle x|\psi\rangle = \begin{cases} \psi_0^+(x)|S_0\rangle + \sum_{S_f} r_{S_f,S_0}\psi_0^-(x)|S_f\rangle & x/\Delta_V \to -\infty \\ \sum_{S_f} t_{S_f,S_0}\psi_0^+(x)|S_f\rangle & x/\Delta_V \to \infty \end{cases} \tag{3.21}$$

with $\psi_0^\pm(x) = \frac{1}{\sqrt{2\pi}} e^{\pm ik_0 x}$ and the initial/final spin state denoted by $|S_{0/f}\rangle$. Thus a freely propagating particle would pass the interaction region undisturbed, which is related to a 100% transmission probability $|t_{S_0,S_0}|^2$ of the initial wave with spin S_0 and momentum k_0.

Let $|\tilde{S}_0\rangle$ be the spin state that results from $|S_0\rangle$ if the spin between two particles is exchanged. For example $|\tilde{S}_0\rangle = |\uparrow,\downarrow\rangle$ is a related to $|S_0\rangle = |\downarrow,\uparrow\rangle$ due to spin exchange. Hence, an interaction would lead to a deviation from the free propagation due to deflection into a different spin channel $|t_{\tilde{S}_0,S_0}|^2$ or reflection in the initial $|r_{S_0,S_0}|^2$ or the flipped spin channel $|r_{\tilde{S}_0,S_0}|^2$. In other words the transmission incorporates information about the interaction, which is related to the conductance[56] and thus of interest for experiments. In the following we derive the transmission amplitude of an incoming wave with momentum k_0 and initial spin S_0 that is elastically scattered into the final spin state S_f. This final spin state can be detected far away from the interaction region. Note that S_0 and S_f are products of

spin states such that the total spin part of the wave function is subject to scattering. As shown in equation 3.21, the transmission amplitude t_{S_f,S_0} is encoded in the wave function far away from the scattering region

$$\lim_{x \gg \Delta_V} \langle S_f, x|\psi\rangle, \tag{3.22}$$

which means in our convention the right hand side of the scattering potential. The Lippmann-Schwinger equation allows to replace the wave function by $|\psi\rangle = |\psi_0\rangle + \hat{G}_0\hat{V}\,|\psi\rangle$, which enables to perform the spacial limit in a convenient way.

$$\begin{aligned} &\lim_{x \gg \Delta_V} \langle S_f, x|\psi\rangle \\ = &\lim_{x \gg \Delta_V} \left(\langle S_f, x|\psi_0\rangle + \sum_{S'} \int dx' \langle S_f, x|\hat{G}_0|S', x'\rangle \langle S', x'|\hat{V}|\psi\rangle \right). \end{aligned} \tag{3.23}$$

Only the one-dimensional Green's function in real space representation depends on the coordinate x. Thus we can use the relation $\lim_{x \gg \Delta_V} |x - x'| = |x| - x'\mathrm{sign}(x)$ to take the limit of the Green's function far away from the scattering region. Here we are interested in the transmission, which means we can take $\mathrm{sign}(x) = 1$. Thus the limit

$$\begin{aligned} \lim_{x \gg \Delta_V} \langle S_f, x|\hat{G}_0|S', x'\rangle &= \lim_{x \gg \Delta_V} \left(-\langle S_f|S'\rangle \frac{im}{\hbar^2 k_0} e^{ik_0|x-x'|} \right) \\ &= -\langle S_f|S'\rangle \frac{im}{\hbar^2 k_0} e^{ik_0 x} e^{-ik_0 x'} \end{aligned} \tag{3.24}$$

can be replaced in equation 3.23 and leads together with $\langle x|k_0\rangle = \frac{1}{\sqrt{2\pi}} e^{ik_0 x}$ to

$$\begin{aligned} &\lim_{x \gg \Delta_V} \langle S_f, x|\psi\rangle \\ = &\langle S_f, x|\psi_0\rangle - \frac{im}{\hbar^2 k_0} e^{ik_0 x} \sum_{S'} \int dx' \langle S_f|S'\rangle e^{-ik_0 x'} \langle S', x'|\hat{V}|\psi\rangle \\ = &\langle S_f, x|\psi_0\rangle - \frac{im\sqrt{2\pi}}{\hbar^2 k_0} e^{ik_0 x} \sum_{S'} \int dx' \langle S_f|S'\rangle \langle k_0|x'\rangle \langle S', x'|\hat{V}|\psi\rangle \\ = &\langle S_f, x|\psi_0\rangle - \frac{im\sqrt{2\pi}}{\hbar^2 k_0} e^{ik_0 x} \langle S_f|\langle k_0|\hat{V}|\psi\rangle \\ = &\ \ldots \quad . \end{aligned} \tag{3.25}$$

At this point, the matrix element of the scattering potential can be replaced by a matrix element of the T-matrix $\langle\psi'|\hat{V}|\psi\rangle = \langle\psi'|\hat{T}|\psi_0\rangle$, which follows from comparison of equation 3.6 and 3.3 and leads to

$$\cdots = \langle S_f, x|\psi_0\rangle - \frac{im\sqrt{2\pi}}{\hbar^2 k_0} e^{ik_0 x} \langle S_f|\langle k_0|\hat{T}|\psi_0\rangle. \tag{3.26}$$

As mentioned before, the initial wave function is specified by $|\psi_0\rangle = |k_0\rangle|S_0\rangle$ and its spacial representation $\langle x|\psi_0\rangle = \frac{1}{\sqrt{2\pi}} e^{ik_0 x}|S_0\rangle$ allows a substitution, such that

$$\lim_{x \gg \Delta_V} \langle S_f, x|\psi\rangle = \langle S_f, x|\psi_0\rangle - \frac{im2\pi}{\hbar^2 k_0} \langle S_f|\langle k_0|\hat{T}|k_0\rangle|S_0\rangle\langle S_0|\langle x|\psi_0\rangle. \tag{3.27}$$

This form shows the relation between the initial wave function and the scattered wave function via the T-matrix. From comparison with equation 3.21 the transmission amplitude

$$t_{S_f,S_0} = \delta_{S_f,S_0} - \frac{im2\pi}{\hbar^2 k_0} \langle S_f|\langle k_0|\hat{T}|k_0\rangle|S_0\rangle \tag{3.28}$$

for an elastic transmission from initial spin S_0 to final spin S_f can be identified. Analogously the derivation can be performed for the limit $x/\Delta_V \to -\infty$ to derive the reflection amplitude

$$r_{S_f,S_0} = -\frac{im2\pi}{\hbar^2 k_0} \langle S_f|\langle -k_0|\hat{T}|k_0\rangle|S_0\rangle. \tag{3.29}$$

Both amplitudes are directly related to the scattering that occurred within the interaction region. Especially information about the localized spin after the scattering is encoded in the spin dependent transmission and reflection amplitude.

3.5 Contact form of exchange interaction

The previous derivation of spin dependent transmission and reflection does not rely on a specific form of the scattering potential. Hence, we begin our discussion with the contact form of the exchange interaction

$$\langle x|\hat{V}|x\rangle = V_0\delta(x-x_0)\vec{\sigma}_c\vec{\sigma}_l, \tag{3.30}$$

which can be solved analytically and thus gives a reference system for further investigations. The vector of Pauli matrices is either labeled with c when acting on the spin of the conduction electron or l for the localized spin. This contact form of the exchange interaction is commonly used, for example in the Kondo model[94]. It can be derived from the s-d model[99] in the case of small characteristic size of the localized spin possessing orbital with respect to the wavelength of the conduction electron[145]. In order to obtain the analytic solution we begin with the operator representation of the delta potential

$$\hat{V} = V_0\vec{\sigma}_c\vec{\sigma}_l|x_0\rangle\langle x_0|, \tag{3.31}$$

which is equivalent to the spacial representation of equation 3.30. The matrix elements $\langle\pm k_0|\hat{T}|k_0\rangle$ of the T-matrix are related to the transmission and reflection probabilities. Hence, we project the main equation of the T-matrix $\hat{T} = \hat{V} + \hat{V}\hat{G}_0\hat{T}$ into momentum representation and utilize its recursiveness. With the operator representation of the scattering potential

$$\begin{aligned}
\langle k_\alpha|\hat{T}|k_\beta\rangle &= \langle k_\alpha|\hat{V}|k_\beta\rangle + \langle k_\alpha|\hat{V}\hat{G}_0\hat{V}|k_\beta\rangle \\
&\quad + \langle k_\alpha|\hat{V}\hat{G}_0\hat{V}\hat{G}_0\hat{V}|k_\beta\rangle + \dots \\
&= \langle k_\alpha|x_0\rangle\langle x_0|k_\beta\rangle V_0\vec{\sigma}_c\vec{\sigma}_l \\
&\quad + \langle k_\alpha|x_0\rangle\langle x_0|\hat{G}_0|x_0\rangle\langle x_0|k_\beta\rangle \left(V_0\vec{\sigma}_c\vec{\sigma}_l\right)^2 \\
&\quad + \langle k_\alpha|x_0\rangle\langle x_0|\hat{G}_0|x_0\rangle\langle x_0|\hat{G}_0|x_0\rangle\langle x_0|k_\beta\rangle \left(V_0\vec{\sigma}_c\vec{\sigma}_l\right)^3 \\
&\quad + \dots \\
&= \dots
\end{aligned} \tag{3.32}$$

and the spacial representation of the Green's function $\langle x|\hat{G}_0|x'\rangle = -\frac{im}{\hbar^2 k_0}e^{ik_0|x-x'|}$ one obtains the series

$$\dots = \frac{V_0}{2\pi}e^{i(k_\beta-k_\alpha)x_0}\vec{\sigma}_c\vec{\sigma}_l\left[\mathbb{1} + \left(-\frac{imV_0}{\hbar^2 k_0}\vec{\sigma}_c\vec{\sigma}_l\right) + \left(-\frac{imV_0}{\hbar^2 k_0}\vec{\sigma}_c\vec{\sigma}_l\right)^2 + \dots\right]. \tag{3.33}$$

Introduction of the characteristic wave vector $v_0 := \frac{mV_0}{\hbar^2}$ and identification of the geometrical series in equation 3.33 allows to write the T-matrix in a compact form

$$\langle k_\alpha|\hat{T}|k_\beta\rangle = \frac{\hbar^2}{m2\pi} v_0 e^{i(k_\beta - k_\alpha)x_0} \vec{\sigma}_c \vec{\sigma}_l \left(\mathbb{1} - \left(-\frac{iv_0}{k_0}\vec{\sigma}_c\vec{\sigma}_l\right)\right)^{-1}. \tag{3.34}$$

For two 1/2 spins the last term of equation 3.34 is a 4×4 matrix that can analytically be inverted. In the product spin basis $S_i \in \{\uparrow_c\uparrow_l, \uparrow_c\downarrow_l, \downarrow_c\uparrow_l, \downarrow_c\downarrow_l\}$ the analytic solution for the T-matrix is given by

$$\langle k_\alpha|\hat{T}|k_\beta\rangle = \tag{3.35}$$
$$\frac{\hbar^2 v_0}{m2\pi} e^{i(k_\beta - k_\alpha)x_0} \begin{pmatrix} \frac{k_0}{4k_0+iv_0} & 0 & 0 & 0 \\ 0 & -\frac{k_0(4k_0+i3v_0)}{16k_0^2-i8k_0v_0+3v_0^2} & \frac{8k_0^2}{16k_0^2-i8k_0v_0+3v_0^2} & 0 \\ 0 & \frac{8k_0^2}{16k_0^2-i8k_0v_0+3v_0^2} & -\frac{k_0(4k_0+i3v_0)}{16k_0^2-i8k_0v_0+3v_0^2} & 0 \\ 0 & 0 & 0 & \frac{k_0}{4k_0+iv_0} \end{pmatrix}.$$

With equation 3.28 the T-matrix can be related to the transmission amplitude and thus gives

$$t = \begin{pmatrix} \frac{1}{i/(4\kappa)+1} & 0 & 0 & 0 \\ 0 & 1+i\frac{(4\kappa+i3)}{16\kappa^2-i8\kappa+3} & i\frac{8\kappa}{16\kappa^2-i8\kappa+3} & 0 \\ 0 & i\frac{8\kappa}{16\kappa^2-i8\kappa+3} & 1+i\frac{(4\kappa+i3)}{16\kappa^2-i8\kappa+3} & 0 \\ 0 & 0 & 0 & \frac{1}{i/(4\kappa)+1} \end{pmatrix} \tag{3.36}$$

and the reflection amplitude with equation 3.29

$$r = \begin{pmatrix} \frac{1}{i4\kappa-1} & 0 & 0 & 0 \\ 0 & i\frac{(4\kappa+i3)}{16\kappa^2-i8\kappa+3} & i\frac{8\kappa}{16\kappa^2-i8\kappa+3} & 0 \\ 0 & i\frac{8\kappa}{16\kappa^2-i8\kappa+3} & i\frac{(4\kappa+i3)}{16\kappa^2-i8\kappa+3} & 0 \\ 0 & 0 & 0 & \frac{1}{i4\kappa-1} \end{pmatrix} \tag{3.37}$$

for $x_0 = 0$ and the unitless parameter $\kappa := k_0/v_0$. The factor 4 in the transmission and reflection amplitude of a parallel spin configuration $\uparrow_c\uparrow_l$ or $\downarrow_c\downarrow_l$ can be eliminated by rescaling V_0 and has no physical meaning. Figure 3.3 shows a difference between the transmission probability for the parallel and antiparallel configuration $\uparrow_c\downarrow_l$ or $\downarrow_c\uparrow_l$. In the antiparallel configuration also spin flip scattering is possible, which leads to the reduced probability for the spin to be transmitted unperturbed. On the right hand side of figure 3.3 the probability for spin flips is shown. We define a switching probability $\Gamma := |t_{\tilde{S}_0,S_0}|^2 + |r_{\tilde{S}_0,S_0}|^2$ for the localized spin. The switching probability indicates, if the combined spin state has performed a transition from the initial state S_0 to the flipped state $\tilde{S}_0$ during the scattering. The switching probability

does not supply information, whether a coherent spin state was created during the scattering. In this thesis, we are interested in the final spin configuration, when some unspecified mechanism, such as a spin measurement of the itinerant electrons, leads to decoherence after the scattering. Since the transmission and reflection into the flipped spin state $\tilde{S}_0$ have the same momentum k_0 dependence, we can write the switching probability in the short form

$$\Gamma(\kappa) = \frac{128\kappa^2}{9 + 32\kappa^2(5 + 8\kappa^2)} \tag{3.38}$$

with a maximum at $\kappa_{\max} \approx 0.43$ of $\Gamma = 1/2$. The maximum position is indicated by a gray line in figure 3.3. This means a delta like exchange interaction can at most lead to an equal mixture of the initial spin state S_0 and the flipped spin state $\tilde{S}_0$ at the maximum position of Γ. This can be seen from both transmission channels

$$|t_{S_0,S_0}(\kappa_{\max})|^2 = |t_{\tilde{S}_0,S_0}(\kappa_{\max})|^2 = \frac{1}{4}, \tag{3.39}$$

which are equal at the maximum point of the switching probability. Same applies for the reflection. Thus both spin orientations of the itinerant electron will be detected with equal probability after it passed the interaction region. 100% probability for full reversal of both spins can not be achieved. Later on, we will focus on the switching probability for an exchange interaction with finite range and elaborate deviations from the delta potential. We demonstrate, that transmission with 100% switching probability can occur in a system with extended exchange interaction.

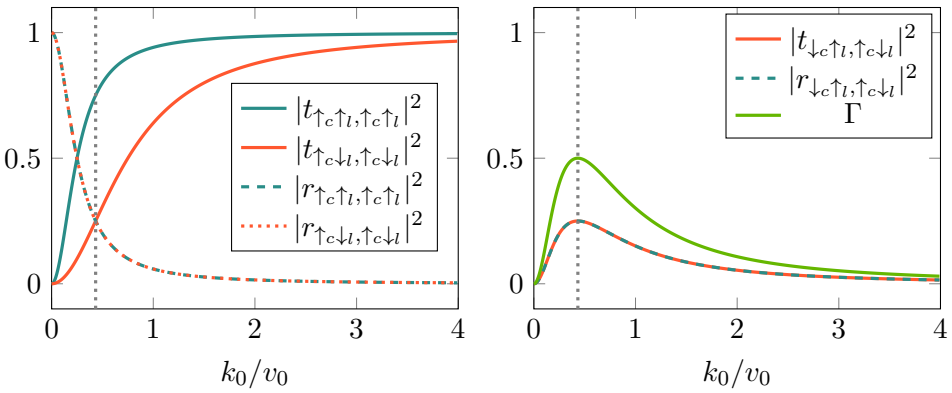

FIGURE 3.3: Transmission and reflection probability of a contact exchange interaction represented by a delta potential $V(x) = V_0\delta(x)\vec{\sigma}_c\vec{\sigma}_l$. When the spins are initially aligned antiparallel $\uparrow_c\downarrow_l$, exchange of the spins can occur. Denoted by the green line is the spin switching probability Γ of the localized spin. The gray line indicates the maximum of the switching probability.

3.6 Transmission probability

Before continuing with results including spin scattering it is important to understand the appearance of resonances in the transmission for attractive potentials. In a scattering theory the two cases of a repulsive potential $V(x) > 0$ acting as a barrier and the attractive potential $V(x) < 0$ acting as a well are usually treated separately. While quantum tunneling is a characteristic effect for a barrier, an attractive potential gives rise to bound states. We demonstrate in the following that bound states close to the continuum lead to an increased transmission probability at small momenta.

The delta potential $V_\delta(x) = V_0\delta(x)$ with $V_0 < 0$ for example bears a single bound state at the energy $\epsilon = -mV_0^2/2\hbar^2$. Thus only in the limit of vanishing potential $V_0 \to 0$ the bound state approaches the transition of becoming a continuum state. The transmission probability

$$|t|^2 = \frac{1}{1 + \left(\frac{v_0}{k_0}\right)^2} \tag{3.40}$$

for an attractive delta potential goes to 1 if the characteristic length $1/v_0 = \hbar^2/mV_0$ goes to infinity. Therefore the effect of bound state transition into the continuum and the absence of a scattering potential $V_0 = 0$ coincides for the delta potential as can be seen in figure 3.4.

This differs for the Pöschl-Teller potential

$$V_{\mathrm{PT}}(x) = V_0 \frac{\lambda(\lambda - 1)}{\cosh^2(x/\Delta_V)} \tag{3.41}$$

with characteristic length Δ_V and unitless parameter λ. The Schrödinger equation including the attractive Pöschl-Teller potential can be solved analytically and one obtains bound state energies $\epsilon_n \propto (\lambda - 1 - n)$ with $n \in \mathbb{N}_0$ [57]. The bound states merge into continuum states for $\lambda \in \mathbb{N}$. In this case the attractive potential becomes transparent for the incoming plane wave, since it is a solution to the full Schrödinger equation as well. In figure 3.4 the periodic appearance of resonances in the transmission is a clear indication of this effect. Note, that results of figure 3.4 were calculated with the spin independent T-matrix formalism using

$$t = 1 - \frac{im2\pi}{\hbar^2 k_0} \langle k_0 | \hat{T} | k_0 \rangle, \tag{3.42}$$

which reproduces the analytic results for the transmission probability

$$|t|^2 = \frac{p^2}{1 + p^2} \tag{3.43}$$

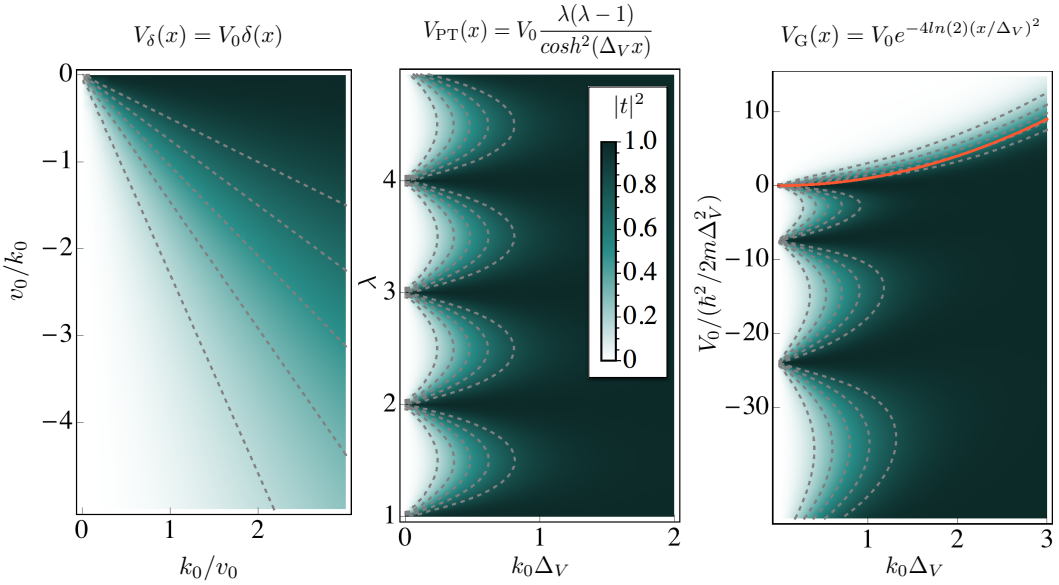

FIGURE 3.4: Transmission probability $|t|^2$ for three different attractive scattering potentials, meaning $V_0 < 0$. The transmission probability for the delta potential (left), the Pöschl-Teller potential (center) and the Gaussian potential (right) are shown. Resonances at $k_0 = 0$ indicate the transition from bound states into the continuum. The red line marks the classical limit for a transmission over the repulsive Gaussian potential.

when choosing $V_0 = \hbar^2/(2m\Delta_V^2)$ and defining $p := \sinh(\pi k\Delta_V)/\sin(\pi\lambda)$ [57].

For a Gaussian potential

$$V_{\mathrm{G}}(x) = V_0 e^{-4ln(2)(x/\Delta_V)^2} \tag{3.44}$$

one needs to refer to perturbation theory or numerical calculation [37] to compute the bound states. In figure 3.4 we see again the resonances from the bound state into continuum state transition for $V_0 < 0$, which are not periodic. This is typical for the Gaussian potential. Further, each resonance can be associated with a specific bound state [68]. For example the resonance at $V_0/(\hbar^2/(2m\Delta_V^2)) \approx -7.5$ belongs to the first excited state, the one at $V_0/(\hbar^2/(2m\Delta_V^2)) \approx -24$ to the second excited state, et cetera. When the potential acts as a barrier, only quantum tunneling leads to a transmission through the barrier, which is restricted by the classical limit $\hbar^2k^2/2m < V_0$. This limit is indicated by a red line in figure 3.4. The rapid increase of the transmission is roughly located around the classical condition $\hbar^2k^2/2m = V_0$ for a step in the transmission. The characteristic features that were elaborated so far allow an interpretation of the following results for a spin dependent Gaussian

scattering potential

$$V(x) = V_0 e^{-4ln(2)(x/\Delta_V)^2} \vec{\sigma}_c \vec{\sigma}_l, \tag{3.45}$$

which includes spin exchange between the itinerant spin $\vec{\sigma}_c$ and localized spin $\vec{\sigma}_l$ within a finite region. We are especially interested in the scattering with the initially antiparallel spin configuration $|S_0\rangle = |\uparrow_c, \downarrow_l\rangle$, since this condition enables to observe spin exchange. Note, that the results for an initial spin state $|S_0\rangle = |\downarrow_c, \uparrow_l\rangle$ would be the same. For convenience we suggest a change of basis to explain the spin flip results with the afore elaborated effects from an attractive and repulsive Gaussian scattering potential. We use the singlet $|0\rangle$ and triplet $|1\rangle$ state to replace the initial spin configuration $|S_0\rangle$ and the spin flip configuration $|\tilde{S}_0\rangle$ in the following manner

$$|0\rangle = \frac{1}{\sqrt{2}} \left(|\uparrow_c \downarrow_l\rangle - |\downarrow_c \uparrow_l\rangle \right) \tag{3.46}$$

$$|1\rangle = \frac{1}{\sqrt{2}} \left(|\uparrow_c \downarrow_l\rangle + |\downarrow_c \uparrow_l\rangle \right) \tag{3.47}$$

$$|S_0\rangle = |\uparrow_c \downarrow_l\rangle = \frac{1}{\sqrt{2}} \left(|1\rangle + |0\rangle \right) \tag{3.48}$$

$$|\tilde{S}_0\rangle = |\downarrow_c \uparrow_l\rangle = \frac{1}{\sqrt{2}} \left(|1\rangle - |0\rangle \right). \tag{3.49}$$

The potential $V(x) = V_\mathrm{G}(x)\vec{\sigma}_c\vec{\sigma}_l$ in equation 3.45 is now diagonal in this representation, since the total spin commutes with the scattering potential $[\hat{V}, \vec{\sigma}_c + \vec{\sigma}_l] = 0$ and the singlet and triplet states are eigenstates of the total spin. Thus for $V_0 > 0$ the single state is subject to an attractive potential with $\langle 0|V(x)|0\rangle = -\frac{3}{4}V_\mathrm{G}(x)$ while the triplet state is effected by a repulsive potential $\langle 1|V(x)|1\rangle = \frac{1}{4}V_\mathrm{G}(x)$. In figure 3.5 the transmission probability shows resonances from the transition of bound states into the continuum, referring to the regions, in which either singlet or triplet state senses an attractive potential. The different scaling of the left an central plot of figure 3.5 is a result of the effective potential height $\tilde{V}_0 = -\frac{3}{4}V_0$ for the singlet and $\tilde{V}_1 = \frac{1}{4}V_0$ for the triplet state. In the region where the effective potentials act as a barrier, the classical transmission step is indicated by a red line. Because we are interested in the deflection of an initial state $|S_0\rangle = |\uparrow_c \downarrow_l\rangle$ into a spin flip state $|\tilde{S}_0\rangle = |\downarrow_c \uparrow_l\rangle$, we also have to determine the phase shift between singlet and triplet state that occurs during the scattering. With the main equation for the T-matrix

$$\hat{T} = \hat{V} + \hat{V}\hat{G}_0\hat{V} + \hat{V}\hat{G}_0\hat{V}\hat{G}_0\hat{V} + \ldots, \tag{3.50}$$

one can demonstrate the commutator relation $[\hat{T}, \vec{\sigma}_c + \vec{\sigma}_l] = 0$ and thus the conservation of total spin by the T-matrix. Hence, the matrix elements $\langle 0|\langle k_0|\hat{T}|k_0\rangle|1\rangle =$

$\langle 1|\langle k_0|\hat{T}|k_0\rangle|0\rangle = 0$ vanish and we can derive the transmission amplitude

$$\begin{aligned} t_{\tilde{S}_0,S_0} &= -\frac{im2\pi}{\hbar^2 k_0}\frac{1}{2}\left(\langle 1| - \langle 0|\right)\langle k_0|\hat{T}|k_0\rangle\left(|0\rangle + |1\rangle\right) \\ &= \frac{1}{2}\left(t_{11} - t_{00}\right) \end{aligned} \tag{3.51}$$

in the singlet and triplet representation. The effect of the relative phase shift between singlet and triplet state, according to the different potentials they have to pass, is included in the last term of

$$|t_{\tilde{S}_0,S_0}|^2 = \frac{1}{4}\left(|t_{11}|^2 + |t_{00}|^2 - 2\Re(t_{11}^* t_{00})\right). \tag{3.52}$$

Figure 3.5 shows the importance of the phase shift when the potential barriers can be surmounted in a classical sense $\hbar^2 k_0^2/2m > \tilde{V}_{0/1}$. A phase shift below this limit, denoted by the black lines on the right of figure 3.5, is a result of quantum tunneling. In the singlet and triplet representation, the complete spin exchange between itinerant and localized spin is denoted by the phase shift $\Re(t_{11}^* t_{00}) = -1$. Effectively no spin is exchanged during the scattering, when $2\Re(t_{11}^* t_{00}) = 1$. Remember, for the delta potential a complete exchange of spin is not possible. The phase relation during the scattering of a finite range potential increases the probability for a complete spin exchange, which is indicated by the dark red regions on the right hand side of figure 3.5. Note, that the results are not symmetric to $V_0 = 0$ due to the asymmetric singlet and triplet splitting, becoming apparent from the ratio $\tilde{V}_0 = -3\tilde{V}_1$. This asymmetry and the focus on spin exchange will be subject to the following, where we look at the switching probability of the local momentum that acts as a scatterer.

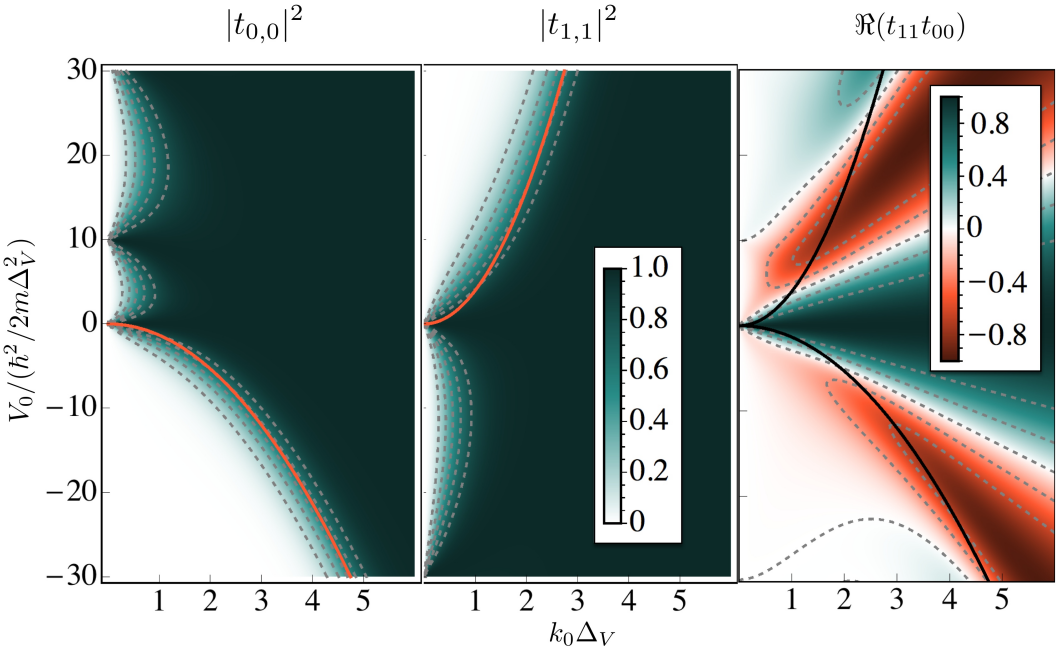

Figure 3.5: Transmission probability for the singlet (left) and triplet (center) part of the initial spin state $|S_0\rangle = |\uparrow_c\downarrow_l\rangle$. The effect of the relative phase between singlet and triplet state on the transmission probability $|t_{\tilde{S}_0,S_0}|^2$ into the spin flipped state $|\tilde{S}_0\rangle = |\downarrow_c\uparrow_l\rangle$ is shown on the right.

3.7 Spin switching probability

Previous results for the transmission demonstrate the momentum k_0 dependent efficiency for a spin exchange between the localized and itinerant spin, leading to a reversal of both spins with respect to the initial spin state, for example $|S_0\rangle = |\uparrow_c\downarrow_l\rangle$. In general, not only transmission but also reflection into the flipped spin state $|\tilde{S}_0\rangle = |\downarrow_c\uparrow_l\rangle$ would reverse the local magnetic moment labeled with l. Both scattering channels,$|r_{\tilde{S}_0,S_0}|^2$ and $|t_{\tilde{S}_0,S_0}|^2$, that lead to a spin reversal of the local spin, are depicted in figure 3.6. The sum of the probabilities $|t_{\tilde{S}_0,S_0}|^2$ from the transmission channel and $|r_{\tilde{S}_0,S_0}|^2$ from the reflection channel give the total probability for the switching of the local magnetic moment $\downarrow_l\rightarrow\uparrow_l$ due to scattering with the itinerant electron. Again, coherent spin states are not considered in the switching probability, since we assume that decoherence occurs after the scattering process is completed.

With increasing momentum k_0 of the itinerant electron, four consecutive situations in the scattering can be differentiated. The occurrence is indicated by the colored lines in figure 3.6 and we exemplarily elaborate them in figure 3.7 taken at $V_0 = -25\frac{\hbar^2}{2m\Delta^2}$ and $V_0 = 25\frac{\hbar^2}{2m\Delta^2}$. For the explanation we decompose the initial $|S_0\rangle$ and flipped spin

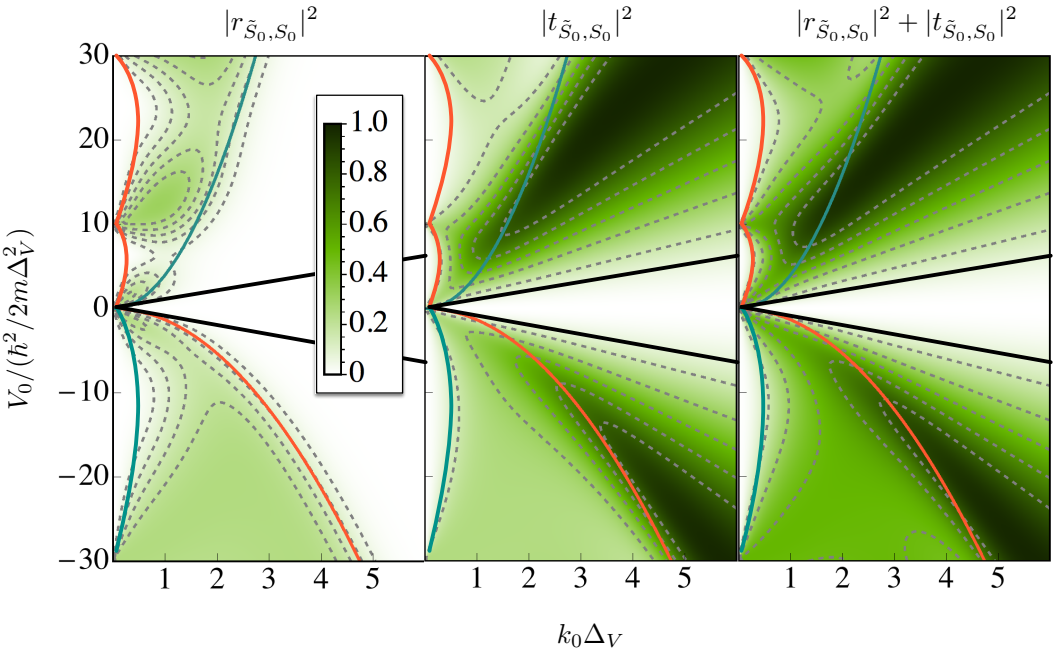

FIGURE 3.6: Spin switching potability due to reflection (left) or transmission (center) into the spin flipped state $\tilde{S}_0$. Total spin flip probability is shown on the right. The colored lines indicate the onset of full transmission for the singlet (red) and triplet (blue) state. The black line limits the region in which no exchange interaction effectively occurs due to the large kinetic energy of the itinerant spin.

state $|\tilde{S}_0\rangle$ into the singlet and triplet representation as demonstrated in equations 3.49 and 3.48. In figure 3.6 for small k_0 only reflection $|r_{S_0,S_0}|^2$ of the unchanged spin state appears if neither the singlet nor the triplet part of $|S_0\rangle$ can be transmitted. Resonances at small k_0 only appear, if bound states are close to the continuum in the singlet and triplet representation, as demonstrated in figure 3.5. When crossing the first colored line in figure 3.6 one enters the region in which either the triplet (blue line) or the singlet (red line) part of the initial state is transmitted, while the other is still reflected. In the case of $V_0 < 0$ the transmission of the triplet state appears at smaller momenta k_0 than the transmission of the singlet. This situation is reversed for $V_0 > 0$ as shown in figure 3.6. While either just the singlet or triplet part of the initial spin state is transmitted, the switching probability remains constant with respect to the energy of the scattered electron. This is an effect of the finite range of the scattering potential and does not appear for a delta like scattering potential, see figure 3.3. The further apart the insets of full transmission of each singlet and triplet sate are with respect to k_0, the wider is the region of constant switching probability. Thus, the plateau with constant probability is more pronounced in the region $V_0 < 0$,

as shown in the comparison of figure 3.7. The inset of the region in which also the second part, either singlet (red line) or triplet (blue line), of the scattered state $|S_0\rangle$ is transmitted indicates the region in which the switching probability is dominated by the transmission. As discussed previously, the relative phase between singlet and triplet state might even lead to a switching probability up to 100% depending on the strength V_0 of the exchange interaction. This high switching probability can only occur due to the transmission through a spatially extended interaction region. The reflection into the spin flipped channel can maximally lead to a switching potability of 25% as shown on the left hand side of figure 3.6. Finally when reaching a momentum k_0 such that the black line in figure 3.6 is crossed, the phase relation between singlet and triplet remains constant and no switching of the local spin occurs. From this point on the correlation between the itinerant and localized spin effectively vanished.

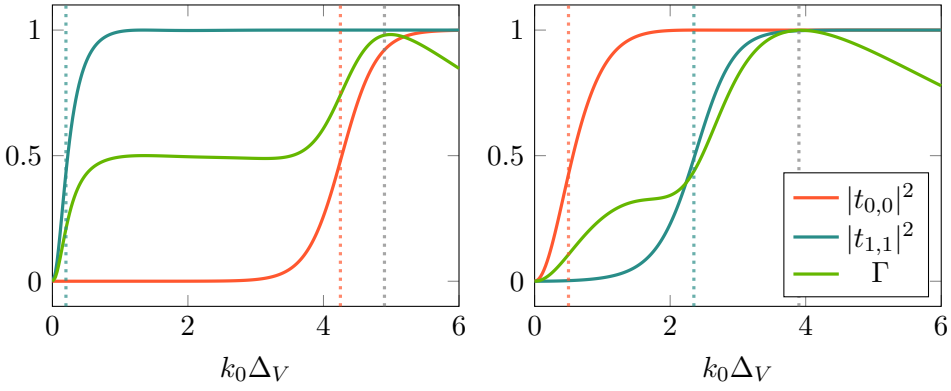

Figure 3.7: Transmission of the triplet state (blue line) and the singlet state (red line) in combination with the switching probability Γ, with its maximum marked by the gray line. The colored dashed lines indicate the onset of full transmission for the singlet (red) and triplet (blue) state. The two different interaction strength $V_0 = -25\frac{\hbar^2}{2m\Delta^2}$ (left) and $V_0 = 25\frac{\hbar^2}{2m\Delta^2}$ (right) were chosen.

3.8 Wave function of the itinerant electron

In the previous discussion we mainly focused on the asymptotic limit $|x/\Delta_V| \to \infty$ of the scattering in terms of transmission and reflection probabilities. Likewise the T-matrix allows to investigate the wave function of the itinerant electron within the interaction region $|x| < \Delta_V$. The initial $|\psi_0\rangle = |k_0\rangle|S_0\rangle$ and scattered wave function

$$|\psi\rangle = |\psi_0\rangle + \hat{G}_0\hat{T}\,|\psi_0\rangle \tag{3.53}$$

are related via the T-matrix. Information about the spatially dependent spin scattering is revealed when looking at the specific spin density $|\phi(x)_{S_f}|^2 = |\langle S_f|\langle x|\psi\rangle|^2$. Thus we project equation 3.53 onto a certain spin state in space by multiplying $\langle S_f|\langle x|$ to the left and make use of the completeness relation $\mathbb{1} = \sum_S \int dk|S\rangle|k\rangle\langle k|\langle S|$. The diagonality of the Green's function $\langle S_l|\langle k_l|\hat{G}_0|k_r\rangle|S_r\rangle = \delta_{S_l,S_r} 2m/(\hbar^2(k_0^2 - k^2))$ further allows to write the wave function

$$\begin{aligned}\langle S_f|\langle x|\psi\rangle &= \delta_{S_f,S_0}\frac{1}{\sqrt{2\pi}}e^{ik_0x} \\ &+\frac{2m}{\hbar^2\sqrt{2\pi}}\int dk\frac{1}{k_0^2-k^2}e^{ikx}\langle S_f|\langle k|\hat{T}|k_0\rangle|S_0\rangle\end{aligned} \tag{3.54}$$

in a form which is suitable for the previously elaborated discretization scheme. Utilizing equation 3.15 and identifying $f(k) = e^{ikx}\langle S_f|\langle k|\hat{T}|k_0\rangle|S_0\rangle$ allows to use the results gathered from the calculation of the T-matrix to compute the wave function

$$\begin{aligned}\langle S_f|\langle x|\psi\rangle &= \delta_{S_f,S_0}\frac{1}{\sqrt{2\pi}}e^{ik_0x} \\ &+\frac{2m}{\hbar^2\sqrt{2\pi}}\sum_{\mu=1}^{2N_g+2} D_\mu e^{i\kappa_\mu x}\langle S_f|\langle \kappa_\mu|\hat{T}|k_0\rangle|S_0\rangle\end{aligned} \tag{3.55}$$

in spacial and spin dependent representation.

In the following two examples, for selected values of the interaction strength V_0, we want to focus on the scattering process from the itinerant electrons point of view. Beside the spin dependent wave function in figure 3.8 and 3.10 we present the transmission and reflection in the representation $|S_0\rangle = |\uparrow_c\downarrow_l\rangle$ and $|\tilde{S}_0\rangle = |\downarrow_c\uparrow_l\rangle$ in figure 3.9 and 3.11. As a reference to the previous discussion, horizontal dashed lines indicate the onset of transmission for the singlet (red line) and triplet (blue line) part of the initial spin state. The gray dashed line marks the maximum of the switching probability Γ. As a first example we take the same value of $V_0 = -25\frac{\hbar^2}{2m\Delta^2}$ as on the left side of figure 3.7, where the difference in representation can be seen in figure 3.9. In the region of constant switching probability $1 < k_0\Delta_V < 4$ the

incoming electron is scattered with equal probability into all four transmission and reflection channels. In this region the wave function in figure 3.8 shows an interference pattern occurring between the incoming wave with initial spin $|S_0\rangle = |\uparrow_c\downarrow_l\rangle$ and the reflected wave $|r_{S_0,S_0}|^2$ with the same spin. Reflection into another spin state $|r_{\tilde{S}_0,S_0}|^2$ does not cause interference in the spin density. Note, the total spin density $(|\phi(x)_{\uparrow_c\downarrow_l}|^2 - |\phi(x)_{\downarrow_c\uparrow_l}|^2)/2$ vanishes behind the spin scatterer while the switching probability is constant at 50%. Even though the itinerant electron is partially transmitted, equal distribution into both transmission channels with spin S_0 and $\tilde{S}_0$ leads to an absence of spin current behind the scatterer. Thus the itinerant spin is efficiently reflected by the localized spin for a wide range of initial momenta k_0. This effect is attributed to the finite range of the exchange interaction and only present for the delta potential at the point of maximal switching probability.

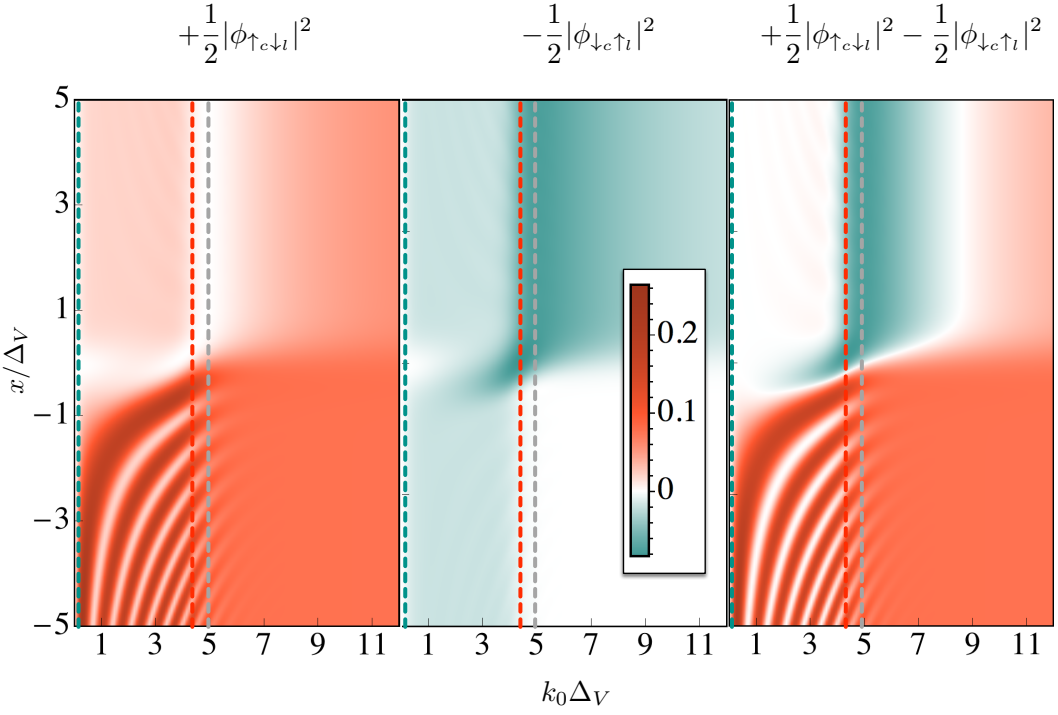

Figure 3.8: Spin and spacial dependent expectation value for spin up (left) and spin down (center) of the itinerant electron. Total spin density of the itinerant electron (right). Parameters are the same as on the left hand side of figure 3.7.

In addition, the total reflection of the spin can only be seen if the onset for singlet and triplet transmission are clearly separated with respect to the momentum k_0. This separation is to small in the second example at $V_0 = 25\frac{\hbar^2}{2m\Delta^2}$, which has already been shown on the right hand side of figure 3.7. Superpositions of the singlet and triplet transmission lead to a clear difference between the $|t_{S_0,S_0}|^2$ and $|t_{\tilde{S}_0,S_0}|^2$

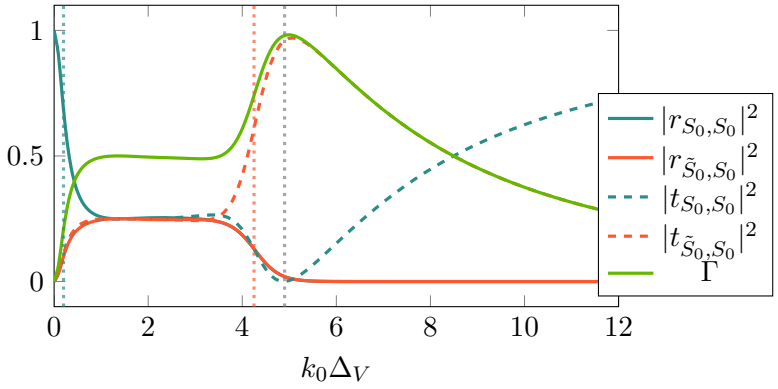

FIGURE 3.9: Spin dependent transmission probability with respect to the initial $|S_0\rangle = |\uparrow_c\downarrow_l\rangle$ and the spin flipped state $|\tilde{S}_0\rangle = |\downarrow_c\uparrow_l\rangle$. Parameters are the same as on the left hand side of figure 3.7.

within the region $0.5 < k_0\Delta_V < 2.3$ as shown in figure 3.11. In the spin density in figure 3.7 a spin current behind the scattering region appears.

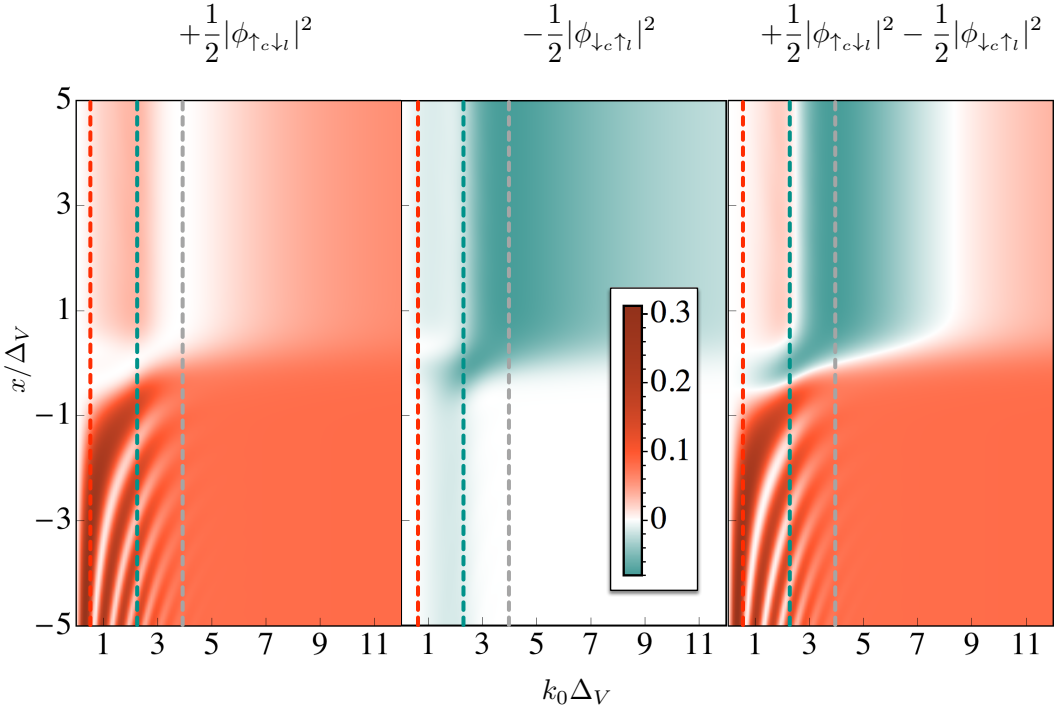

FIGURE 3.10: Spin and spacial dependent expectation value for spin up (left) and spin down (center) of the itinerant electron. Total spin density of the itinerant electron (right). Parameters are the same as on the right hand side of figure 3.7.

Both examples exhibit the same k_0 behavior after the maximum of the switching

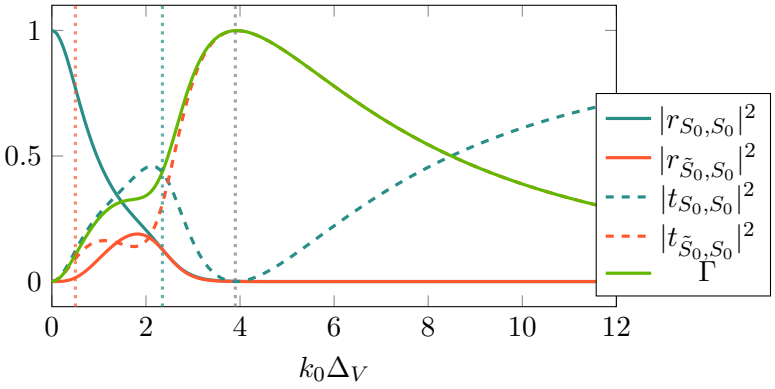

Figure 3.11: Spin dependent transmission probability with respect to the initial $|S_0\rangle = |\uparrow_c\downarrow_l\rangle$ and the spin flipped state $|\tilde{S}_0\rangle = |\downarrow_c\uparrow_l\rangle$. Parameters are the same as on the right hand side of figure 3.7.

probability was reached. At the maximum point of the switching probability, indicated by the gray dashed line, the initial spin of the itinerant electron is fully reversed due to the exchange with the localized spin. Since this effect appears due to the transmission, the interference pattern before the scattering region vanishes. When the momentum of the itinerant electron is further increased, the spin exchange effectively decreases until the spin state is not effected by the scattering anymore.

Driven magnetization reversal for a single spin 4

In the following, a model for the description of the current-driven dynamics of a magnetic adatom on a metallic surface and coupled to a spin-polarized tip is presented. We approximate the magnetic atom by a single spin in an anisotropic potential, resulting from the crystal field of the surface. Further, the metallic surface and tip are treated as electron reservoirs that represent a continuos source of electrons. In correspondence to the previous chapter we indicate the relation between the T-matrix and the master equation approach, utilized in this chapter.

4.1 Stevens operators and crystal field symmetries

Magnetism in single atoms is manly based on the electron configuration, which follows Hund's rules. If the intra-atomic spin-orbit coupling dominates and leads to a strong interaction between the total orbital momentum $\vec{L}$ and the total spin $\vec{S}$, they form a combined spin $\vec{J} = \vec{L} + \vec{S}$. The combined magnetic moment $g\mu_B\sqrt{J(J+1)}$ of the atom, with the Landé factor g and the Bohr magneton μ_B, can be quantified by the total angular momentum quantum number J. When an atom is placed in an electronic environment, its magnetic moment can change due to the hybridization of the momentum bearing orbitals. Commonly this effect is smaller for the rare earth $4f$-elements, than for transition metal 3d-elements, since the electron density is more localized in the core of the atom. Minor deviations for 3d-adatoms from the free magnetic moment were also reported [81;100;113;167] and depend on the hybridization with the substrate. The magnetic moment of an adatom can be studied in more detail with first-principle models such as density functional theory [154].

Without further specifications, we refer in the following to an adatom on a metallic substrate that exhibits strong spin-orbit coupling with respect to the crystal field interaction. Thus the magnetic degrees of the adatom are represented by a single total spin $\vec{J}$. The degenerate spin states of the multiplet can be labeled by the magnetic quantum number $m \in \{-J, ..., J\}$. Because of the interaction with the anisotropic crystal field of the substrate, degeneracy between the $2J + 1$ spin states in the J multiplet is partially lifted. We show in the following how to derive an effective Hamiltonian for $\vec{J}$ that results from the crystal field and thus obeyes all the rotational symmetries of the adatom and substrate complex.

Each of the N ligands, meaning ions in the crystal structure that surround the adatom, creates an electrostatic potential $V(\vec{R}_i)$ that adds up to the total crystal field

$$H_{\mathrm{cf}} = -|e| \sum_{i=1}^{N} V(\vec{R}_i), \tag{4.1}$$

experienced by electrons in the momentum bearing outer shell of the adatom. In first approximation, the ionic ligands can be described by point charges q_i. It is convenient for later symmetry arguments to switch to spherical coordinates (r, θ_r, ϕ_r) and expand the field in spherical harmonics Y_{pk} leading to

$$\begin{aligned} V(\vec{R}_i) &= \frac{1}{4\pi\epsilon_0} \sum_{i}^{N} \frac{q_i}{|\vec{R}_i - \vec{r}|} \\ &= \frac{1}{\epsilon_0} \sum_{i}^{N} q_i \sum_{p=0}^{\infty} \frac{r^p}{R_i^{p+1}} \sum_{m=-p}^{p} \frac{1}{2p+1} Y^*_{pm}(\theta_r, \phi_r) Y_{pm}(\theta_{R_i}, \phi_{R_i}). \end{aligned} \tag{4.2}$$

Deploying the Wigner-Eckart theorem allows to replace spacial coordinates with a complete set of spherical tensor operators namely $\hat{J}_z$ and the ladder operators $\hat{J}_+, \hat{J}_-$. Bear in mind, the operator representation is just an alternative to the description of the crystal field in cartesian coordinates. An example is $x^2 - y^2 \propto (\hat{J}_+^2 + \hat{J}_-^2)$ [110]. This leads to the operator equivalent representation of the crystal field

$$H_{\mathrm{cf}} = \sum_{p,m} B_p^m O_p^m \tag{4.3}$$

with the so called Stevens operators O_p^m [151] and the coefficient B_p^m that can explicitly be calculated from the ligand distribution. Note, that the tesseral harmonics can substitute the spherical harmonics, which proofs that the coefficients B_p^m are real numbers. Because of the orthogonality of the spherical harmonics all odd terms in p vanish [9] and the remaining Stevens operators up to fourth order are

$p=2$	$O_2^0 \propto 3\hat{J}_z^2 - J(J+1)$
	$O_2^1 \propto \{\hat{J}_z, \hat{J}_+ + \hat{J}_-\}$
	$O_2^2 \propto (\hat{J}_+^2 + \hat{J}_-^2)$
$p=4$	$O_4^0 \propto 35\hat{J}_z^4 - 30J(J+1)\hat{J}_z^2 + 25\hat{J}_z^2 - 6J(J+1) + 3J^2(J+1)^2$
	$O_4^1 \propto \{7\hat{J}_z^2 - (3J(J+1)+1)\hat{J}_z, \hat{J}_+ + \hat{J}_-\}$
	$O_4^2 \propto \{7\hat{J}_z^2 - J(J+1) - 5, \hat{J}_+^2 + \hat{J}_-^2\}$
	$O_4^3 \propto \{\hat{J}_z, \hat{J}_+^3 + \hat{J}_-^3\}$
	$O_4^4 \propto (\hat{J}_+^4 + \hat{J}_-^4)$

from which O_2^0 is the most prominent, representing the uniaxial anisotropy $D\hat{J}_z^2$ with $D = 3B_2^0$.

The symmetry of the crystal field is now directly related to the Stevens coefficients B_p^m and thus restricts the operators O_p^m that occur in the single spin Hamiltonian we want to derive. We refer to section 5.1 for an illustration of the potential that is described by the Stevens operators.

Since we consider a single magnetic adatom on a crystalline surface, the only remaining symmetry transformations are discrete rotations around the z-axis of the atom, which is chosen perpendicular to the surface. These transformations belong to the cyclic point groups C_χ with χ-fold rotations that map the system onto itself. For the moment we restrict our considerations to maximally *4*-fold symmetric systems. The remaining *6*-fold rotational symmetry will be discussed at a later point. In figure 4.1 we illustrate the rotational point groups of an adatom on a crystalline substrate with different planes of a face-centered cubic (fcc) crystal.

The coefficients B_p^m of the Stevens operators depend on the point symmetry of the atom within the ligand field. To show this we separately look at the sum over the ligands

$$B_p^m = \cdots \sum_i \frac{q_i}{R_i^{p+1}} Y_{pm}(\theta_{R_i}, \phi_{R_i}) \tag{4.4}$$

$$= \ldots \int d^3R \frac{n(\vec{R})}{R^{p+1}} Y_{pm}(\theta_R, \phi_R) \tag{4.5}$$

and introduced the ligand density $n(\vec{R})$. A χ-fold rotation symmetry means the ligand density is invariant under χ-fold rotations, $n(\vec{R}) = n(r, \theta, 2\pi j/\chi)$ with $j \in \{0, \ldots, \chi - 1\}$. Integration over the radial part r and the polar angle θ can be performed separately. The integral over the azimuthal angle ϕ can be separated into a sum over $\chi - 1$ equal integrals, due to rotational symmetry, with the factor

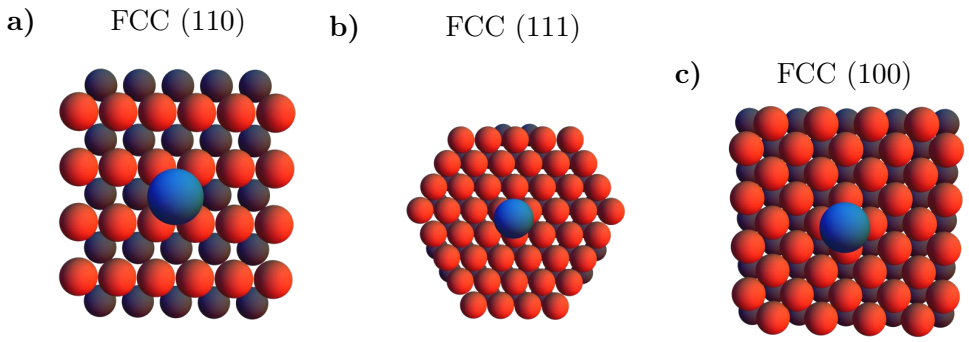

Figure 4.1: Visualization of point symmetries on a crystall plane of a FCC crystal defined by Miller indices. The blue sphere represents the adatom while the red spheres are surface atoms. The adatom on the (110) plane in (a) has a two-fold symmetry (C_2), in (b) a three-fold symmetry (C_3) on the (111) plane is shown and in (c) the adatom on the (100) plane has a four-fold symmetry (C_4).

$e^{i2\pi mj/\chi}$ resulting from the invariance in the angle dependence of Y_{pm}. Identifying the geometrical sum

$$B_p^m = \cdots \sum_{j=0} e^{i2\pi mj/\chi} = \ldots \frac{1 - e^{i2\pi m}}{1 - e^{i2\pi m/\chi}}, \tag{4.6}$$

generates an expression that is always zero unless m is an integer multiple of χ. Hence only coefficients $B_p^{i\chi}$, with integer i, do not vanish. In the table

	O_2^0	O_2^1	O_2^2	O_4^0	O_4^1	O_4^2	O_4^3	O_4^4
C_2	X	0	X	X	0	X	0	X
C_3	X	0	0	X	0	0	X	0
C_4	X	0	0	X	0	0	0	X

X/O marks the non-/vanishing coefficients of a specific point symmetry C_χ. In conclusion this means that the crystal field experienced by the adatom depends on the rotational point symmetry the system posses.

4.2 Single spin in a crystal field

In general, a crystal field lifts the degeneracy of the $2J+1$ spin states of an atom in the ground state multiplet J. It was shown that the point symmetry of an adatom on a crystalline substrate has a large effect on the form of the crystal field in terms of Stevens operators. We consider three relevant rotational symmetries with a rotational axes perpendicular to the crystal surface. The index $\chi \in \{2, 3, 4\}$ labels the number of rotations leading to a symmetry transformation. The previous table visualizes the non-vanishing coefficients B_k^m of the Stevens operators O_k^m for the point group of the system. This means every symmetry is represented by a characteristic spin Hamiltonian $\hat{H}_\chi$ that contains the interaction of the magnetic atom with the crystal field. For simplicity we take into account only operators O_2^0 and the lowest order perturbation O_p^m that includes ladder operators $\hat{J}_\pm$, since we are interested in their capability to mix spin states. Stevens operators such as O_4^0 can create the situation, in which the ground states do not posses the maximal absolute magnetic moment [50]. For sake of simplicity we neglect those terms but they might be included, if referring to a specific system. Contributions of $J(J+1)$ can also be omitted since in the J multiplet it is just a constant energy shift of all levels.

The simplified spin Hamiltonian

$$\hat{H}_2 = D_2 \hat{J}_z^2 + \tilde{B}\hat{J}_z + E_2(\hat{J}_+^2 + \hat{J}_-^2) \tag{4.7}$$

$$\hat{H}_3 = D_3 \hat{J}_z^2 + \tilde{B}\hat{J}_z + E_3\left(\hat{J}_z(\hat{J}_+^3 + \hat{J}_-^3) + (\hat{J}_+^3 + \hat{J}_-^3)\hat{J}_z\right) \tag{4.8}$$

$$\hat{H}_4 = D_4 \hat{J}_z^2 + \tilde{B}\hat{J}_z + E_4(\hat{J}_+^4 + \hat{J}_-^4) \tag{4.9}$$

includes the uniaxial anisotropy constant D_χ, the Zeeman energy $\tilde{B} := \mu_B g B/\hbar$ and transversal anisotropy constant E_χ. The Stevens operator coefficients are thus replaced by some general constants, since we focus only on the symmetry effects of a general crystal field.

In the following we explain each term of the single spin Hamiltonian $\hat{H}_\chi$ shown in equations (4.7,4.8,4.9). Starting with the first part that appears in each Hamiltonian, the uniaxial anisotropy, lifts all but double degeneracies. Since $[\hat{J}_z^2, \hat{J}_z] = 0$ the eigenstates of the uniaxial part can be labeled by the magnetic quantum number $|m\rangle$. Since $D_\chi < 0$, the eigenstates with energy ϵ_i align along an inverted parabola with respect to their expectation value $\langle \hat{J}_z \rangle$ as depicted in figure 4.2. In this case, the two ground states $|\pm m\rangle$ with opposite magnetic orientation are separated by an anisotropy barrier that is depicted in figure 4.2 by a gray line. Later, we will focus on the switching between these ground states. In a classical system one

needs to surmount the barrier of height $\Delta_0 := max(|\epsilon_i - \epsilon_j|) = |D_\chi|J^2$ to switch the magnetization direction. Note, that the barrier $|D_\chi|(J^2 - 1/4)$ slightly differs for a half integer spin. We will show that in a quantum system low energy paths become accessible for switching between the ground states due to the transversal anisotropy. A characteristic energy is given by the largest energy difference between adjacent spin states Δ_{01} , that can be found between the ground state $|\pm m\rangle$ and the first excited state $|\pm m \mp 1\rangle$. The second part of each Hamiltonian $\hat{H}_\chi$ describes the interaction of the total magnetic moment $\vec{J}$ with a magnetic field along the z-axis. This simply increases or decreases the energy gap between adjacent spin states by $\pm\tilde{B}$, depending on the relative orientation of the spin to the magnetic field. Still the magnetic quantum number m remains a good quantum number. This changes when the third term of the Hamiltonian $\hat{H}_\chi$ is included, since $[\hat{H}_\chi, \hat{J}_z] \neq 0$. Every transversal anisotropy field, with constant E_χ, creates coherences between $\hat{J}_z$ eigenstates. Thus, the energy eigenstates are mixtures of $|m\rangle$ states, and hence, m is not a good quantum number anymore. Which states contribute to the mixture is specified by the order χ of the ladder operators $\hat{J}_\pm$. For example the expansion of the ground states in $\hat{J}_z$ eigenstates

$$|\phi_0^s\rangle = \sum_{n=0}^{\lfloor (2J-1)/\chi \rfloor} c_n^{s,0} |J - \chi n\rangle \tag{4.10}$$

$$|\phi_0^{s'}\rangle = \sum_{n=0}^{\lfloor (2J-1)/\chi \rfloor} c_n^{s',0} |-J + \chi n\rangle \tag{4.11}$$

holds a superposition of every χs spin state $|m\rangle$ with coefficients $c_n^{s,i}$. Those coefficients become important in the case of transitions between the energy eigenstates that are related to the matrix element $\langle\phi_0^{s'}|\hat{J}_\pm|\phi_0^s\rangle$. We will illustrate the dependence of the transition probability on the transversal anisotropy E_χ, which is encoded in the coefficients $c_n^{s,i}$. Notice, an alternative representation for the energy eigenstates allows to see immediately if the transition probability between two states vanishes. Later, we will introduce such a representation but continue with the present picture, since it allows in a convenient way to quantify the transition probability. Hence, we continue by labeling the χ different species of energy eigenstates $|\phi_i^s\rangle$ with s . Each species can be formed by their own disjoint group of $|m\rangle$ states. Whenever two degenerate ground states belong to different groups, we label the group with $s = +/-$ if it contains the $|+/-J\rangle$ spin state. The lower index i counts the position of the eigenstate in energy space within the species. For example $i = 0$ is the ground

state and $i = 1$ the first excited state. As an example the energy levels are shown in figure 4.2 for the three-fold symmetry and a spin $J = 4$. States of the same color rely on the same subset of $|m\rangle$ states. The degeneracy of the green states is lifted by the transversal anisotropy and they exhibit tunnel splitting while reducing their magnetic expectation value $\langle \hat{J}_z \rangle$. One can approximate these states by

$$|\phi_0^0\rangle \approx 1/\sqrt{2}(|3\rangle - |-3\rangle) \tag{4.12}$$

$$|\phi_1^0\rangle \approx 1/\sqrt{2}(|3\rangle + |-3\rangle), \tag{4.13}$$

the antisymmetric and symmetric superposition of spin states on each side of the barrier. The formation of these tunnel split states within the barrier emerges when naively a degeneracy of two eigenstates from the same species is suspected and the main contributing spin states are not half integers with the same absolute value. Latter condition is a result of Kramers theorem that states a double degeneracy between half integer spin states for a time-reversally symmetric Hamiltonian. In other words, without a magnetic field $\hat{H}_\chi$ is time-reversal symmetric and a system with half-integer J does not show tunnel splitting between states from the same species. For an integer J we can conclude further that tunnel splitting between the ground states due to the transversal anisotropy only occurs if the ratio $2J/\chi$ is an integer number.

We will later see that the time-reversal symmetry of the three-fold symmetric system and the tunnel split states within the barrier have a great impact on the electron induced switching rate between the ground states.

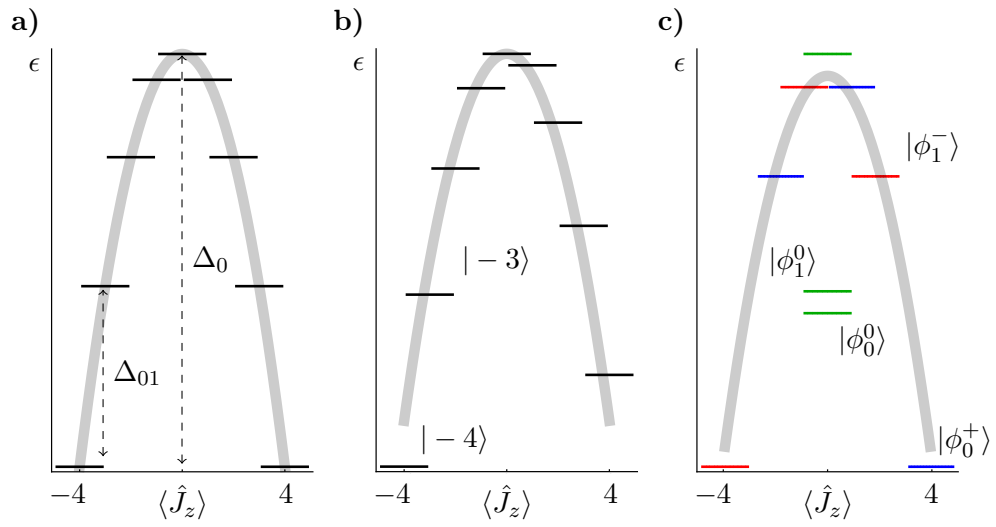

Figure 4.2: Energy levels of $\hat{H}_\chi$ as a function of the expectation value $\langle \phi_i^s | \hat{J}_z | \phi_i^s \rangle$ with just uniaxial anisotropy (a) and additional magnetic field (b). The gray line indicates the unperturbed anisotropy barrier. A three-fold symmetric system $\hat{H}_\mathcal{3}$ with transversal anisotropy is shown in (c) in the absence of magnetic field. The different species of states are colored blue (+), red (−) and green (0). Tunnel splitting between the green states occurs due to the transversal anisotropy.

4.3 Master equation for current-driven magnetization dynamics

The considered model is used to describe transport in a spin polarized scanning tunneling microscope setup, where the tip and the substrate are sources of tunneling electrons. This setup allows for a non-equilibrium configuration in which a current flows from the tip to the substrate and conduction electrons interact with the adatom via spin-spin interaction. Transitions between spin states of the magnetic adatom are thus induced by elastic and inelastic spin scattering with conduction electrons [46;105]. The tunneling electrons can also detect the spin orientation of the adatom due to the magnetoresistance effect. A sketch of the model is shown in figure 4.3.

The total Hamiltonian reads as

$$\hat{H} = \underbrace{\hat{H}_\chi + \overbrace{\hat{H}_T + \hat{H}_S}^{\hat{H}_\mathrm{res}}}_{\hat{H}_0} + \hat{H}_t \tag{4.14}$$

and includes the tip $\hat{H}_T$, the substrate $\hat{H}_S$ Hamiltonian and the single spin Hamiltonian $\hat{H}_\chi$ that incorporates the interaction with the crystal field of the

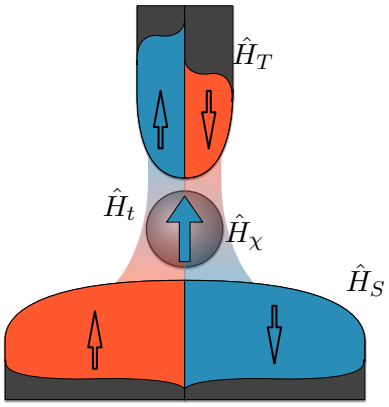

FIGURE 4.3: Schematic view of the single magnetic spin coupled to two electron reservoirs. The upper part, characterized by $\hat{H}_T$, represents a spin polarized tip, which has a different chemical potential with respect to the unpolarized substrate, described by $\hat{H}_S$. The interaction of the adatom with the crystal field is included in $\hat{H}_\chi$, while exchange interaction with the conduction electrons is included by $\hat{H}_t$.

substrate. Both reservoirs ($\hat{H}_{\text{res}}$) are treated as non-interacting Fermi liquids $\hat{H}_r = \sum_{k,\sigma} \epsilon_{r,k,\sigma} a^\dagger_{rk\sigma} a_{rk\sigma}$ with k denoting the momentum. The single particle energy $\epsilon_{r,k,\sigma}$ is given by the free electron dispersion relation and includes the chemical potential μ_r for the reservoir. $a^{(\dagger)}_{rk\sigma}$ are the annihilation (creation) operators in tip $r = T$ and substrate $r = S$, where σ denotes the spin of a conduction electron. Since $\hat{H}_{res}$ is diagonal, the eigenstates of the uncoupled system $\hat{H}_0$ can be determined by diagonalizing $\hat{H}_\chi$. An Appelbaum Hamiltonian [4]

$$\hat{H}_t = \frac{1}{2} \sum_{rr'kk'\sigma\sigma'} v_r v_{r'} a^\dagger_{rk\sigma} \vec{\sigma}_{\sigma,\sigma'} \cdot \hat{\vec{J}} a_{r'k'\sigma'}, \tag{4.15}$$

models the coupling between conduction electrons and the magnetic adatom in the limit of half filled orbitals and large Coulomb energy compared to the hybridization energy [10;43;58;145]. The vector of Pauli matrices $\vec{\sigma}_{\sigma,\sigma'}$ is associated with the spin of the tunneling electrons. Note, $\hat{H}_t$ is already second order in the tunnel coupling v_r and thus describes the effect of cotunneling, known from the Anderson model.

Next, we outline the derivation of a master equation and refer to Timm [160] for details. The von Neumann equation expresses the time evolution of the density matrix

$$\frac{d\rho}{dt} = -i[\hat{H}_l(t), \rho] =: -i\mathcal{L}_l(t)\rho \tag{4.16}$$

and can be written in a compact form with the Liouville superoperator $\mathcal{L}_l$, where l refers to a specific Hamiltonian. A description of driven dynamics in the reduced

system $\hat{H}_\chi$ can be achieved by tracing over the reservoir degrees of freedom. Further, it is assumed that coherences, represented by off-diagonal elements of the reduced density matrix, decay much faster than the relaxation time [44;159]. While coherences are also created by environment-induced superselection [58;87], this effect can be neglected in the weak coupling limit we consider. Thus the definition of a superoperator

$$\tilde{\mathcal{P}}\rho(t) := \sum_\alpha |\alpha\rangle\langle\alpha|\mathbf{tr}_{res}(\rho(t))|\alpha\rangle\langle\alpha| \otimes \rho^0_{res} \tag{4.17}$$

allows to project the density matrix of the total system ρ onto the diagonal elements $P_{(\alpha,\alpha)}$ of the reduced density matrix with respect to eigenstates $|\alpha\rangle$ of $\hat{H}_\chi$. This is achieved by tracing over the reservoir degrees of freedom ($\mathbf{tr}_{res}$) and then projecting onto the diagonal elements of the reduced density matrix. The reservoir permanently remains in equilibrium ρ^0_{res}. We assume the coupling to be turned on at time $t = -\infty$, by replacing $\hat{H}_t \to \hat{H}_t e^{\eta t}$. One can solve the von Neumann equation with

$$\tilde{\mathcal{P}}\rho(t) = \tilde{\mathcal{P}} T_{\leftarrow} \exp\left(-i\int_{t_0}^{t} dt'(\mathcal{L}_0 + \mathcal{L}_t e^{\eta t'})\right)\tilde{\mathcal{P}}\rho(t_0) \tag{4.18}$$

under the mentioned conditions. $T_\leftarrow$ denotes the time ordering operator, that orders according to the direction of the arrow the following expression ascending in time. Taking the time derivative of equation 4.18 leads to a rate equation

$$\frac{d}{dt}\tilde{\mathcal{P}}\rho(t) = \tilde{\mathcal{R}}(t,t_0)\tilde{\mathcal{P}}\rho(t_0) \tag{4.19}$$

for the diagonal elements of the reduced density matrix. Writing the superoperator $\tilde{\mathcal{R}}(t,t_0)$ in the representation of $\hat{H}_0$ eigenstates allows to define rates

$$\Gamma_{fi} := \langle f|(\tilde{\mathcal{R}}(t,t_0)|i\rangle\langle i|)|f\rangle \tag{4.20}$$

between eigenstates i and f. When making equation 4.19 local in time, known as Markov approximation $\rho(t_0) \to \rho(t)$, Timm demonstrated [160] that the rates

$$\Gamma_{fi} = 2\pi\delta(E_i - E_f)|\langle f|\hat{T}(E_i)|i\rangle|^2 \tag{4.21}$$

can be expressed in terms of the T-matrix. This matrix

$$\hat{T}(E_i) = \sum_{n=0}^{\infty} \hat{H}_t\left(\hat{G}_0(E_i)\hat{H}_t\right)^n \tag{4.22}$$

is equivalent to the one we have used in the previous chapter, where $\hat{H}_t$ represents the spin interaction and $\hat{G}_0(E_i) = 1/(E_i - \hat{H}_0 + i0^+)$ is the free Greens function within the adiabatic coupling approximation $\eta \to 0^+$. Next we assume to be in the weak

coupling limit, meaning $\hat{T} \approx \hat{H}_t$, also known as Born approximation. In this regime the thermal energy k_bT in the reservoirs is large compared to the level broadening [168]. The weak coupling also justifies the Markov approximation [86;159], which can be seen from a comparison of rates from the T-matrix and the time-convolution-less approach with respect to an expansion in $\hat{H}_t$ [160]. Thus, within the lowest order expansion of the T-matrix in $\hat{H}_t$ and a summation over all reservoir ($\hat{H}_{res}$) eigenstates $|f'\rangle$ and $|i'\rangle$, the rate between $\hat{H}_\chi$ eigenstates $|\alpha\rangle$ and $|\beta\rangle$ is given by

$$\tilde{\mathcal{W}}_{\alpha\beta} = 2\pi \sum_{i'f'} |\langle f'|\langle \alpha|\hat{H}_t|\beta\rangle|i'\rangle|^2 \delta(\epsilon_\beta + E_i - \epsilon_\alpha - E_f). \tag{4.23}$$

Further, we only take into account terms that lead to transitions between $\hat{H}_\chi$ eigenstates, meaning $\alpha \neq \beta$. This determines a master equation

$$\frac{dP_\alpha}{dt} = \sum_\beta \left(\mathcal{W}_{\alpha\beta} P_\beta - \mathcal{W}_{\beta\alpha} P_\alpha\right) \tag{4.24}$$

for the diagonal elements of the reduced density matrix $P_\alpha := \langle\alpha|\tilde{\mathcal{P}}\rho|\alpha\rangle$. The rates

$$\mathcal{W}_{\alpha\beta} = \pi \sum_{rr' \in \{\mathrm{T,S}\}} |v_r v_{r'}|^2 \Sigma^{rr'}_{\alpha\beta}\, \zeta\left(\mu_r - \mu'_r - \Delta_{\alpha\beta}\right) \tag{4.25}$$

now only include transitions between states of the reduced system [46]. First, each addend of a rate depends on the tunnel coupling $|v_r v_{r'}|^2$ and differentiates electron transport between tip and substrate or just tip and just substrate. The fourth order in tunnel coupling corresponds to the cotunneling in the Anderson model. The second part is the spectral weight

$$\begin{aligned} \Sigma^{rr'}_{\alpha\beta} \;=\; & |\langle\alpha|\hat{J}_+|\beta\rangle|^2 \rho_{r\downarrow}\rho_{r'\uparrow} + |\langle\alpha|\hat{J}_-|\beta\rangle|^2 \rho_{r\uparrow}\rho_{r'\downarrow} \\ & + |\langle\alpha|\hat{J}_z|\beta\rangle|^2 \left(\rho_{r\uparrow}\rho_{r'\uparrow} + \rho_{r\downarrow}\rho_{r'\downarrow}\right), \end{aligned} \tag{4.26}$$

including matrix elements of the ladder operators describing $\hat{J}_\pm$ the angular momentum transfer of the tunneling electrons and $\hat{J}_z$ matrix elements giving rise to the tunnel magnetoresistance. The last part $\zeta(x) = x/(1 - exp(-x/k_bT))$ gives the energy dependence of the rates, which results from a convolution of two fermi distributions. μ_r is the chemical potential for the electron reservoir r such that $eV = \mu_T - \mu_S$ is the voltage between the tip and the surface. $\Delta_{\alpha\beta} = \epsilon_\alpha - \epsilon_\beta$ is the energy difference between eigenstates.

The formal solution of equation 4.24 can be expanded in terms of eigenvectors of the kernel $K_{\alpha,\beta} = (1 - \delta_{\alpha,\beta})\mathcal{W}_{\alpha\beta} + \delta_{\alpha,\beta} \sum_\beta \mathcal{W}_{\alpha\beta}$. The time evolution of each

eigenvector $\vec{\kappa}_i$ follows an exponential behavior $exp(-\Gamma_i t)$, with Γ_i the i-th eigenvalue of $\mathbf{K}$. The solution is thus given by

$$\vec{P}(t) = \sum_i c_i \vec{\kappa}_i e^{-\Gamma_i t}, \tag{4.27}$$

with expansion coefficients c_i, specifying the initial state. We solve the master equation numerically. The smallest eigenvalue $\Gamma_0 = 0$ denotes the stationary limit where the probability distribution $\vec{P}_0 = \vec{\kappa}_0$ does not change with time. At this point, we refer to the actual structure of $\hat{H}_\chi$, discussed in the previous section. In the case of strong relaxation compared to excitation of the spin, the switching between the ground states $|\phi_0^{\pm}\rangle$ denotes the longest time scale for a transition between states. Thus we can identify the longest non-vanishing eigenvalue Γ with the switching rate between the ground states. All other rates between states are on a much shorter time scale. On the time scale of the ground state transition $|\phi_0^+\rangle \leftrightarrow |\phi_0^-\rangle$, we can thus write the solution of equation 4.24 as

$$\begin{pmatrix} P_{+,0} \\ P_{-,0} \\ \vdots \end{pmatrix} \approx c_0 \vec{P}_0 + c_1 \begin{pmatrix} 1 \\ -1 \\ \vec{0} \end{pmatrix} e^{-\Gamma t}. \tag{4.28}$$

In Γ all possible paths from one ground state to the other are included. We have shown the relation between the switching rate and the two state telegraph noise that has been detected in recent experiments in a different publication [89]. In the following we will elaborate the contribution of special paths from quantum tunneling and classical switching to the total rate Γ, which we normalize to the total spin flip rate $\Gamma_0 = \pi\hbar^2 v_T^2 v_S^2 (\rho_{T\uparrow}\rho_{S\downarrow} + \rho_{T\downarrow}\rho_{S\uparrow})/|D_\chi|(2J_\chi - 1)$ for electrons inelastically tunneling from the tip to the surface.

4.4 Single electron induced switching

Even if the ground states are separated by an anisotropy barrier, the quantum nature of the spin allows for a finite switching probability. A single electron can induce this transition when transversal anisotropy is present. Electrons that induce direct transitions between the ground states come mainly from the substrate, since it is more strongly coupled to the adatom than the tip. We label the ground states with $|\phi_0^{\pm}\rangle$. For the comparison of symmetry effects on single electron switching, we consider a spin $J = 5/2$. Two-, three- and four-fold symmetry all have a non-vanishing probability for the spin to switch from one ground state to the other with a single electron. Taking the limit $\zeta(x/k_bT \to 0) = k_bT$ for states with energy splitting smaller than the temperature gives the rate for this process

$$\mathcal{W}_{\phi_0^{\mp}\phi_0^{\pm}} \propto \left(|\langle \phi_0^{\mp} | \hat{J}_+ | \phi_0^{\pm} \rangle|^2 + |\langle \phi_0^{\mp} | \hat{J}_- | \phi_0^{\pm} \rangle|^2 \right) k_bT \tag{4.29}$$

that is proportional to the temperature. The part of the spectral weight $|\langle \phi_i^{\mp} | \hat{J}_z | \phi_i^{\pm} \rangle|^2 = 0$ because each ground state consists of a superposition of $\hat{J}_z$ eigenstates, which form two disjoint sets. The two matrix elements, within equation 4.29, thus determine the magnitude of the switching probability. In figure 4.4 this is manifested in a finite switching rate at zero voltage ($V = 0$).

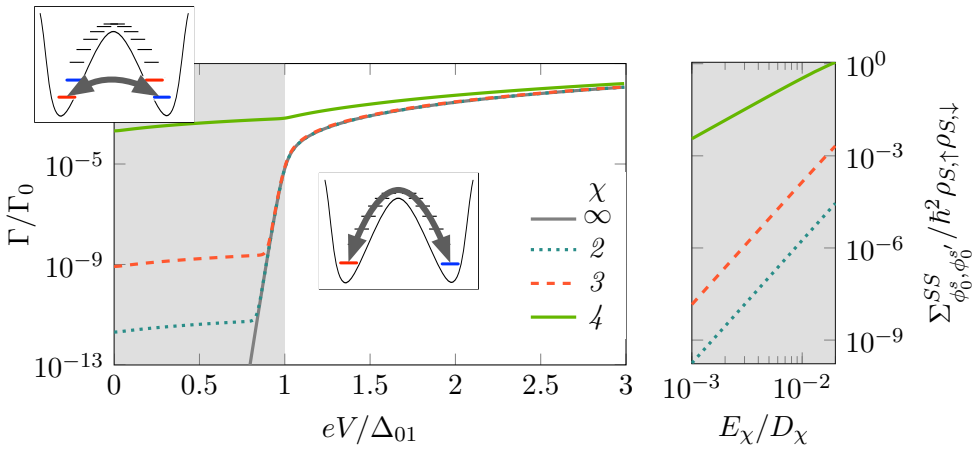

FIGURE 4.4: (left) Switching rate Γ/Γ_0 is shown in units of the total spin flip rate for the different symmetries $\chi \in \{2, 3, 4\}$ with $J = 5/2$. For comparison a system with just uniaxial anisotropy is shown, which is labeled with $\chi = \infty$. For voltages above the first excitation energy Δ_0 transitions across the barrier dominate the switching with respect to single electron induced tunneling that is present at lower voltages. (right) The matrix elements within the spectral weight, shown in equation 4.29, are presented with respect to the transversal anisotropy E_χ.

A system without transversal anisotropy, labeled with $\chi = \infty$, does not show single electron ground state switching since the spin can only be switched when at least $2J$ inelastic scattering processes occur. The threshold voltage $eV = \Delta_{01}$ denotes the minimal energy that is needed to excite from the ground state and thus start a cascade of subsequent transitions. An excitation can be made even slightly below the first excitation energy, when the fermi edge of the conduction electrons is thermally broadened. The probability to surmount the barrier then further increases with increasing voltage, since more electrons posses enough energy to excite the system. In the following we will focus on the regime below the threshold voltage. The different magnitude of the direct transition at $V = 0$ is a result of the mixing of $|m\rangle$ states by the transversal anisotropy. The groups, within which mixing occurs, are shown color coded in figure 4.5. Lets focus on the induced transition from $|\phi_0^+\rangle$ to $|\phi_0^-\rangle$. The spectral weight of the direct rate includes the non-vanishing matrix elements $\langle m \pm 1|\hat{J}_\pm|m\rangle$ that are proportional to $(E_2/D_2)^2$. This results from a perturbation expansion of the ground states in E_χ/D_χ with respect to $\hat{J}_z$ eigenstates, as demonstrated in the appendix 7.6. For example $\langle\frac{5}{2}|\hat{J}_+|\frac{3}{2}\rangle$ appears due to the second order expansion of $|\phi_0^-\rangle$ and the unperturbed order of $|\phi_0^+\rangle$. In general the matrix element $\langle\phi_0^\pm|\hat{J}_\pm|\phi_0^\mp\rangle \propto (E_2/D_2)^{(2J-1)/\chi}$ for a two-fold symmetric system if the transversal anisotropy can be treated as small perturbation.

Such a generalization can not be made for the three-fold symmetric systems. In our example with $J = \frac{5}{2}$ the only non-vanishing matrix element for the transition from the $s = +$ to the $s = -$ ground states is $\langle-\frac{1}{2}|\hat{J}_+|\frac{1}{2}\rangle$. This part of the expansion is proportional to $(E_3/D_3)^2$ since it comes from the first perturbation expansion of both ground states. On the right hand side of figure 4.4 we therefore see the same slope for the spectral weight $\Sigma^{SS}_{\phi_0^s,\phi_0^{s'}}$ in a two- and three-fold symmetric system.

In a four-fold symmetric system with $J = \frac{5}{2}$ there are only two non-vanishing matrix elements contributing to the spectral weight of the transition from $|\phi_0^+\rangle$ to $|\phi_0^-\rangle$. For example the element $\langle-\frac{5}{2}|\hat{J}_-|-\frac{3}{2}\rangle$ gives a proportionality of E_4/D_4 since only the first perturbation order of both ground states is needed. This results in a different slope for the spectral weight as shown in figure 4.4.

Even though the proportionality of the matrix elements within the spectral weight can not be generalized, a good approximation is given by $(E_\chi/D_\chi)^{(2J-1)/\chi}$ in the limit of small transversal anisotropy $E_\chi \ll D_\chi$.

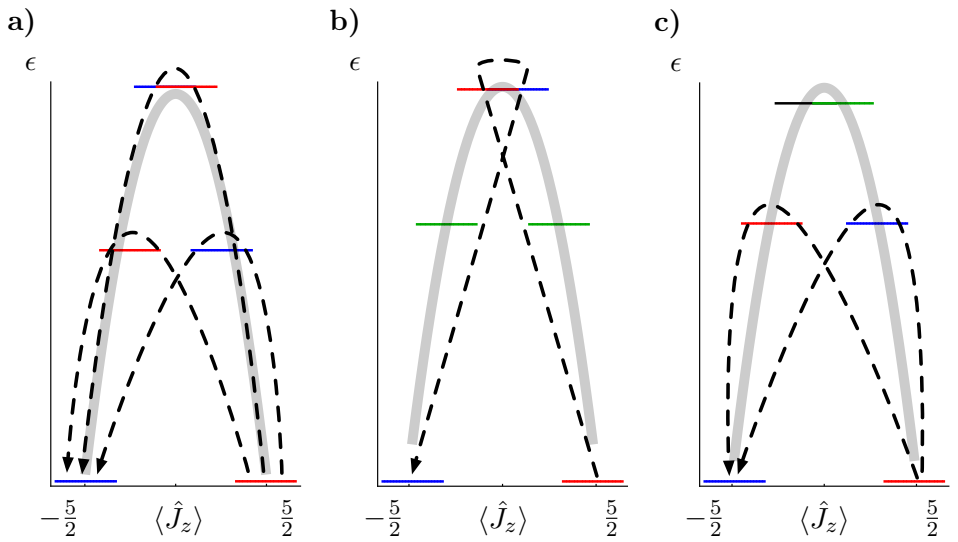

FIGURE 4.5: Energy levels of $\hat{H}_\chi$ as a function of the expectation value $\langle \phi_i^s | \hat{J}_z | \phi_i^s \rangle$ for the two-fold (a), three-fold (b) and four-fold symmetry (c). The different species of states are color coded. The two ground states belong to different groups blue (+), red (−). The dashed arrows visualize the different matrix elements $\langle m \pm 1 | \hat{J}_\pm | m \rangle$ that contribute to the spectral weight in equation 4.29.

4.5 Protection against single electron induced switching

Recently a mechanism that prevents the adatom spin from switching induced by a single electron has been investigated by Miyamachi et al.[118] and related to experimental data. The stated protection occurs in a three-fold symmetric system with a spin that is not an integer multiplet of 3. They demonstrate that the magnetic moment of the adatom is protected from single electron induced switching under time reversal symmetry. In appendix 7.7 we demonstrate that such a protection relies on the time reversal symmetry breaking due to exchange interaction. From the general relation $\hat{J}_\pm \hat{T} = -\hat{T} \hat{J}_\mp$, with the time reversal operator $\hat{T}$, we can derive for an integer spin J the condition

$$\langle \phi_0^- | \hat{J}_\pm | \phi_0^+ \rangle = -\langle \phi_0^- | \hat{J}_\pm | \phi_0^+ \rangle^* \tag{4.30}$$

that must be valid at zero magnetic field, meaning $[\hat{H}_\chi, \hat{T}] = 0$. In this case, $\hat{H}_\chi$ is symmetric and the spectral theorem states, that real eigenvectors can always be found. This means a basis transformation with orthogonal matrices diagonalizes the symmetric Hamiltonian. Thus $\hat{J}_\pm$ is also a real matrix in the representation of $\hat{H}_\chi$ eigenstates. Hence, the real number $\langle \phi_0^- | \hat{J}_\pm | \phi_0^+ \rangle$ must vanish according to equation 4.30. In the degenerate case, other linear combinations of $|\phi_0^+\rangle$ and $|\phi_0^-\rangle$

might also represent ground states, but we assume coherent superpositions of these states to be constantly destroyed due to the scattering with conduction electrons.

In our recent publication [84] we showed the linear increase of the matrix elements, when time reversal symmetry is broken with a magnetic field. The consequence can be seen in figure 4.6 for a $J = 5$ spin in a three-fold symmetric system.

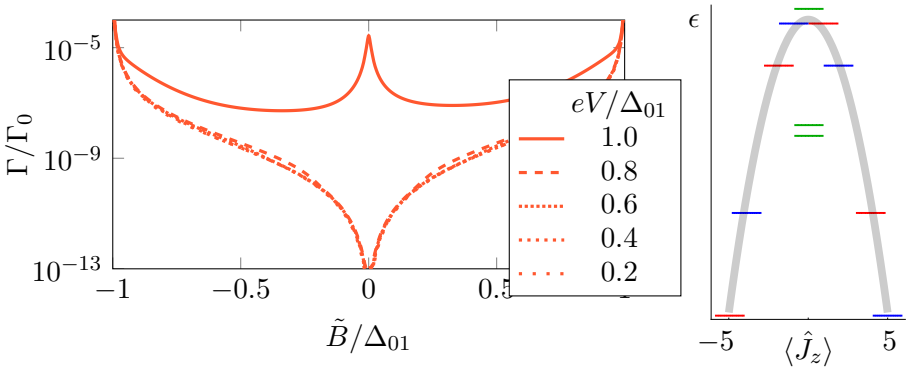

Figure 4.6: Switching rate for a spin with $J = 5$ in a three-fold symmetric system as a function of external magnetic field $\tilde{B}$. The separate lines denote different voltages eV. The level scheme is shown on the right side. Transitions through the green short cuts lead to an increased switching rate at vanishing magnetic field if excitations occur.

The switching rate is only zero for vanishing magnetic field, which marks the only point where the system can be protected form single electron induced switching. This rate increases drastically with magnetic field. Thus, apart from the zero field point, direct ground state transitions induced by a single electron are present. With increasing voltage, also excited states contribute to the switching rate. The peak at $eV = \Delta_{01}$ and $\tilde{B} = 0$ is a result from the states $|\phi_0^0\rangle$ and $|\phi_1^0\rangle$, which generate a short cut through the anisotropy barrier. We will elaborate on this in more detail in the next section.

The four-fold symmetric system with the same spin $J = 5$ shows a similar behavior shown in figure 4.7. A short cut is now created by the first and second excited state. This creates a resonance at zero magnetic field, if inelastic excitations from the ground states are present. The resonance from the short cut is even leaking into the region with voltages below the first excitation energy because of the finite temperature. The protection mechanism in the four-fold symmetric system does not rely on time reversal symmetry but is a consequence of the maximal angular momentum a conduction electron can exchange with the spin of the adatom. Thus, this mechanism is robust with respect to changes in the magnetic field. Transversal anisotropy in the four-fold

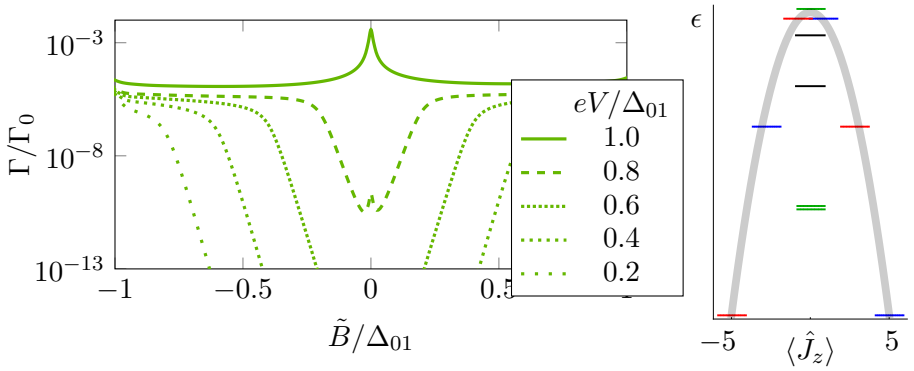

FIGURE 4.7: Switching rate for a spin with $J = 5$ in a four-fold symmetric system as a function of external magnetic field $\tilde{B}$. The separate lines denote different voltages eV. The level scheme on the right side shows that transitions between states of the $s = +$ and $s = -$ subgroup can not be induced by a single electron. Transitions through the green and black short cuts lead to an increased switching rate at vanishing magnetic field if excitations occur.

symmetric system mixes every fourth $|m\rangle$ state. That means the states $|m\rangle$ and $|m'\rangle$ contributing to each ground state are at least $|m - m'| \geq 2$ apart if the spin J is an integer. Only higher order coherent tunneling can induce direct transitions between the ground states but is suppressed by $|v_S|^4$ in the weak coupling limit.

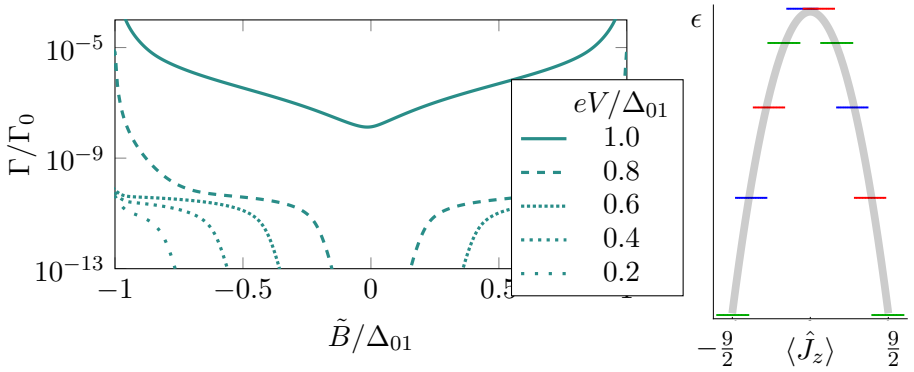

FIGURE 4.8: Switching rate for a spin with $J = 9/2$ in a three-fold symmetric system as a function of external magnetic field $\tilde{B}$. The separate lines denote different voltages eV. The level scheme on the right side shows that the ground states belong to the same subgroup. Short cuts, single electron induced switching and ground state splitting are absent.

An even more robust protection against higher order tunneling can be found in the three-fold symmetric system for half integer spins if the numerator of the spin quantum number is an integer multiplet of three. There is no tunnel splitting for half integer spins in a time reversal symmetric system due to Kramers theorem [92;98].

This means there is no tunnel splitting between the two states with the same absolute magnetic moment, even if they are from the same group of states. A short cut is thus forbidden in zero field by Kramers theorem. For comparison with the other protection mechanisms we choose a spin $J = 9/2$ that is close to the before mentioned $J = 5$. In figure 4.8 one can clearly see that no resonance of a short cut exists even for voltages above the first excitation energy. The energy levels in figure 4.8 show that direct transitions between the ground states can only occur from a process with $\hat{J}_{\pm}^{3}$, which is proportional to $|v_S|^6$ and thus very improbable in the weak coupling regime. This implies a robust protection mechanism with respect to changes in the magnetic field and to the energy of scattering electrons. To prevent a spin from switching one could also increase the size of the spin and thus diminish the quantum coherences. Tunneling through the barrier is then forbidden and the height of the barrier defines the robustness of the system against perturbations.

4.6 Resonant switching

The switching probability is enhanced when a short cut through the anisotropy barrier appears due to quantum tunneling transitions. This happens in general when two spin states are tunnel split due to the transversal anisotropy. Known as quantum tunneling of magnetization (QTM) this is well known for molecular magnets[155]. A magnetic field is used to shift the energy levels according to the Zeeman energy. Whenever the magnetic field shifts the energy levels towards the crossing point of two levels from the same group, the tunnel splitting leads to an avoided crossing. The resulting energy eigenstates possess a vanishing $\langle \hat{J}_z \rangle$ expectation value since they have an equal contribution of spin states on both sides of the barrier. Short cuts through the anisotropy barrier are formed by these states.

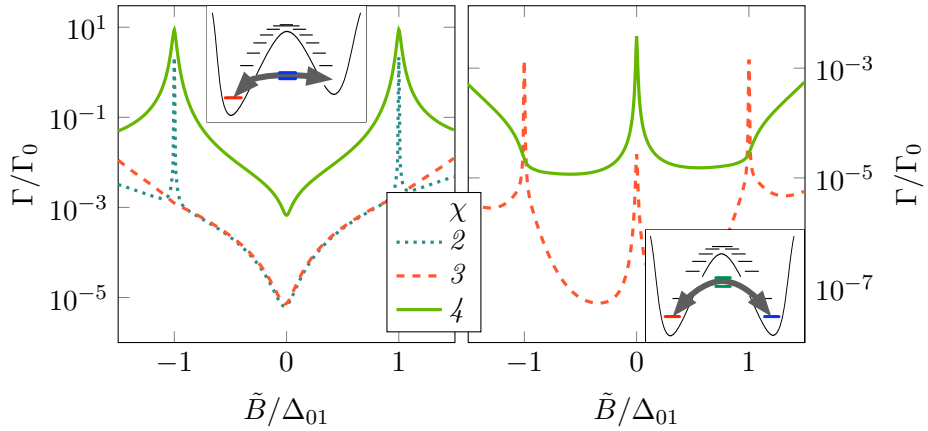

FIGURE 4.9: Switching rate against the magnetic field for different symmetries $\chi \in \{2, 3, 4\}$ for voltages above the first exication energy. (left) A spin $J = 5/2$ has no short cut resonance at zero field but shows a dependence of the resonance from quantum tunneling of magnetization (QTM - see inset) with respect to the symmetry. (right) A spin $J = 5$ has a central resonance from short cut tunneling (see inset) and allows to distinguish between the symmetries at the QTM resonance.

On the left side of figure 4.9 the switching rate is shown against the magnetic field for a spin $J = \frac{5}{2}$. Resonance peaks at $\tilde{B} = \Delta_{01}$ come from QTM. A broader peak can be observed for the four-fold symmetric system in contrast to the two-fold. The width is correlated with the level splitting that is caused by the transversal anisotropy. Larger splitting at the resonance point causes broader resonance peaks. The three-fold symmetric system shows QTM not until $\tilde{B} = 2\Delta_{01}$ since the corresponding spin states from the same group are further separated in energy. Certainly the absence of a resonance at the first level crossing point is determined by the spin quantum number.

A spin $J = 5$ for example would show QTM at $\tilde{B} = \Delta_{01}$ for the three-fold symmetric system, while it appears at higher magnetic fields for the four-fold symmetric system. The right hand side of figure 4.9 shows the switching rate for a spin $J = 5$ system. Besides QTM a central resonance can be seen for both symmetries. This is produced by tunnel split states at zero field. The situation is slightly different to the case of QTM. While for the quantum tunneling of magnetization a former ground state shows tunnel splitting with an excited state occurs and thus a fast relaxation channel is created, the zero field resonance results from tunnel splitting between two excited states. They create a short cut through the barrier. Since excited states need to be involved for the complete magnetization switching, either thermal or excitations due to a non-equilibrium situation are necessary to excess short cuts. From the presence or absence of resonance peaks one can draw conclusions to the spin or symmetry of the observed system. Similar to a spectrum the increased switching rate due to tunnel split states allows to resolve the features in the level structure that would otherwise be hidden.

4.7 Categorization of spin and symmetry combinations

We have shown that the switching rate of a single spin shows characteristics that are unique for the total spin quantum number J as well as the symmetry of the system. The presence of two ground states with opposite magnetic orientation is a key requirement for magnetization switching. Thus we exclude from our consideration those systems in which **g**round **s**tate **s**plitting (**GSS**) is caused by the transversal anisotropy. The lowest two energy states are tunnel split if J and $2J/\chi$ are both integers. Excluding this set of spins for each symmetry we can now focus on the presence of **s**ingle **e**lectron induced **s**witching (**SES**) between the double degenerate ground states. Previously we showed examples of two different mechanisms that protect the spin from switching. The first one, that has been reported in the publication of Miyamachi *et al.*[118], is a consequence of time reversal symmetry breaking by a spin flip with a conduction electron while the single spin Hamiltonian is invariant under time reversal. We therefore call this **p**rotection under **t**ime reversal symmetry (**PT**). The second protection mechanism, which is present even with magnetic field, is a consequence of total spin conservation during the scattering of the conduction electron with the spin of the adatom. We therefore call this **p**rotection due to **s**pin conservation (**PS**). In the following we introduce an alternative representation to visualize the PS mechanism. The total Hamiltonian $\hat{H} = \hat{H}_\chi + \hat{H}_t + \hat{H}_T + \hat{H}_S$ needs to be invariant under a rotation that is consistent with the rotation symmetry of the substrate. This is equivalent to translation symmetries in crystal structures. Since our system is reduced to the spin degree of freedom, we can introduce a rotation operator $R_\chi(\hat{S}_z) := e^{-i(2\pi/\chi)(\hat{S}_z/\hbar)}$ that performs a rotation of the coordinate system in spin space. Therefore, the total Hamiltonian must be invariant under a rotation of the coordinate system, that is consistent with the crystal symmetry. Thus, the commutator

$$[H, e^{-i\frac{2\pi}{\chi}(\hat{J}_z/\hbar+\hat{\sigma}_z)}] = 0 \tag{4.31}$$

must vanish, while a rotation around the z-axis is considered for the single spin and the spin of the conduction electrons. The single spin Hamiltonian itself must obey the commutator relation $[\hat{H}_\chi, R_\chi(\hat{J}_z)] = 0$, without specifying its representation in spin operators. Hence, eigenstates $|\phi\rangle$ of $\hat{H}_\chi$

$$R_\chi(\hat{J}_z)|\phi\rangle = e^{-i\frac{2\pi}{\chi}(\hat{J}_z/\hbar)}|\varphi, x\rangle = e^{i\varphi}|\varphi, x\rangle \tag{4.32}$$

can be labeled by the phase of the eigenvalues $z = e^{i\varphi}$. Distinguishing the energy eigenstates by a phase φ is equivalent to the previously used color coding or the

classification into groups by the label s. The other part of the wave function x specifies the state within this group. In figure 4.10 the χ possible eigenvalues z for each substrate symmetry, including the six-fold symmetry C_6, are shown in the complex plane. All eigenvalues z have the same absolute value, while adjacent states posses a phase difference of $2\pi/\chi$. Now total spin conservation during scattering with the conduction electron, which appears due to the commutator $[\hat{H}_t, \hat{J}_z + \hat{\sigma}_z] = 0$, also dictates the conservation of the total phase $i\varphi - i(2\pi/\chi)\sigma_z$. This can be shown by the matrix element

$$\begin{aligned} 0 &= \langle\varphi', x'|\langle\sigma_z'|\hat{H}_t R_\chi(\hat{J}_z)R_\chi(\hat{\sigma}_z) - R_\chi(\hat{J}_z)R_\chi(\hat{\sigma}_z)\hat{H}_t|\sigma_z\rangle|\varphi, x\rangle \\ &= \langle\varphi', x'|\langle\sigma_z'|\hat{H}_t|\sigma_z\rangle|\varphi, x\rangle \left(e^{i\varphi - i(2\pi/\chi)\sigma_z} - e^{i\varphi' - i(2\pi/\chi)\sigma_z'}\right) \\ &= \langle\varphi', x'|\langle\sigma_z'|\hat{H}_t|\sigma_z\rangle|\varphi, x\rangle e^{i\varphi - i(2\pi/\chi)\sigma_z}\left(1 - e^{i(\varphi'-\varphi) - i(2\pi/\chi)(\sigma_z' - \sigma_z)}\right) \end{aligned} \tag{4.33}$$

where the unitarity of the rotation was utilized. Thus, a conduction electron that reverses its spin from $|\pm 1/2\rangle$ to $|\mp 1/2\rangle$, which is related to the Pauli matrix $\hat{\sigma}_\mp$, changes its phase by $\pm 2\pi/\chi$. Therefore, only adjacent eigenstates of $\hat{H}_\chi$, meaning a phase difference of $|\varphi - \varphi'| = 2\pi/\chi$, can exhibit single electron induced switching. This is shown in figure 4.10.

For example in a three-fold symmetric system with $J = 3(2n+1)/2$ both ground states have the same phase. Thus an interaction with at least two electrons is needed to exhibit single electron induced ground state switching. In a four-fold symmetric system with $J = 2n + 1$ also two electrons are needed since the phase difference is $4\pi/\chi$. Both are examples for PS. In the following table we summarize our results for all combinations of rotation symmetry C_χ and spin J.

χ	**GSS**	**SES**	**PT**	**PS**
C_2	$\{n\}$	$\{\frac{2n+1}{2}\}$	$\{n\}$	$\{\}$
C_3	$\{3n\}$	$\{\frac{2n+1}{2}\} \setminus \{\frac{3(2n+1)}{2}\}$	$\{n\}$	$\{\frac{3(2n+1)}{2}\}$
C_4	$\{2n\}$	$\{\frac{2n+1}{2}\}$	$\{n\}$	$\{2n+1\}$
C_6	$\{6n\}$	$\{\frac{2n+1}{2}\} \setminus \{\frac{3(2n+1)}{2}\}$	$\{n\}$	$(\{n\} \setminus \{6n\}) \cup \left(\{\frac{3(2n+1)}{2}\}\right)$

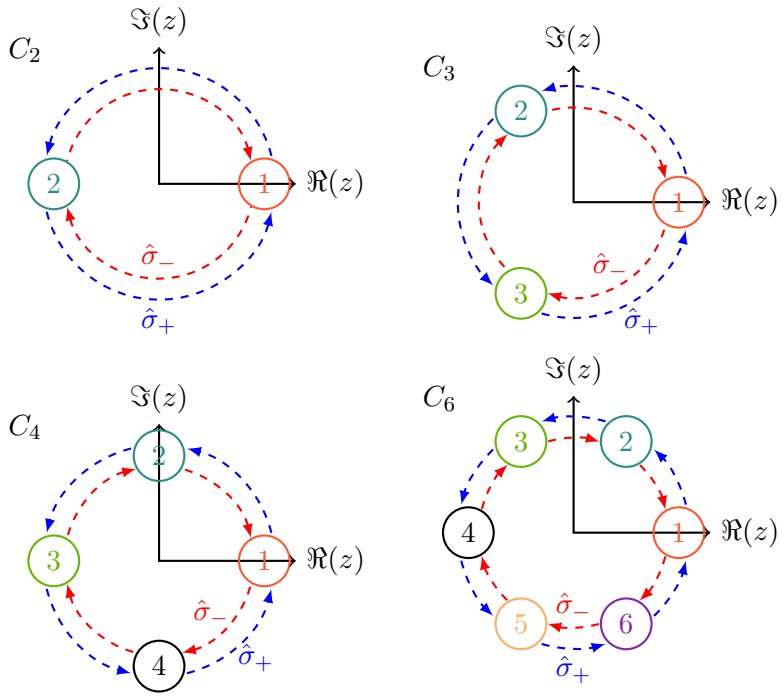

FIGURE 4.10: Phase representation of energy eigenstates with respect to the eigenvalue z of the spin rotation $e^{-(2\pi/\chi)(\hat{J}_z/\hbar)}$. The arrows indicate transitions that are related to the Pauli matrix $\hat{\sigma}_\pm$.

Classical magnetization reversal 5

Magnetization reversal has extensively been studied with fully- or semiclassical approaches. Since the master equation is derived from a quantum mechanical model, we want to point out its connection to classical descriptions.

5.1 Anisotropy potential

In the previous chapters the transversal anisotropy was treated as a small perturbation that barely changes the energy landscape the spin experiences from the dominating uniaxial anisotropy. Each part of the crystal field, represented by the Stevens operators O_p^m, creates an energy landscape that favors specific orientations of the spin. We use the rotation operator $D(\theta,\phi) := exp\left(-i\phi\frac{\mathbf{e_z}\vec{J}}{\hbar}\right) exp\left(-i\theta\frac{\mathbf{e_x}\vec{J}}{\hbar}\right)$ to probe the energy landscape for different orientations of a spin on the Bloch sphere defined by the azimuthal ϕ and polar angle θ. Figure 5.1 visualizes the energy of a spin pointing in a specific spacial direction interacting with a field represented by the Stevens operator O_p^m.

The energy, given by an expectation value $\langle D(\theta,\phi)O_p^m D^{-1}(\theta,\phi)\rangle$, is represented by the distance between the origin and the surface point in the direction defined by θ and ϕ. The color denotes the sign, red means positive and blue negative energy. As a reference we start with a magnetic field that is parallel to the z-axis of our coordinate system. Due to the Zeeman term $\frac{g\mu_B}{\hbar}\vec{B}\vec{J}$ a spin tends to point into the opposite direction of the local magnetic field. The energy expectation value is thus minimal for a polarized state $|-J\rangle$ and maximal for the opposite direction $|J\rangle$. A spin state in the x-y-plane is not energetically effected. The transversal anisotropy

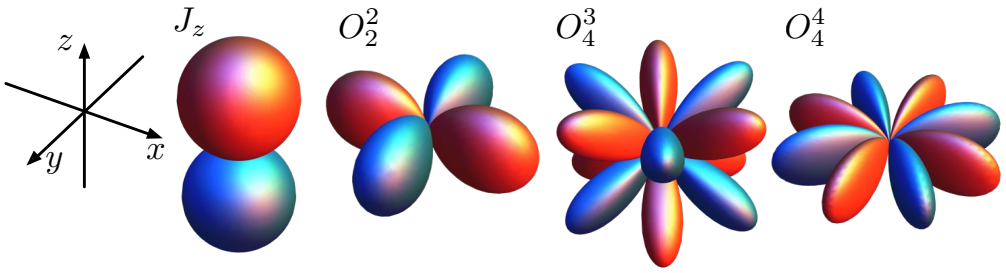

Figure 5.1: Field representation of the Stevens operator O_p^m in cartesian coordinates. The field is probed by rotating a spin in any direction and taking the energy expectation value $\langle D(\theta,\phi)O_p^m D^{-1}(\theta,\phi)\rangle$.

fields, that are related to the operators O_2^2, O_4^3 and O_4^4, reproduce the same rotational symmetry as the crystal substrate they originate from. The potential created by O_4^3 even energetically favors spins that are pointing out of the x-y-plane. The uniaxial anisotropy O_2^0 is rotational symmetric around the z-axis. With $D < 0$ both polarized spin states $|\pm J\rangle$ represent the ground states since they maximally align with the easy axis of the anisotropy potential. This is shown in figure 5.2.

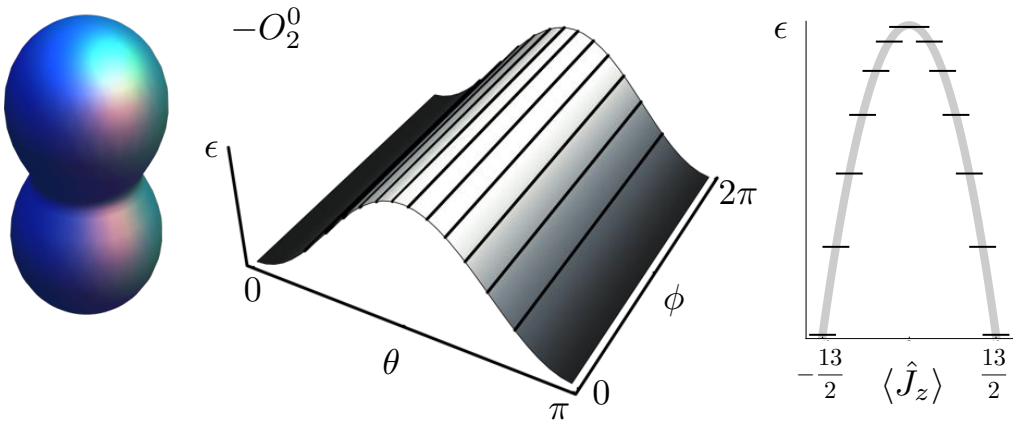

Figure 5.2: Visualization of uniaxial anisotropy. Anisotropy potential plotted in three dimensional cartesian coordinates (left) as in figure 5.1. (center) Potential landscape in spherical coordinates with polar θ and azimuthal angle ϕ. The energy expectation values of a $J = 13/2$ spin are displayed as contour lines. (right) Energy eigenvalues with respect to the expectation value $\langle \hat{J}_z \rangle$ for $J = 13/2$.

Any orientation perpendicular to this axis costs energy. This creates the often stated anisotropy barrier that needs to be exceeded to change the spin from $|\pm J\rangle$ to $|\mp J\rangle$. Since the field is rotational symmetric, the barrier is of same height

in every direction. One can therefore map the three dimensional representation of the barrier onto the previously used representation that displays the energy eigenvalues with respect to the $\hat{J}_z$ expectation value. This reduced two dimensional representation can be misleading, when the rotational symmetry is broken by a transversal anisotropy field. The operator O_2^2 creates a biaxial anisotropy in the x-y-plane and thus breaks the rotational symmetry. Combined with the uniaxial anisotropy, the energy landscape is shown in figure 5.3.

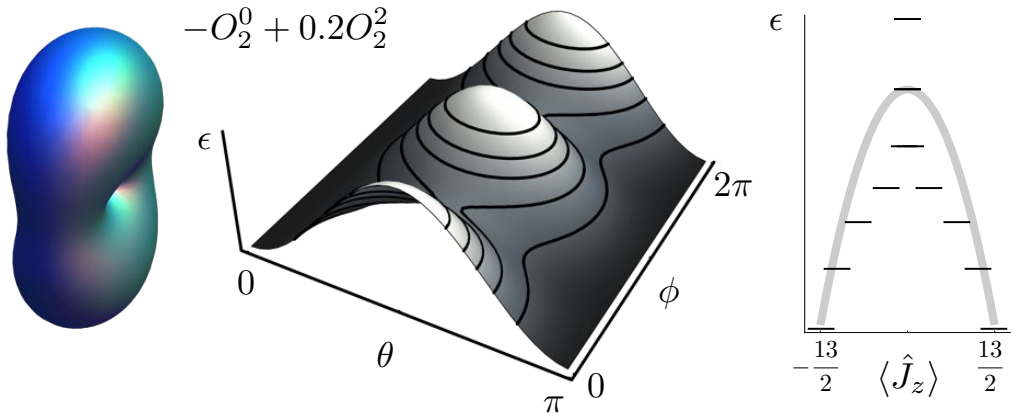

FIGURE 5.3: Mixed anisotropy given by $-O_2^0 + 0.2O_2^2$. The mixed anisotropy potential shown in a three dimensional cartesian coordinates (left) as in figure 5.1 has no continuos rotational symmetry around the z-axis. (center) Potential landscape in spherical coordinates denoting saddle points at polar angle $\theta = \pi/2$ and azimuthal angles $\phi \in \{\pi/2, 3\pi/2\}$. The energy expectation values of a $J = 13/2$ spin are displayed as contour lines. (right) Energy eigenvalues with respect to the expectation value $\langle \hat{J}_z \rangle$ for $J = 13/2$.

The height of the barrier now depends on the azimuthal angle ϕ and is reduced at the saddle points shown in figure 5.3. Since saddle points can not be resolved in the two dimensional representation of the level scheme, the barrier height could be mistaken with the largest energy difference. Certainly this is just a problem of interpretation. The master equation very well includes switching via the saddle points since transitions occur between energy eigenstates. In figure 5.2 and 5.3 the discrete energies of the spin are marked by contours on the anisotropy potential. Hence, switching from one potential minimum to the other is mediated via states that are intermediate in energy and are close to the saddle point. In contrast to the previously elucidated resonant switching, which is of quantum nature, the surmounting of an energy barrier has a classical character. Thus in the following we compare the results of our master equation with the switching of a classical magnetic moment.

5.2 Superparamagnetic relaxation

Brown[30] adapted the idea of Kramer's escape rate of a particle over a barrier onto the classical concept of a single-domain magnetic particle exposed to thermal agitation. The interaction with a heat bath results in fluctuations and dissipation that can reverse the orientation of the magnetic moment even if it is stabilized by an anisotropy field. This reversal is known as Néel-Brown relaxation and the characteristic time is referred to superparamagnetic relaxation time. Its inverse is equivalent to the switching rate Γ between the orientations of the magnet with minimal energy. Brown derived from the phenomenological Gilbert equation[67] a Fokker-Planck equation. It describes the evolution of a distribution function $\rho(\theta, \phi, t)$ for the magnetic moment on a Bloch sphere

$$\frac{d}{dt}\rho(\theta, \phi, t) = L_{\mathrm{FP}}\rho(\theta, \phi, t). \tag{5.1}$$

Since the absolute value of the magnetic moment is constant, only the polar θ and azimuthal angle ϕ appear. The relaxation time can now be numerically determined by discretizing the Fokker-Planck operator L_{FP} and taking its smallest non vanishing eigenvalue. This method of lowest eigenvalue is commonly used[75] and equivalent to the one we utilized for the master equation. The similarities are even clearer when formulating the Focker-Planck equation in energy representation. In the limit of fast equilibration on the orbits of constant energy, namely the Stoner-Wohlfarth orbits[174], energy and time are the remaining free variables. Consequently the Fokker-Planck equation and the master equation are of the same form[34], which can be solved numerically. Analytic solutions for the relaxation time highly depend on the symmetry of the anisotropy potential. When Brown investigated thermal fluctuations of a single-domain particle he considered axial symmetric potentials. Hence, in the Fokker-Planck equation, the differential equations for polar and azimuthal angular motion decouple. Analytic expressions were found for mixed anisotropy potentials that provide no continuos rotational symmetry[36;41]. Apalkov and Vischer[3] used a potential of the form $V(\vec{M}) = -h_z M_z^2 + h_y M_y$ with M being the magnetic moment of a classical spin. This is equivalent to the potential described by the Hamilton operator

$$\begin{aligned} \hat{H}_2 &= D\hat{J}_z^2 + E(\hat{J}_+^2 + \hat{J}_-^2) \\ &= D\hat{J}_z^2 + 2E(\hat{J}_x^2 - \hat{J}_y^2) \end{aligned} \tag{5.2}$$

when applying a rotation around the x-axis such that $z \to y$ and $y \to -z$. Substituting $D = 1/2(h_z - h_y)$ and $2E = -1/2(h_z + h_x)$ the Hamiltonian can be brought to the form Apalkov and Visher used. Within the Arrhenius-Néel limit, meaning a high barrier compared to the temperature, the authors found an analytic expression for the dwell time

$$\tau = \omega e^{-\frac{E_b}{k_B T}} \tag{5.3}$$

in one of the potential minima that includes the azimuthal angle $\theta = 0$ or π respectively. E_b denotes the barrier height at the saddle point and the constant ω is known from the Arrhenus law as attempt frequency. Remember the switching rate is inverse proportional to the dwell time $\Gamma \propto 1/\tau$ thus we can compare the results of the master equation with the analytic expression from a classical theory. We want to show the potential of the master equation to describe equally magnetization switching in the quantum and the classical regime. The Hamiltonian of equation 5.2 describes an anisotropy potential used in classical systems that provides transversal anisotropy [27;127]. Exemplarily we choose a sufficiently large spin of $J = 13/2$ which still allows to detect single electron induced ground state switching.

Only a single electron bath, namely the unpolarized substrate is coupled to the spin $\vec{J}$. Thus, only thermal excitations occur. In figure 5.4 the change of the switching rate with the temperature is shown for different values of transversal anisotropy. For small temperatures $k_b T < 10^{-1}\Delta_{01}$ only thermally induced direct transitions between the ground states occur. In this region the linearity in the temperature, magnified in figure 5.4 (b), is a result of the direct rate in equation 4.29. The slope is proportional to $\langle \phi_0^{\pm} | \hat{J}_{\pm} | \phi_0^{\mp} \rangle \propto (E/D)^{(2J-1)/\chi}$ and slowly changes with transversal anisotropy because of the large spin J. In general with decreasing transversal anisotropy, the direct transition becomes less probable until they vanish for $E = 0$. Deviations from the constant slope occur for $k_b T \approx 0.1$ when temperature induced excitations become relevant. This also means that the system enters the region in which it starts to behave classically, meaning excitations across the barrier are more common. This is similar to the case in figure 4.4 when the voltage leads to subsequent excitations that allow to surmount the barrier. For temperatures $k_b T > 10^{-1}\Delta_{01}$ the switching rate in figure 5.4 (c) clearly follows an Arrhenius law shown in equation 5.3. A semilogarithmic plot of the rate against the inverse temperature allows to determine the barrier height E_b that is expected from a classical system. From the results of the master equation we extrapolated the exponent in the classical regime and compared it in figure 5.4 (d) with the actual saddle point and maximum of the anisotropy

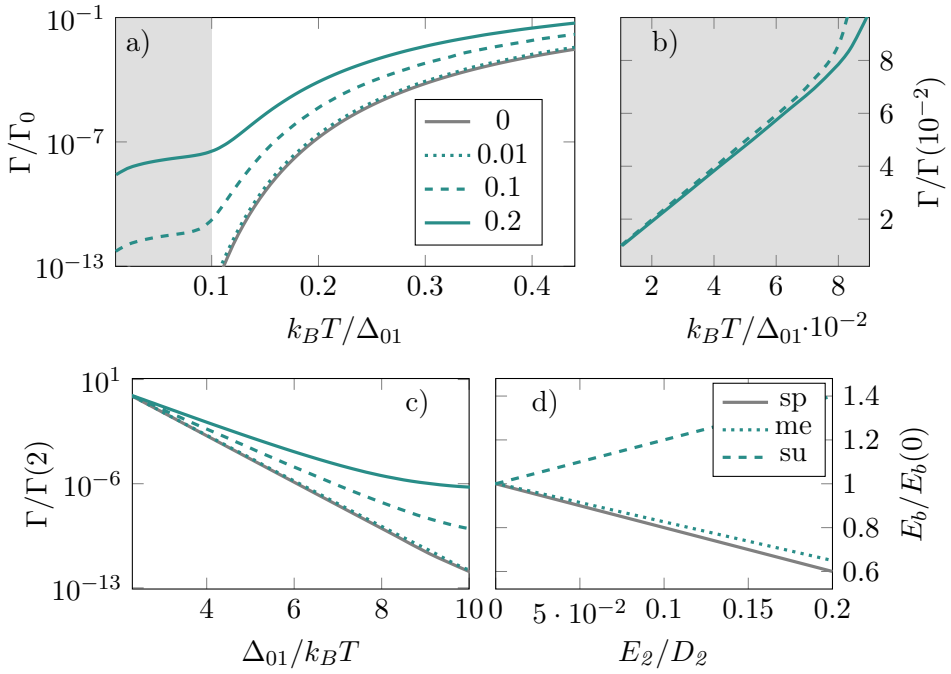

Figure 5.4: (a) Switching rate for a spin $J = 13/2$ experiencing an anisotropy potential with $E/D \in \{0, 0.01, 0.1, 0.2\}$. The spin is solely coupled to the substrate electrons. (b) Low temperature region $k_bT < 10^{-1}\Delta_{01}$ is magnified at which the single electron induced transitions dominate. The rates are normalized to the value at $k_bT = 10^{-2}\Delta_{01}$. (c) Switching rate, as expected for classical system, following the Arrhenus law. The rates are normalized to the value at $1/k_bT = 2/\Delta_{01}$. (d) Saddle point energy (sp), maximal energy of anisotropy potential (su) and energy barrier determined from master equation (me) is shown with respect to the transversal anisotropy.

potential that is expected with transversal anisotropy. The master equation gives a barrier height close to the saddle point energy, which means most switching paths are taken through the saddle point. This is a purely classical behavior that was derived from the master equation.

5.3 Classical limit of master equation

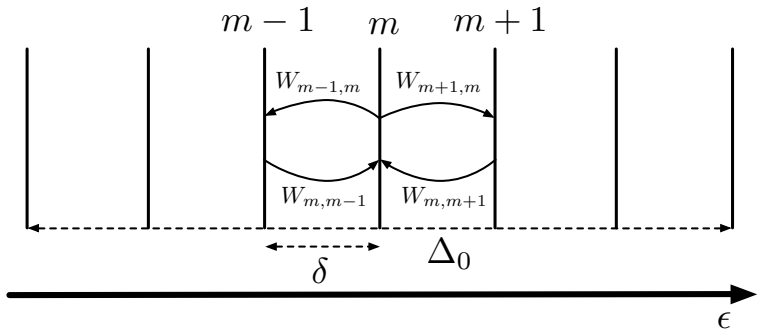

FIGURE 5.5: Scheme for master equation with rates W between adjacent states labeled wit m. The spin states are assumed to be separated equally in energy by a magnetic field. The maximal energy difference is given by Δ_0 and the minimal by δ.

The derivation of the master equation started from a quantum mechanical description of the system. In consequence of just considering rates between energy eigenstates, the rate equation gets the character of a classical equation of motion. Previously we showed that especially a large spin exhibits classical behavior. Thus, we will show for a simple system the derivation of the Fokker-Planck equation from the master equation. For simplicity we start with the Fokker-Planck equation that describes the time evolution of a probability distribution in terms of statistical mechanics. The distribution $\rho(E,t)$ evolves in time according to a probability current, which conserves the total probability. Thus the Fokker-Planck equation can be written in energy space

$$\frac{d\rho}{dt} = \frac{d^2}{dE^2}A\rho + \frac{d}{dE}B\rho \tag{5.4}$$

where A and B are time independent functions of the energy E. Creating a grid of finite differences allows to discretize the derivatives

$$\frac{d\rho_m}{dt} = \left(\frac{A_{m-1}}{\delta^2} - \frac{B_{m-1}}{2\delta}\right)\rho_{m-1} - \frac{2A_m}{\delta^2}\rho_m + \left(\frac{A_{m+1}}{\delta^2} + \frac{B_{m+1}}{2\delta}\right)\rho_{m+1} \tag{5.5}$$

with m finite elements. In this form the Fokker-Planck equation is equal to the master equation for

$$A_m = \frac{\delta^2}{2}\left(W_{m-1,m} + W_{m+1,m}\right) \tag{5.6}$$

$$B_m = \delta\left(W_{m-1,m} - W_{m+1,m}\right) \tag{5.7}$$

where $W_{i,j}$ are rates. For simplicity we consider a system in which only rates between adjacent energy eigenstates exist as depicted in figure 5.5. Explicitly we consider a spin that is exposed to a magnetic field, which sets the quantization axis. Degeneracy between spin states $|m\rangle$ is lifted by the Zeeman energy. The maximal splitting between spin states $|-S\rangle$ and $|S\rangle$ is $\Delta_0 := 2\tilde{B}S$, which denotes the energy scale. Zeeman splitting between adjacent energy states is then given by $\delta_m^{\pm} := (\epsilon_{m\pm1} - \epsilon_m)/\Delta_0 = \pm\delta$. When coupling the spin to an unpolarized electron bath, such as the previously used substrate, only transitions between spin states with $|m' - m| = 1$ are allowed. The rates

$$W_{m\pm1,m} = \alpha\Sigma_{m+1,m}\zeta(\delta_m^{\pm}) \tag{5.8}$$

consist of three parts. The first part $\alpha = \pi|v|^4\rho_{\downarrow}\rho_{\uparrow}\hbar^2$ holds the units while $\Sigma_{m+1,m} = |\langle m\pm1|\hat{J}_{\pm}|m\rangle|^2/\hbar^2$ is the spectral weight and $\zeta(\delta_m^{\pm}) = -\tilde{T}\frac{\delta_m^{\pm}}{\tilde{T}}/(1-e^{\frac{\delta_m^{\pm}}{\tilde{T}}})$ is the energy dependency, which we expand for large temperatures $\tilde{T} = k_bT/\Delta_0$ compared to the level spacing. We also replace the magnetic quantum number by the energy $E := \epsilon_m/\Delta_0 = m/2S$. The classical limit is specified by increasing the spin $S \to \infty$ and thus decreasing the level spitting $\delta = \frac{1}{2S} \to 0$ while keeping the energy Δ_0 constant. In the classical limit

$$A_m \quad \to \quad A(E) = \frac{\alpha}{4}(1-4E^2)\tilde{T} \tag{5.9}$$

$$B_m \quad \to \quad B(E) = -\alpha\left[\frac{1}{4}(1-4E^2) - 2E\tilde{T}\right] \tag{5.10}$$

we can replace the discrete values A_m and B_m by functions depending on energy. $A(E)$ denotes the substrate induced diffusion $\frac{\alpha}{4}(1-4E^2)\tilde{T}$, which is in agreement with the fluctuation-dissipation theorem[169] linear in temperature. The drift $\alpha\left[\frac{1}{4}(1-4E^2) - 2E\tilde{T}\right]$ is given by the function $B(E)$. The stationary solution of the Fokker-Planck equation, with the drift and diffusion derived from the master equation, is a Boltzmann distribution. This is what one would expect, since the coupling to the substrate leads to equilibration. We thus showed the derivation of the classical Fokker-Planck equation from a quantum mechanical master equation approach.

Conclusion 6

6.1 Summary

This thesis was conducted for the purpose of investigating the dynamic and static properties of a correlated system consisting of a single magnetic moment, which is exchange coupled to itinerant electrons. In the first part of this work we focused on the exchange interaction between a localized spin and a single itinerant electron. We introduce a model that takes into account the extended nature of the localized spin. From the time evolution of a spin associated Gaussian wave package, representing the itinerant electron, we can observe the exchange of momentum. We found that the amount of exchanged momentum depends on the mean kinetic energy of the moving electron and is thus related to the time it spends within the interaction region.

In chapter 3 we develop a scattering formalism to gain further insight into the dependence on kinetic energy and see the effect on the conduction properties of the itinerant electron. The scattering formalism, which is based on the T-matrix approach, is presented in a simple representation and allows to obtain solutions beyond Born approximation. We derived the relations between the T-matrix and scattering amplitudes, as well as the T-matrix and the scattered wave function. We presented an analytic solution for the contact form of the exchange interaction by making use of the delta distribution properties. The numerically exact solution of the T-matrix for an exchange interaction with arbitrary shape was obtained by Gaussian quadrature in combination with a discretized momentum representation [8]. We find multiple resonances in the transmission of an electron at small momentum for a Gaussian shaped exchange interaction with varying maximum value. The appearance

of these resonances is explained by transitions from bound states to continuum states for an attractive potential. The itinerant electron is subject to an attractive or repulsive potential, when it forms a singlet or triplet state with the local spin. In the antiparallel spin configuration of itinerant and local spin a momentum exchange during the scattering can be interpreted as a phase shift between the singlet and triplet part of the initial two particle spin state. This phase shift and the amount of exchanged spin highly depends on the maximum value of the exchange interaction and the kinetic energy of the incoming electron. We showed that an exchange region with finite width can lead to a full exchange of spin, meaning the orientation of the local spin is fully reversed, while a delta spin scatterer can only lead to a switching probability of 50%. Additionally we show that the switching probability of a spatially extended impurity leads to a constant switching probability within a certain range of kinetic energy for the itinerant spin. In this region a momentum independent exchange constant is justified. Further we show the spin density of the itinerant electron and explain occurring interference patterns with a spin barrier, that is created by interaction with the localized spin.

In chapter 4 we include the interaction of a single spin with a weakly coupled bath of electrons in terms of an Appelbaum Hamiltonian and incorporate a crystal and magnetic field. We demonstrated in our publication [89] that the derived non-equilibrium master equation approach is suitable to describe electron induced magnetization dynamics of a ferromagnetic cluster with a few atoms in a spin polarized scanning tunneling microscope. In a second publication [84] we applied the same formalism to investigate crystal symmetry effects on the magnetization reversal of a single spin. We determine the time for a full reversal by calculating the switching rate from a master equation. In this thesis we explain the concept of taking into account crystal field symmetries in the resulting anisotropic spin Hamiltonian for a single magnetic adatom. Spin operators, the so called Stevens operators, are used to represent the crystal field and can be written in a convenient way for magnetic rare earth adatoms, that create a total magnetic moment due to the strong spin orbit coupling. We assumed the uniaxial anisotropy to be dominant while creating an anisotropy barrier that separates the two spin ground states with opposite magnetic orientation. For various symmetries we point out the appearance of electron induced direct transitions between the two ground states that result in a finite switching rate even if inelastic excitations, mandatory to surmount the barrier, are exponentially suppressed. Following the example of Miyamachi et al. [118] we studied symmetry caused protection agains single electron induced ground state transitions and the

stability of this protection against breaking of time reversal symmetry with a magnetic field. We demonstrate that the protection mechanism is a direct result of a fundamental commutator relation and rapidly breaks down in presence of a magnetic field. Additionally we propose combinations of spin and crystal symmetry that are protected even in the presence of a magnetic field and relate this to the conservation of total spin during the scattering with a tunneling electron. An alternative representation is presented in this work, which allows to predict in a simple way the occurrence of a protection mechanism in a system with any spin or rotation symmetry. Finally we elaborate the concept of short cut tunneling and quantum tunneling of magnetization, which create resonances in the switching rate and are of mere quantum mechanical origin. We suggest that these resonances can be used to determine the spin and symmetry from experimental measurements.

The last chapter elaborates the relation between the quantum mechanical approach of a master equation and the classical or semiclassical approach of a Fokker-Planck equation, as we did in our recent publication[34]. In this thesis we show quantum mechanical and classical behavior in the temperature induced magnetization reversal, also known as superparamagnetic relaxation. While at low temperatures the switching mainly appears due to single electron induced switching, which is a quantum effect, at high temperatures the switching rate follows an Arrhenius law. In this classical regime we were able to determine from the master equation that all switching paths go over a saddle point in the anisotropy potential that is created by transversal anisotropy. To demonstrate the equivalence of the quantum and classical approach in the classical limit, we derived from the master equation a Fokker-Plack equation. This allows to determine the diffusion and drift from a quantum mechanical model.

6.2 Outlook

Beside the historical background we elaborated in the introduction and our own contribution to the topic of electron induced magnetization dynamics, we also want to point out possible future research activities. For example the scattering formalism, introduced in chapter 3, could be extended to describe quasi two dimensional systems[8], such as magnetic impurities in between a quantum point contact. Also the time dependent scattering[158] or the inclusion of oszillating electric and magnetic fields is possible[162] to investigate real time dynamics in transport with the T-matrix approach.

The currently more popular topic of magnetic adatoms on metallic substrates has been subject to many recent publications and creates a large amount of open questions and research topics. Especially the symmetry caused protection was discussed recently. Substrates with a high degree of rotational symmetry, such as graphene, are promising candidates to find symmetry caused protection. The magnetic moment of a few transition-metal adatoms on graphene was already calculated [32;49;170] but little is known about the anisotropy potential. We think Mn on graphene is a good candidate to be protected against single electron switching, if two minima are created by the uniaxial anisotropy.

We also suggest to further investigate rare earth elements, which provide a large total spin [50]. Still, the relevance of orbital momentum and spin of the adatom for the spin dependent transport is not clear yet. Same applies for the role of magnetic orbitals that form underneath the adatom within the substrate. Also, the question arrises, if a symmetry caused protection mechanism would sustain in proximity of a magnetic tip with arbitrary magnetization direction, that was studied in a simple system by Frahm [58], who takes into account the full quantum master equation.

Together with the authors Karlewski et al. [87] we strongly emphasize to study experimentally the magnetic field dependency of symmetry protected systems and also the closing of short cuts in the anisotropy barrier due to increased scattering with tunneling electrons. Similar findings from Delgado et al. [45] and Yan et al. [178] demonstrate the relevance of substrate and tip induced energy renormalization. The impact of symmetries in higher order terms of the perturbation expansion and thus the relevance for Kondo physics [125;156] is also unknown. Important for this is the connection between the symmetry and the tunnel current as well as the current noise [10]. For example, a signal from quantum tunneling of magnetization only appears in the current for a spin polarized tip [115]. Therefore it would be interesting to systematically investigate the effects of symmetry protection or short cut tunneling onto the conductivity. Dubout et al. [51] already demonstrated that the spin and symmetry can be determined from the differential conductance, similar to our suggestion in chapter 4. But also other advances in experimental techniques allow to characterize the system by mapping the three dimensional anisotropy potential [179]. Also, light field induced spin manipulation of the adatom [180] and pump probe scanning tunneling microscopy [178] on the nano second time scale present great tools for further investigation of spin dynamics.

Todays experiments also allow to have control over many properties of the studied system. For example, the spin of a complex, composed of a single or few atoms on

a substrate, can be adjusted by hydrogen absorption[51]. Likewise, the anisotropy can be modified by positioning magnetic atoms in the neighborhood[31]. Thus, more complex systems, like spin chains[64] or logic structures[91], could be studied further and represent an interesting set-up for a theoretical investigation of more sophisticated correlated spin systems.

6.3 Danksagungen

Ich möchte an dieser Stelle die Chance nutzen mich bei einigen Personen zu bedanken, die mich während meiner Doktorarbeit begleitet haben.

An erster Stelle steht Prof. Dr. Daniela Pfannkuche, die meinen Werdegang als Physiker vom ersten Tag meines Studiums bis zum jetzigen Zeitpunkt verfolgt hat. Ich bin sehr dankbar dafür, dass sie mir immer mit Rat beiseite stand und mir stets großes Vertrauen schenkte. Somit konnte ich mich mit vielen Themen frei beschäftigen, die dann auch stets einer schweren Probe unterzogen wurden. Auch diese Erfahrungen möchte ich nicht missen. Von Danielas Kochkünsten bei unseren Weihnachtsessen schwärme ich noch immer.

Auch den weiteren Mitgliedern unserer Gruppe, wie Alexander Chudnovskiy, Daniel Becker, Eva-Maria Richter, Holger Niehus, Ole Berg, Marta Prada und Simon Leiß, danke ich für die spannende gemeinsame Zeit. Ganz besonders hervorheben, möchte ich dabei meine Bürokollegen Benjamin Baxevanis, Lars-Hendrik Frahm und Maximilian Hollstein. Diskussionen mit ihnen habe ich immer sehr zu schätzen gewusst und bin der Überzeugung, dass wir ein gutes Team gebildet haben. Besonders Benjamin möchte ich dafür danken, dass er mir Anstöße in vielen Bereichen gegeben hat.

Bei Dr. Katrin Buth und bei Prof. Dr. Ulrich Merkt möchte ich mich für die Leitung des Graduiertenkollegs 1286 und bei Prof. Dr. Klaus Sengstock für die des Sonderforschungsbereiches 925 bedanken.

Des Weiteren möchte ich mich bei Prof. Dr. Vidar Gudmundsson für die Übernahme des Zweitgutachten bedanken und dass er mich in Island so herzlich empfangen hat. Er hat mir nicht nur bei dem Thema des Streuformalismus geholfen, sondern mir auch gezeigt, wie man durch Magnetfeldsensoren Nordlichter beobachten kann ohne in den Himmel zu schauen. Zugleich danke ich auch Prof. Dr. Andrei Manolescu, dass er meinen Aufenthalt in Island zu einem spannenden und unvergesslichen Erlebnis gemacht hat. Stets habe ich mich über Diskussionen mit ihm gefreut und empfand sein generelles Interesse, sowohl an Physik als auch anderen Themengebieten, immer sehr beeindrucken und erfrischend. Vielmehr möchte ich mich auch bei meinen isländischen Bürokollegen Abhishek Kumar, Ania Sitek, Einar Jon Erlingsson, Gunnar Thorgilsson, Kristinn Torfason, Lahcen Bouhlali, Maria Gudjonsdottir, Rauan Meirbekova und Thorsten Arnold bedanken, die mich gleich am ersten Tag freundlich empfangen haben.

Auch bedanken möchte ich mich bei meinen Kollegen aus der Experimentalphysik,

nämlich Alexander Ako Khajetoorians, Andreas Sonntag, Jens Wiebe, Manuel Steinbrecher, Sebastian Loth und Shichao Yan. Durch die enge Zusammenarbeit mit ihnen ist mir die betrachtete Physik noch einmal in einem ganz anderen Licht erschienen. Besonders Alexander danke ich, dass er mir stets neue interessante Forschungsthemen deutlich gemacht hat.

Prof. Dr. Gerd Schön und Prof. Dr. Wulf Wulfhekel möchte ich für ihre Gastfreundschaft am Karlsruher Institut für Technologie danken. Besonders die Gespräche während und nach der Arbeitszeit mit Christian Karlewski und Panagiotis Kotetes habe ich sehr genossen. Die gemeinsame und sich ergänzende Arbeit mit Christian war mir sehr wichtig und hat sehr viel Spaß gemacht.

Ein wichtiger Bestandteil eines jeden Arbeitstages war das gemeinsame Mittagessen in der Mensa. Ich möchte mich bei den noch nicht aufgezählten Mitgliedern unserer Essensgruppe bedanken, nämlich Alexander Hampel, Claas Abert, Michael Karolak, Raphael Richter und Theo Gerhardt. Die Gespräche bei Tisch haben mich immer schwer beeindruckt, vor allem wenn sich jemand als ein unerwarteter Experte offenbart hat. Michael möchte ich noch gesondert für das nicht einhalten des Eulenvertrages danken. Theo möchte ich auch noch einmal an dieser Stelle hervorheben. Wir haben zusammen unser gesamtes Studium bestritten, wofür ich mir keinen besseren Kollegen hätte vorstellen können.

Auch meinen anderen Kommilitonen wie Axel Frauen, Cornelius Bausch, Jens Ehlermann, Malte Weinberg und Michael Salz danke ich für die gemeinsame Zeit. Besonders Axel möchte ich dafür danken, dass er lange ein so guter Mitbewohner war und guter Freund ist. Axel, Jens und Fjorden: wir müssen mal wieder die Welt retten!

Auch meinen unzähligen Skateboardkollegen möchte ich danken, dass sie immer ein offenes Ohr für mich hatten und mir geholfen haben mal abzuschalten.

Der Familie Sato und Toriumi möchte ich dafür danken, dass sie mir meinen Aufenthalt in Japan ermöglichten und mich wie einen Sohn behandelt haben.

Besonders wichtig ist mir meine Freundin Alena Mohr. Sie hat mir in den letzten Monaten der Doktorarbeit Kraft gegeben und mich in allen Situationen unterstützt. Für den Rückhalt den ich in ihrer Familie bekommen habe bin ich auch sehr dankbar.

Zuletzt möchte ich mich bei meiner Familie bedanken. Ich danke allen meinen Verwandten dafür, dass sie immer so viel Interesse und Verständnis für meine Arbeit gezeigt haben. Meinem Bruder Andreas und seiner Verlobten Josefin danke ich für ihre Art. Mit ihnen konnte ich immer auf eine entspannte Weise alles diskutieren.

Der größte Dank gilt meinen Eltern. Sie haben mir und meinem Bruder alles

ermöglicht. Wir konnten uns frei, ohne Sorgen, entwickeln und mit dem beschäftigen was uns Freude macht. Dafür bin ich ihnen sehr dankbar.

Appendix 7

7.1 Appendix - Parameter used in figures

Figure 2.2 and 2.3:
$\Delta_c/\Delta_V = 0.1$; $k_0\Delta_V = 100$; $V_0/\left(\frac{\hbar^2 k_0^2}{2m}\right) = 9 \cdot 10^{-3}$

Figure 4.4:
$k_bT/\Delta_{01} = 10^{-2}$; $E_\chi/D_\chi = 10^{-3}$; $v_T/v_S = 0.15$; $\tilde{B}/D_\chi = 0$; $(\rho_\uparrow - \rho_\downarrow)/(\rho_\uparrow + \rho_\downarrow) = 0.1$

Figures 4.6, 4.7 and 4.8:
$k_bT/\Delta_{01} = 10^{-2}$; $E_\chi/D_\chi = 10^{-3}$; $v_T/v_S = 0.15$; $(\rho_\uparrow - \rho_\downarrow)/(\rho_\uparrow + \rho_\downarrow) = 0.1$

Figure 4.9:
$k_bT/\Delta_{01} = 10^{-2}$; $E_\chi/D_\chi = 10^{-3}$; $v_T/v_S = 0.15$; $(\rho_\uparrow - \rho_\downarrow)/(\rho_\uparrow + \rho_\downarrow) = 0.1$; $eV/\Delta_{01} = 1.5$

Figure 5.4:
$E_\chi/D_\chi = 10^{-3}$; $v_T/v_S = 0$; $eV/\Delta_{01} = 1.5$; $\tilde{B}/D_\chi = 0$;

7.2 Appendix - Discretization with Gaussian quadrature

In the following we elaborate a discretization scheme for the expression

$$\int_{-\infty}^{\infty} \frac{f(k)}{k_0^2 - k^2} dk, \tag{7.1}$$

that is based on Gaussian quadrature and was used for scattering approaches in multiple systems[7;8;70;71;158;161;162]. We begin by shifting the singularity into the

complex plane and utilizing the Sokhotski-Plemelj theorem

$$\begin{aligned} & \int_{-\infty}^{\infty} \frac{f(k)}{k_0^2 - k^2 + i\eta} dk \\ = \; & \mathcal{P} \int_{-\infty}^{\infty} \frac{f(k)}{k_0^2 - k^2} dk - i\pi \int_{-\infty}^{\infty} f(k)\delta(k_0^2 - k^2) dk. \end{aligned} \tag{7.2}$$

With the general relation $\delta(x^2 - \alpha^2) = \frac{1}{2|\alpha|}(\delta(x - \alpha) + \delta(x + \alpha))$ the integral, containing the delta distribution, can be solved.

$$= \mathcal{P} \int_{-\infty}^{\infty} \frac{f(k)}{k_0^2 - k^2} dk - \frac{i\pi}{2|k_0|}(f(k_0) + f(-k_0)) \tag{7.3}$$

Further, we make use of $\int_{-\infty}^{\infty} \frac{1}{k_0^2 - k^2} dk = 0$ for the principle value integral, thus we can add the vanishing integral $\int_{-\infty}^{\infty} \frac{f(\pm k_0)}{k_0^2 - k^2} = 0$, that vanished due to symmetry reasons and avoid the diverging points of the principle integral.

$$\begin{aligned} = \; & \int_0^{\infty} \frac{f(k) - f(k_0)}{k_0^2 - k^2} dk + \int_{-\infty}^{0} \frac{f(k) - f(-k_0)}{k_0^2 - k^2} dk - \frac{i\pi}{2|k_0|}(f(k_0) + f(-k_0)) \\ = \; & \int_0^{\infty} \frac{f(k) - f(k_0)}{k_0^2 - k^2} dk + \int_0^{\infty} \frac{f(-k) - f(-k_0)}{k_0^2 - k^2} dk - \frac{i\pi}{2|k_0|}(f(k_0) + f(-k_0)) \end{aligned} \tag{7.4}$$

The integrals do not contain singularities anymore and can thus be solved by Gaussian quadrature within finite intervals. The integrals are thus replaced by sums over weighted functions at Gauss nodes k_j. With a coordinate

$$q_j = \begin{cases} -k_{N_g - j + 1} & j = 1, \ldots, N_g \\ k_{j - N_g} & j = N_g + 1, \ldots, 2N_g \end{cases} \tag{7.5}$$

and weight mapping

$$\omega_j = \begin{cases} \omega'_{N_g - j + 1} & j = 1, \ldots, N_g \\ \omega'_{j - N_g} & j = N_g + 1, \ldots, 2N_g \end{cases} \tag{7.6}$$

one can recombine the two sums

$$\begin{aligned} = \; & \sum_{j=N_g+1}^{2N_g} \frac{f(q_j) - f(k_0)}{k_0^2 - q_j^2} \omega_j + \sum_{j=1}^{N_g} \frac{f(q_j) - f(-k_0)}{k_0^2 - q_j^2} \omega_j - \frac{i\pi}{2|k_0|}(f(k_0) + f(-k_0)) \\ = \; & \sum_{j=1}^{2N_g} \omega_j \frac{f(q_j)}{k_0^2 - q_j^2} - \sum_{j=N_g+1}^{2N_g} \omega_j \frac{1}{k_0^2 - q_j^2} f(k_0) - \sum_{j=1}^{N_g} \omega_j \frac{1}{k_0^2 - q_j^2} f(-k_0) \\ & - \frac{i\pi}{2|k_0|}(f(k_0) + f(-k_0)). \end{aligned} \tag{7.7}$$

Since $\sum_{j=1}^{N_g} \omega_j \frac{1}{k_0^2 - q_j^2} = \sum_{j=N_g+1}^{2N_g} \omega_j \frac{1}{k_0^2 - q_j^2}$ we can combine both sums and factorize the $(f(k_0) + f(-k_0))$ term.

$$= \sum_{j=1}^{2N_g} \omega_j \frac{f(q_j)}{k_0^2 - q_j^2} - \left(\sum_{j=1}^{N_g} \omega_j \frac{1}{k_0^2 - q_j^2} + \frac{i\pi}{2|k_0|} \right) (f(k_0) + f(-k_0)) \tag{7.8}$$

By mapping again onto a discrete momentum representation

$$\kappa_\mu := \begin{cases} q_\mu & \mu = 1, \ldots, 2N_g \\ -k_0 & \mu = 2N_g + 1 \\ k_0 & \mu = 2N_g + 2 \end{cases} \tag{7.9}$$

and defining

$$D_\mu := \begin{cases} \omega_\mu \frac{1}{k_0^2 - q_\mu^2} & \mu = 1, \ldots, 2N_g \\ -\left(\sum_{j=1}^{N_g} \omega_j \frac{1}{k_0^2 - q_j^2} + \frac{i\pi}{2|k_0|} \right) & \mu = 2N_g + 1, 2N_g + 2 \end{cases} \tag{7.10}$$

one can write the result in a short form.

$$\int_{-\infty}^{\infty} \frac{f(k)}{k_0^2 - k^2} dk = \sum_{\mu=1}^{2N_g+2} D_\mu f(\kappa_\mu) \tag{7.11}$$

7.3 Appendix - Relation between T-matrix and scattering potential

One can project the Lippmann-Schwinger equation

$$|\psi\rangle = |\psi_0\rangle + \hat{G}_0 \hat{V} |\psi\rangle \,, \tag{7.12}$$

onto an eigenstate $|\psi^0_{k',S'}\rangle$ of the unperturbed system without $\hat{V}$, which is characterized by the wave vector k' and the spin product state labeled by S'. This will lead to an equation for each component of $|\psi\rangle$,

$$\begin{aligned} \langle \psi^0_{k',S'} | \, |\psi\rangle &= \langle \psi^0_{k',S'} | \, |\psi^0_{k,S}\rangle + \langle \psi^0_{k',S'} | \, \hat{G}_0 \hat{1}_{\hat{H}_0} \hat{V} \, |\psi\rangle & (7.13) \\ &= \delta_{k,k'} \delta_{S,S'} + \langle \psi^0_{k',S'} | \, \hat{G}_0 \, |\psi^0_{k',S'}\rangle \, \langle \psi^0_{k',S'} | \, \hat{V} \, |\psi\rangle & (7.14) \end{aligned}$$

where we also inserts the unitary operator $\hat{1}_{\hat{H}_0} = \sum_{S_1} \int dk_1 \, |\psi^0_{S_1,k_1}\rangle \, \langle \psi^0_{S_1,k_1}|$. Notice $\hat{G}_0$ is diagonal in the basis $|\psi^0_{k,S}\rangle$. Proceeding in the same manner with the equation

$$|\psi\rangle = |\psi_0\rangle + \hat{G}_0 \hat{T} \, |\psi_0\rangle \tag{7.15}$$

leads to

$$\langle \psi^0_{k',S'} | \, |\psi\rangle = \delta_{k,k'} \delta_{S,S'} + \langle \psi^0_{k',S'} | \, \hat{G}_0 \, |\psi^0_{k',S'}\rangle \, \langle \psi^0_{k',S'} | \, \hat{T} \, |\psi^0_{k,S}\rangle \,. \tag{7.16}$$

The equality of the left hand side of both equations leads to the relation

$$\langle \psi^0_{k',S'} | \, \hat{T} \, |\psi^0_{k,S}\rangle = \langle \psi^0_{k',S'} | \, \hat{V} \, |\psi\rangle \tag{7.17}$$

between the matrix elements of the potential and the T-matrix.

7.4 Appendix - Wave function with T-matrix

In the following we derive an expression for the spin dependent wave function from the T-matrix equation

$$|\psi\rangle = |\psi_0\rangle + \hat{G}_0\hat{T}\,|\psi_0\rangle\,. \tag{7.18}$$

We project into the real and and spin space by multiplying $\langle S_f|\langle x|$ to the left. Further, we make use of the completeness relation $\mathbb{1} = \sum_s \int dk|s\rangle|k\rangle\langle k|\langle s|$ and the diagonality of the Green's function $\langle S_l|\langle k_l|\hat{G}_0|k_r\rangle|S_r\rangle = \delta_{S_l,S_r} 2m/(\hbar^2(k_E^2 - k^2))$.

$$\begin{aligned}&\langle S_f|\langle x|\psi\rangle = \langle S_f|\langle x|\psi_0\rangle \\ &+\sum_{S_1,S_2}\int\int dk_1 dk_2 \langle S_f|\langle x|k_1\rangle|S_1\rangle\langle S_1|\langle k_1|\hat{G}_0|k_1\rangle|S_1\rangle\langle S_1|\langle k_1|\hat{T}|k_2\rangle|S_2\rangle\langle S_2|\langle k_2|\psi_0\rangle\end{aligned} \tag{7.19}$$

Since the initial state is given by $|\psi_0\rangle = |k_E\rangle|S_E\rangle$, we can simplify the expression to

$$\begin{aligned}\langle S_f|\langle x|\psi\rangle &= \delta_{S_f,S_E}\langle x|k_E\rangle \\ &\quad +\frac{2m}{\hbar^2}\int dk\langle x|k\rangle\frac{1}{k_E^2-k^2}\langle S_f|\langle k|\hat{T}|k_E\rangle|S_E\rangle \\ &= \delta_{S_f,S_E}\frac{1}{\sqrt{2\pi}}e^{ik_E x} \\ &\quad +\frac{2m}{\hbar^2\sqrt{2\pi}}\int dk\frac{1}{k_E^2-k^2}e^{ikx}\langle S_f|\langle k|\hat{T}|k_E\rangle|S_E\rangle.\end{aligned} \tag{7.20}$$

Now, we can simply identify $f(k) = e^{ikx}\langle S_f|\langle k|\hat{T}|k_E\rangle|S_E\rangle$ and make use of the discretization scheme that is based on Gaussian quadrature. This leads to the expression

$$\begin{aligned}&\langle S_f|\langle x|\psi\rangle = \delta_{S_f,S_E}\frac{1}{\sqrt{2\pi}}e^{ik_E x} \\ &+\frac{2m}{\hbar^2\sqrt{2\pi}}\sum_{\mu=1}^{2N_g+2} D_\mu e^{i\kappa_\mu x}\langle S_f|\langle \kappa_\mu|\hat{T}|k_E\rangle|S_E\rangle\end{aligned} \tag{7.21}$$

for the wave function.

7.5 Appendix - Reflection amplitude

Equivalent to the derivation of the transmission amplitude, we derive the reflection amplitude from

$$\lim_{|x|\gg\Delta_V}\langle S_f, x|\psi\rangle = \langle S_f, x|\psi_0\rangle - \frac{im}{\hbar^2 k_E}e^{ik_E|x|}\sum_{s'}\int dx'\langle S_f|s'\rangle e^{-ik_E\mathrm{sign}(x)x'}\langle s', x'|\hat{V}|\psi\rangle, \tag{7.22}$$

with $x < 0$ such that $\text{sign}(x) = -1$. This leads to

$$= \langle S_f, x|\psi_0\rangle - \frac{im\sqrt{2\pi}}{\hbar^2 k_E} e^{-ik_E x} \sum_{s'} \int dx' \langle S_f|s'\rangle\langle -k_E|x'\rangle\langle s', x'|\hat{V}|\psi\rangle, \tag{7.23}$$

where we can use the completeness of the basis and write

$$= \langle S_f, x|\psi_0\rangle - \frac{im\sqrt{2\pi}}{\hbar^2 k_E} e^{-ik_E x} \langle S_f|\langle -k_E|\hat{V}|\psi\rangle. \tag{7.24}$$

The relation $\langle\psi'|\hat{V}|\psi\rangle = \langle\psi'|\hat{T}|\psi_0\rangle$ between the scattering potential and the T-matrix allows to express the scattered wave function in terms of the T-matrix

$$= \langle S_f, x|\psi_0\rangle - \frac{im\sqrt{2\pi}}{\hbar^2 k_E} e^{-ik_E x} \langle S_f|\langle -k_E|\hat{T}|\psi_0\rangle. \tag{7.25}$$

We define the initial wave function as $|\psi_0\rangle = |k_E\rangle|S_E\rangle$ wich gives in spacial representation $\langle x|\psi_0\rangle = \frac{1}{\sqrt{2\pi}} e^{ik_E x}|S_E\rangle$. Thus,

$$= \langle S_f, x|\psi_0\rangle - \frac{im2\pi}{\hbar^2 k_E} \langle S_f|\langle k_E|\hat{T}|\psi_0\rangle\langle\psi_0|x\rangle|S_E\rangle \tag{7.26}$$

allows to identify the reflection amplitude for a wave that has been initialized with momentum k_E and spin S_E.

$$r_{S_f,S_e} = -\frac{im2\pi}{\hbar^2 k_E} \langle S_f|\langle -k_E|\hat{T}|k_E\rangle|S_E\rangle \tag{7.27}$$

7.6 Appendix - Perturbation expansion for transversal anisotropy

In the following we derive the eigenstates of $\hat{H}_\chi$ up to second-order perturbation expansion in the transversal anisotropy $E_\chi/D_\chi \ll 1$. For two and four-fold symmetric systems $\chi \in \{2, 4\}$, the Hamiltonian reads as

$$\hat{H}_\chi = D_\chi \hat{J}_z^2 + E_\chi \left(\hat{J}_+^\chi + \hat{J}_-^\chi\right). \tag{7.28}$$

The perturbation expansion of the eigenstates up to second order gives

$$
\begin{aligned}
& |\phi_0^+\rangle \qquad (7.29)\\
\approx\ & |J\rangle \\
& + \frac{E}{D}\frac{\langle J-\chi|\hat{J}_-^\chi|J\rangle}{(J^2-(J-\chi)^2)}|J-\chi\rangle \\
& + \left(\frac{E}{D}\right)^2 \frac{\langle J-2\chi|\hat{J}_-^\chi|J-\chi\rangle\langle J-\chi|\hat{J}_-^\chi|J\rangle}{(J^2-(J-2\chi)^2)(J^2-(J-\chi)^2)}|J-2\chi\rangle \\
& - \frac{1}{2}\left(\frac{E}{D}\right)^2 \frac{\langle J|\hat{J}_+^\chi|J-\chi\rangle\langle J-\chi|\hat{J}_-^\chi|J\rangle}{(J^2-(J-\chi)^2)^2}|J\rangle \\
=\ & \left[1-\frac{1}{2}\left(\frac{E}{D}\right)^2 \frac{|\langle J-\chi|\hat{J}_-^\chi|J\rangle|^2}{(J^2-(J-\chi)^2)^2}\right]|J\rangle \\
& + \frac{E}{D}\frac{\langle J-\chi|\hat{J}_-^\chi|J\rangle}{(J^2-(J-\chi)^2)}|J-\chi\rangle \\
& + \left(\frac{E}{D}\right)^2 \frac{\langle J-2\chi|\hat{J}_-^\chi|J-\chi\rangle\langle J-\chi|\hat{J}_-^\chi|J\rangle}{(J^2-(J-2\chi)^2)(J^2-(J-\chi)^2)}|J-2\chi\rangle,
\end{aligned}
$$

which can be written in a short form

$$
= c_0^+(J,\chi)|J\rangle + c_1^+(J,\chi)|J-\chi\rangle + c_2^+(J,\chi)|J-2\chi\rangle \qquad (7.30)
$$

by defining

$$
\begin{aligned}
c_0^\pm(J,\chi) &= 1-\frac{1}{2}\left(\frac{E}{D}\right)^2 \frac{|\langle J-\chi|\hat{J}_\mp^\chi|J\rangle|^2}{(J^2-(J-\chi)^2)^2} && (7.31)\\
c_1^\pm(J,\chi) &= \frac{E}{D}\frac{\langle J-\chi|\hat{J}_\mp^\chi|J\rangle}{(J^2-(J-\chi)^2)} && (7.32)\\
c_2^\pm(J,\chi) &= \left(\frac{E}{D}\right)^2 \frac{\langle J-2\chi|\hat{J}_\mp^\chi|J-\chi\rangle\langle J-\chi|\hat{J}_\mp^\chi|J\rangle}{(J^2-(J-2\chi)^2)(J^2-(J-\chi)^2)}. && (7.33)
\end{aligned}
$$

Likewise, we can proceed with the other ground state

$$
\begin{aligned}
& |\phi_0^-\rangle \qquad (7.34)\\
= \; & |-J\rangle \\
& + \frac{E}{D}\frac{\langle -J+\chi|\hat{J}_+^\chi|-J\rangle}{(J^2-(-J+\chi)^2)}|-J+\chi\rangle \\
& + \left(\frac{E}{D}\right)^2 \frac{\langle -J+2\chi|\hat{J}_+^\chi|-J+\chi\rangle\langle -J+\chi|\hat{J}_+^\chi|-J\rangle}{(J^2-(-J+2\chi)^2)(J^2-(-J+\chi)^2)}|-J+2\chi\rangle \\
& - \frac{1}{2}\left(\frac{E}{D}\right)^2 \frac{\langle -J|\hat{J}_-^\chi|-J+\chi\rangle\langle -J+\chi|\hat{J}_+^\chi|-J\rangle}{(J^2-(-J+\chi)^2)^2}|-J\rangle \\
= \; & \left[1-\frac{1}{2}\left(\frac{E}{D}\right)^2 \frac{|\langle -J+\chi|\hat{J}_+^\chi|-J\rangle|^2}{(J^2-(-J+\chi)^2)^2}\right]|-J\rangle \\
& + \frac{E}{D}\frac{\langle -J+\chi|\hat{J}_+^\chi|-J\rangle}{(J^2-(-J+\chi)^2)}|-J+\chi\rangle \\
& + \left(\frac{E}{D}\right)^2 \frac{\langle -J+2\chi|\hat{J}_+^\chi|-J+\chi\rangle\langle -J+\chi|\hat{J}_+^\chi|-J\rangle}{(J^2-(-J+2\chi)^2)(J^2-(-J+\chi)^2)}|-J+2\chi\rangle
\end{aligned}
$$

with the short version

$$= c_0^-(-J,-\chi)|-J\rangle + c_1^-(-J,-\chi)|-J+\chi\rangle + c_2^-(-J,-\chi)|-J+2\chi\rangle. \qquad (7.35)$$

Thus, for a system with $J = 5/2$ and $\chi = 2$ we can now, for example calculate the matrix element

$$
\begin{aligned}
\langle\phi_0^-|\hat{J}_-|\phi_0^+\rangle \; = \; & \langle\frac{3}{2}|\hat{J}_-|\frac{5}{2}\rangle c_0^+(5/2,2)c_2^-(-5/2,-2) \qquad (7.36)\\
& + \langle -\frac{1}{2}|\hat{J}_-|\frac{1}{2}\rangle c_1^+(5/2,2)c_1^-(-5/2,-2) \\
& + \langle -\frac{5}{2}|\hat{J}_-|-\frac{3}{2}\rangle c_2^+(5/2,2)c_0^-(-5/2,-2)
\end{aligned}
$$

which contains coefficients of the perturbation expansion $c_i^+ c_{2-i}^- \propto (E_2/D_2)^2$ with $i \in \{0,1,2\}$, where higher orders in (E_2/D_2) are omitted.

For the matrix element

$$
\begin{aligned}
\langle\phi_0^-|\hat{J}_-|\phi_0^+\rangle \; = \; & \langle\frac{3}{2}|\hat{J}_-|\frac{5}{2}\rangle c_0^+(5/2,4)c_1^-(-5/2,-4) \qquad (7.37)\\
& + \langle -\frac{5}{2}|\hat{J}_-|-\frac{3}{2}\rangle c_1^+(5/2,4)c_0^-(-5/2,-4)
\end{aligned}
$$

in a system with $J = 5/2$ and $\chi = 4$, the lowest order in the transversal anisotropy is given by $c_i^+ c_{1-i}^- \propto (E_4/D_4)$ with $i \in \{0,1\}$.

Same perturbation expansion can be done for a three-fold symmetric system $\chi = 3$ with the Hamiltonian

$$\hat{H}_\chi = D_\chi \hat{J}_z^2 + E_\chi\left(\hat{J}_z\left(\hat{J}_+^\chi + \hat{J}_-^\chi\right) + \left(\hat{J}_+^\chi + \hat{J}_-^\chi\right)\hat{J}_z\right) \qquad (7.38)$$

leading to different expansion coefficients. Up to second-order the states are given by

$$
\begin{aligned}
& |\phi_0^+\rangle && (7.39)\\
= \; & |J\rangle \\
& + \frac{E}{D}\frac{\langle J-\chi|\hat{J}_-^\chi|J\rangle}{(J^2-(J-\chi)^2)}(J-\chi+J)|J-\chi\rangle \\
& + \left(\frac{E}{D}\right)^2 \frac{\langle J-2\chi|\hat{J}_-^\chi|J-\chi\rangle\langle J-\chi|\hat{J}_-^\chi|J\rangle}{(J^2-(J-2\chi)^2)(J^2-(J-\chi)^2)} \\
& (J-2\chi+J-\chi)(J-\chi+J)|J-2\chi\rangle && (7.40)\\
& -\frac{1}{2}\left(\frac{E}{D}\right)^2 \frac{\langle J|\hat{J}_+^\chi|J-\chi\rangle\langle J-\chi|\hat{J}_-^\chi|J\rangle}{(J^2-(J-\chi)^2)^2}(J+J-\chi)^2|J\rangle \\
= \; & \left[1-\frac{1}{2}\left(\frac{E}{D}\right)^2 \frac{|\langle J-\chi|\hat{J}_-^\chi|J\rangle|^2}{(J^2-(J-\chi)^2)^2}(J+J-\chi)^2\right]|J\rangle \\
& + \frac{E}{D}\frac{\langle J-\chi|\hat{J}_-^\chi|J\rangle}{(J^2-(J-\chi)^2)}(J-\chi+J)|J-\chi\rangle \\
& + \left(\frac{E}{D}\right)^2 \frac{\langle J-2\chi|\hat{J}_-^\chi|J-\chi\rangle\langle J-\chi|\hat{J}_-^\chi|J\rangle}{(J^2-(J-2\chi)^2)(J^2-(J-\chi)^2)} \\
& (J-2\chi+J-\chi)(J-\chi+J)|J-2\chi\rangle
\end{aligned}
$$

and can be written in a short form

$$
= c_0'^+(J,\chi)|J\rangle + c_1'^+(J,\chi)|J-\chi\rangle + c_2'^+(J,\chi)|J-2\chi\rangle \qquad (7.41)
$$

by definition of

$$
\begin{aligned}
c_0'^\pm(J,\chi) &= 1-\frac{1}{2}\left(\frac{E}{D}\right)^2 \frac{|\langle J-\chi|\hat{J}_\mp^\chi|J\rangle|^2}{(J^2-(J-\chi)^2)^2}(J+J-\chi)^2 && (7.42)\\
c_1'^\pm(J,\chi) &= \frac{E}{D}\frac{\langle J-\chi|\hat{J}_\mp^\chi|J\rangle}{(J^2-(J-\chi)^2)}(J-\chi+J) && (7.43)\\
c_2'^\pm(J,\chi) &= \left(\frac{E}{D}\right)^2 \frac{\langle J-2\chi|\hat{J}_\mp^\chi|J-\chi\rangle\langle J-\chi|\hat{J}_\mp^\chi|J\rangle}{(J^2-(J-2\chi)^2)(J^2-(J-\chi)^2)} \\
&\quad (J-2\chi+J-\chi)(J-\chi+J). && (7.44)
\end{aligned}
$$

For the other ground state, the expansion leads to

$$
\begin{aligned}
& |\phi_0^-\rangle && (7.45)\\
= \; & |-J\rangle \\
& + \frac{E}{D}\frac{\langle -J+\chi|\hat{J}_+^\chi|-J\rangle}{(J^2-(-J+\chi)^2)}(-J+\chi-J)|-J+\chi\rangle \\
& + \left(\frac{E}{D}\right)^2 \frac{\langle -J+2\chi|\hat{J}_+^\chi|-J+\chi\rangle\langle -J+\chi|\hat{J}_+^\chi|-J\rangle}{(J^2-(-J+2\chi)^2)(J^2-(-J+\chi)^2)} \\
& (-J+2\chi-J+\chi)(-J+\chi-J)|-J+2\chi\rangle && (7.46)\\
& -\frac{1}{2}\left(\frac{E}{D}\right)^2 \frac{\langle -J|\hat{J}_-^\chi|-J+\chi\rangle\langle -J+\chi|\hat{J}_+^\chi|-J\rangle}{(J^2-(-J+\chi)^2)^2}(-J-J+\chi)^2|-J\rangle \\
= \; & \left[1-\frac{1}{2}\left(\frac{E}{D}\right)^2 \frac{|\langle -J+\chi|\hat{J}_+^\chi|-J\rangle|^2}{(J^2-(-J+\chi)^2)^2}(-J-J+\chi)^2\right]|-J\rangle \\
& + \frac{E}{D}\frac{\langle -J+\chi|\hat{J}_+^\chi|-J\rangle}{(J^2-(-J+\chi)^2)}(-J+\chi-J)|-J+\chi\rangle \\
& + \left(\frac{E}{D}\right)^2 \frac{\langle -J+2\chi|\hat{J}_+^\chi|-J+\chi\rangle\langle -J+\chi|\hat{J}_+^\chi|-J\rangle}{(J^2-(-J+2\chi)^2)(J^2-(-J+\chi)^2)} \\
& (-J+2\chi-J+\chi)(-J+\chi-J)|-J+2\chi\rangle
\end{aligned}
$$

with the short form

$$= c_0'^-(-J,-\chi)|-J\rangle + c_1'^-(-J,-\chi)|-J+\chi\rangle + c_2'^-(-J,-\chi)|-J+2\chi\rangle. \quad (7.47)$$

Thus, for a system with $J = 5/2$ and $\chi = 3$ the matrix element

$$\langle\phi_0^-|\hat{J}_-|\phi_0^+\rangle \;=\; \langle\frac{1}{2}|\hat{J}_-|-\frac{1}{2}\rangle c_1^+(5/2,3)c_1^-(-5/2,-3) \quad (7.48)$$

contains coefficients $c_1^+c_1^- \propto (E_3/D_3)^2$.

7.7 Appendix - Protection due to time reversal symmetry

Without a magnetic field the single spin Hamiltonian commutes with the time reversal operator $\left[\hat{H}_\chi, \hat{T}\right] = 0$, which means one can find a basis in which both operators posses a diagonal matrix representation. This basis is given by

$$|t_s\rangle \;=\; \frac{1}{\sqrt{2}}\left(|\phi_0^+\rangle + |\phi_0^-\rangle\right) \quad (7.49)$$

$$|t_a\rangle \;=\; \frac{1}{\sqrt{2}}\left(|\phi_0^+\rangle - |\phi_0^-\rangle\right) \quad (7.50)$$

where t_s and t_a are the eigenvalues of the time reversal operator $\hat{T}$. The states $|t_s\rangle$ and $|t_a\rangle$ are also energy eigenstates. A unitary matrix

$$\mathbf{U} := \frac{1}{\sqrt{2}} \begin{pmatrix} 1 & 1 \\ 1 & -1 \end{pmatrix} \tag{7.51}$$

transforms the initial two state basis $\{|\phi_0^+\rangle, |\phi_0^-\rangle\}$. This unitary transformation holds for an arbitrary value of the transversal anisotropy E_χ since the relation $\hat{J}_z\hat{T} = -\hat{T}\hat{J}_z$ must always be true. We can see from

$$\begin{aligned} 0 &= \langle t_s|\hat{J}_z\hat{T}|t_s\rangle + \langle t_s|\hat{T}\hat{J}_z|t_s\rangle & (7.52)\\ &= |t_s|^2 \left(\langle \phi_0^+|\hat{J}_z|\phi_0^+\rangle + \langle \phi_0^-|\hat{J}_z|\phi_0^-\rangle\right) & (7.53) \end{aligned}$$

that a different choice of the transformation U would violate the anticommutator relation. The eigenvalues of $\hat{T}$ can not depend on E_χ since $\hat{H}_\chi$ is diagonal in the $\{|t_s\rangle, |t_a\rangle\}$ basis. Thus an expansion in $\hat{J}_z$ eigenstates would just allow combinations of $|m\rangle$ and $|-m\rangle$ that have the same time reversal symmetry. Thus one can set $E_\chi = 0$ leading to

$$\begin{aligned} |t_s\rangle &= \frac{1}{\sqrt{2}}\left(|J\rangle + |-J\rangle\right) & (7.54)\\ |t_a\rangle &= \frac{1}{\sqrt{2}}\left(|J\rangle - |-J\rangle\right) & (7.55) \end{aligned}$$

and derive the $\hat{T}$ eigenvalue with the relation $\hat{T}|m\rangle = (-1)^m|m\rangle$. In the representation of $\{|t_s\rangle, |t_a\rangle\}$ the time reversal operator can be written as a matrix

$$\mathbf{T} = (-1)^J \begin{pmatrix} 1 & 0 \\ 0 & -1 \end{pmatrix} \tag{7.56}$$

since $\hat{T}\left(|J\rangle \pm |-J\rangle\right) = \pm(-1)^J\left(|J\rangle \pm |-J\rangle\right)$. This leads to a matrix representation

$$\mathbf{T}' = \mathbf{U}^\dagger\mathbf{T}\mathbf{U} = (-1)^J \begin{pmatrix} 0 & 1 \\ 1 & 0 \end{pmatrix} \tag{7.57}$$

in the basis $\{|\phi_0^+\rangle, |\phi_0^-\rangle\}$. Now we will demonstrate that the condition $\langle\phi_0^-|\hat{J}_\pm|\phi_0^+\rangle = -\langle\phi_0^-|\hat{J}_\pm|\phi_0^+\rangle^*$ for an integer spin J is a direct result of the time reversal symmetry breaking due to a spin exchange, which is related to the general relation $\hat{J}_\pm\hat{T} + \hat{T}\hat{J}_\mp = 0$. We look at a matrix element of this relation by applying $|\phi_0^+\rangle$ to both sides and use the representation of $\hat{T}$ in this basis.

$$
\begin{aligned}
0 &= \langle\phi_0^+|\hat{J}_\pm\hat{T}|\phi_0^+\rangle + \langle\phi_0^+|\hat{T}\hat{J}_\mp|\phi_0^+\rangle && (7.58)\\
&= (-1)^J\langle\phi_0^+|\hat{J}_\pm|\phi_0^-\rangle + \left((-1)^J\right)^*\langle\phi_0^-|\hat{J}_\mp|\phi_0^+\rangle && (7.59)\\
&= (-1)^J\langle\phi_0^+|\hat{J}_\pm|\phi_0^-\rangle + \left((-1)^J\right)^*\langle\phi_0^+|\hat{J}_\pm|\phi_0^-\rangle^*. && (7.60)
\end{aligned}
$$

For a integer spin $J \in \{n\}$ the factor $(-1)^J \in \mathbb{R}$ and can only be ± 1. This leads to the afore mentioned condition

$$0 = (-1)^J(\langle\phi_0^+|\hat{J}_\pm|\phi_0^-\rangle + \langle\phi_0^+|\hat{J}_\pm|\phi_0^-\rangle^*) \tag{7.61}$$

or in other words the real part of the matrix element $\Re(\langle\phi_0^-|\hat{J}_\pm|\phi_0^+\rangle) = 0$ must vanish. On the other hand, for a half integer spin $J \in \{(2n+1)/2\}$ the factor $(-1)^J \in \mathbb{C}$ and can only have the values $\pm i$, which leads to the condition

$$0 = (-1)^J(\langle\phi_0^+|\hat{J}_\pm|\phi_0^-\rangle - \langle\phi_0^+|\hat{J}_\pm|\phi_0^-\rangle^*) \tag{7.62}$$

and thus only restricts the imaginary part of the matrix element $\Im(\langle\phi_0^-|\hat{J}_\pm|\phi_0^+\rangle) = 0$.

7.8 Appendix - Relation between Fokker-Planck and master equation

In the following, we take the classical limit of the master equation. The classical equivalent to the master equation is the Fokker-Planck equation. It describes the time evolution of a probability distribution in terms of statistical mechanics. The distribution $\rho(E,t)$ evolves in time according to a probability current j. The general form of a Fokker-Planck equation reads as

$$
\begin{aligned}
\frac{d\rho}{dt} &= \frac{d}{dE}j(E) && (7.63)\\
\frac{d\rho}{dt} &= \frac{d}{dE}\left[\left(B(E) + \frac{dA(E)}{dE}\right)\rho + A(E)\frac{d\rho}{dE}\right] && (7.64)\\
&= \frac{d^2}{dE^2}A\rho + \frac{d}{dE}B\rho
\end{aligned}
$$

with some functions A and B that depend on energy E. Within the finite difference approximation the derivatives can be replaced, such that

$$
\begin{aligned}
\frac{d\rho_m}{dt} &\approx \frac{A_{m-1}\rho_{m-1} - 2A_m\rho_m + A_{m+1}\rho_{m+1}}{\delta^2}\\
&\quad + \frac{B_{m+1}\rho_{m+1} - B_{m-1}\rho_{m-1}}{2\delta} && (7.65)\\
&= \left(\frac{A_{m-1}}{\delta^2} - \frac{B_{m-1}}{2\delta}\right)\rho_{m-1} - \frac{2A_m}{\delta^2}\rho_m + \left(\frac{A_{m+1}}{\delta^2} + \frac{B_{m+1}}{2\delta}\right)\rho_{m+1}.
\end{aligned}
$$

This form is equivalent to the master equation

$$\frac{d\rho_m}{dt} = W_{m,m-1}\rho_{m-1} - (W_{m+1,m} + W_{m-1,m})\,\rho_m + W_{m,m+1}\rho_{m+1} \tag{7.66}$$

if

$$A_m = \frac{\delta^2}{2}\,(W_{m-1,m} + W_{m+1,m}) \tag{7.67}$$

$$B_m = \delta\,(W_{m-1,m} - W_{m+1,m})\,. \tag{7.68}$$

and δ denotes the energy difference between adjacent energy eigenstates. For a single electron reservoir the rates are given by

$$W_{m\pm1,m} = \pi|v|^4\rho_\downarrow\rho_\uparrow|\langle m\pm1|J_\pm|m\rangle|^2\frac{-(\epsilon_{m\pm1}-\epsilon_m)}{1-e^{(\epsilon_{m\pm1}-\epsilon_m)/k_BT}}. \tag{7.69}$$

Written with energies in units of the total barrier height Δ_0 meaning $\tilde{T} = k_BT/\Delta_0$ and $\delta_m^\pm = (\epsilon_{m\pm1}-\epsilon_m)/\Delta_0$ the rates become

$$W_{m\pm1,m} = \pi|v|^4\rho_\downarrow\rho_\uparrow\Delta_0\tilde{T}|\langle m\pm1|J_\pm|m\rangle|^2\frac{-\frac{\delta_m^\pm}{\tilde{T}}}{1-e^{\frac{\delta_m^\pm}{\tilde{T}}}}, \tag{7.70}$$

or in a short form

$$W_{m\pm1,m} = \alpha\Sigma_{m+1,m}\zeta(\delta_m^\pm) \tag{7.71}$$

with $\alpha = \pi|v|^4\rho_\downarrow\rho_\uparrow$, $\Sigma_{m+1,m} = |\langle m\pm1|J_\pm|m\rangle|^2$ and $\zeta(\delta_m^\pm) = \tilde{T}\frac{-\frac{\delta_m^\pm}{\tilde{T}}}{1-e^{\frac{\delta_m^\pm}{\tilde{T}}}}$.

Further, we can write

$$\begin{aligned} & W_{m+1,m} + W_{m-1,m} \qquad (7.72)\\ = \;& \alpha\left[(S(S+1)-m(m+1))\zeta(\delta_m^+) + (S(S+1)-m(m-1))\zeta(\delta_m^-)\right]\\ = \;& \alpha\left[(S(S+1)-m^2)(\zeta(\delta_m^+)+\zeta(\delta_m^-)) + m(\zeta(\delta_m^+)-\zeta(\delta_m^-))\right] \end{aligned}$$

and

$$\begin{aligned} & W_{m+1,m} - W_{m-1,m} \qquad (7.73)\\ = \;& \alpha\left[(S(S+1)-m(m+1))\zeta(\delta_m^+) - (S(S+1)-m(m-1))\zeta(\delta_m^-)\right]\\ = \;& \alpha\left[(S(S+1)-m^2)(\zeta(\delta_m^+)-\zeta(\delta_m^-)) + m(\zeta(\delta_m^+)+\zeta(\delta_m^-))\right]. \end{aligned}$$

an take the high temperature limit $\tilde{T} \gg \delta_m^\pm$ of $\zeta(\delta_m^\pm)$, which gives

$$(\zeta(\delta_m^+)+\zeta(\delta_m^-)) \approx 2\tilde{T} - \frac{1}{2}(\delta_m^+ + \delta_m^-) \tag{7.74}$$

$$(\zeta(\delta_m^+)-\zeta(\delta_m^-)) \approx -\frac{1}{2}(\delta_m^+ - \delta_m^-). \tag{7.75}$$

At this point, we specify the spin system as a single spin S that is subject to a magnetic field $\tilde{B}$. The spin states are equally separated in energy according to the Zeeman splitting, which defines the expressions

$$\begin{aligned} -S \leq \quad m \quad &\leq S && (7.76)\\ \Delta_0 \quad &= \quad 2\tilde{B}S && (7.77)\\ \delta \quad &= \quad |(\epsilon_{m\pm1} - \epsilon_m)|/\Delta_0 = \frac{1}{2S} && (7.78)\\ \delta_m^{\pm} \quad &= \quad (\epsilon_{m\pm1} - \epsilon_m)/\Delta_0 = \pm\delta && (7.79)\\ E \quad &:= \quad \epsilon_m/\Delta_0 = m/2S. && (7.80) \end{aligned}$$

Specific in the chosen system, the high temperatures limit leads to

$$\begin{aligned} (\zeta(\delta_m^+) + \zeta(\delta_m^-)) \quad &= \quad 2\tilde{T} && (7.81)\\ (\zeta(\delta_m^+) - \zeta(\delta_m^-)) \quad &= \quad -\delta. && (7.82) \end{aligned}$$

Additionally we take the classical limit by assuming $S \xrightarrow{\text{class}} \infty$ and $\delta \xrightarrow{\text{class}} 0$ while keeping Δ_0 constant. Within the classical limit, the expressions A_m and B_m are given by

$$\begin{aligned} & A_m && (7.83)\\ = \quad & \frac{\delta^2}{2}(W_{m+1,m} + W_{m-1,m})\\ = \quad & \alpha\frac{\delta^2}{2}\left[(S(S+1) - m^2)2\tilde{T} + m(-\delta)\right]\\ \xrightarrow{\text{class}} \quad & \alpha\frac{\delta^2}{2}(S^2 - m^2)2\tilde{T}\\ = \quad & \frac{\alpha}{4}(1 - 4E^2)\tilde{T} \end{aligned}$$

and

$$\begin{aligned} & B_m && (7.84)\\ = \quad & \delta(W_{m+1,m} - W_{m-1,m})\\ = \quad & \alpha\delta\left[(S(S+1) - m^2)(-\delta) + m2\tilde{T}\right]\\ \xrightarrow{\text{class}} \quad & \alpha\left[-\delta^2(S^2 - m^2) + 2m\delta\tilde{T}\right]\\ = \quad & \alpha\left[-\frac{1}{4}(1 - 4E^2) + 2E\tilde{T}\right] \end{aligned}$$

Bibliography

[1] Smartphone Users Worldwide Will Total 1.75 Billion in 2014 - eMarketer.

[2] P. Anderson. Localized Magnetic States in Metals. *Phys. Rev.*, 124(1):41–53, 1961.

[3] D. Apalkov and P. Visscher. Spin-torque switching: Fokker-Planck rate calculation. *Physical Review B*, 72(18):180405, Nov. 2005.

[4] J. A. Appelbaum. Exchange Model of Zero-Bias Tunneling Anomalies. *Physical Review*, 154(3):633–643, Feb. 1967.

[5] E. Artacho and L. Miláns Del Bosch. Nonorthogonal basis sets in quantum mechanics: Representations and second quantization. *Physical Review A*, 43(11):5770–5777, 1991.

[6] M. N. Baibich, J. M. Broto, A. Fert, F. Nguyen Van Dau, F. Petroff, P. Etienne, G. Creuzet, A. Friederich, and J. Chazelas. Giant Magnetosresistance of (001)Fe/(001)Cr Magnetic Superlattices. *Physical Review Letters*, 61(21):2472–2475, 1988.

[7] J. Bardarson. Grid-Free Ground State of Molecules and Transport in Nanosystems. Master's thesis, University of Iceland, 2004.

[8] J. H. Bardarson, I. Magnusdottir, G. Gudmundsdottir, C. S. Tang, A. Manolescu, and V. Gudmundsson. Coherent electronic transport in a multimode quantum channel with Gaussian-type scatterers. *Physical Review B*, 70(24):245308, Dec. 2004.

[9] M. Bauer, E. and Rotter. Magnetism of Complex Metallic Alloys: Crystalline Electric Field Effects. *ChemInform*, 41(40):1522–2667, 2010.

[10] B. Baxevanis. *Dynamics in Nanosystems.* PhD thesis, Hamburg University, 2014.

[11] D. Becker. *Interplay of decoherence and quantum correlations in time-dependent transport through small quantum dots*. PhD thesis, University Hamburg, 2011.

[12] D. Becker and D. Pfannkuche. Coulomb-blocked transport through a quantum dot with spin-split level: Increase of differential conductance peaks by spin relaxation. *Phys. Rev. B*, 77(20):205307, 2008.

[13] C. W. J. Beenakker. Theory of Coulomb-blockade oscillations in the conductance of a quantum dot. *Physical Review B*, 44(4):1646–1656, 1991.

[14] R. Bennewitz, J. N. Crain, A. Kirakosian, J. L. Lin, J. L. McChesney, D. Y. Petrovykh, and F. J. Himpsel. Atomic Scale Memory at a Silicon Surface. *Nanotechnology*, 13(4):499, 2002.

[15] A. Bhattacharjee and C. Benoit à la Guillaume. Model for the Mn acceptor in GaAs. *Solid State Communications*, 113(1):17–21, 1999.

[16] A. K. Bhattacharjee. Wavevector dependence of exchange interaction in semimagnetic semiconductors. In *20th International Conference on the Physics of Semiconductors : Thessaloniki*, pages 763–766, 1990.

[17] G. Binasch, P. Grünberg, F. Saurenbach, and W. Zinn. Enhanced magnetoresistance in layered magnetic structures with antiferromagnetic interlayer exchange. *Physical Review B*, 39(7):4828–4830, 1989.

[18] G. Binnig and H. Rohrer. Scanning tunneling microscopy. *Surface Science*, 126(1-3):236–244, 1983.

[19] R. Blick, D. Pfannkuche, R. Haug, K. Klitzing, and K. Eberl. Formation of a Coherent Mode in a Double Quantum Dot. *Physical Review Letters*, 80(18):4032–4035, 1998.

[20] R. H. Blick, R. J. Haug, J. Weis, D. Pfannkuche, K. v. Klitzing, and K. Eberl. Single-electron tunneling through a double quantum dot: The artificial molecule. *Physical Review B*, 53(12):7899–7902, 1996.

[21] M. Bode. Spin-polarized scanning tunnelling microscopy. *Reports on Progress in Physics*, 66(4):523–582, 2003.

[22] M. Bode, O. Pietzsch, A. Kubetzka, and R. Wiesendanger. Shape-dependent thermal switching behavior of superparamagnetic nanoislands. *Physical review letters*, 92(6):067201, 2004.

[23] N. Bode, L. Arrachea, G. S. Lozano, T. S. Nunner, and F. von Oppen. Current-induced switching in transport through anisotropic magnetic molecules. *Physical Review B*, 85(11):115440, Mar. 2012.

[24] L. Bogani and W. Wernsdorfer. Molecular spintronics using single-molecule magnets. *Nature materials*, 7(3):179–186, Mar. 2008.

[25] R. E. Bohn and J. E. Short. How Much Information? 2009 Report on American Consumers. *Scholarly Communications Report*, pages 1–36, 2009.

[26] M. Born. Quantenmechanik der Stoßvorgänge. *Zeitschrift für Physik*, 38(11-12):803–827, 1926.

[27] H.-B. Braun. Kramers's rate theory, broken symmetries, and magnetization reversal (invited). *Journal of Applied Physics*, 76:6310, 1994.

[28] M. Braun, J. König, and J. Martinek. Theory of transport through quantum-dot spin valves in the weak-coupling regime. *Physical Review B*, 70(19):195345, Nov. 2004.

[29] L. Brey and G. Gómez-Santos. Magnetic properties of GaMnAS from an effective Heisenberg Hamiltonian. *Physical Review B*, 68(11):115206, 2003.

[30] W. Brown. Thermal Fluctuations of a Single-Domain Particle. *Physical Review*, 130(5):1677–1686, June 1963.

[31] B. Bryant, A. Spinelli, J. J. T. Wagenaar, M. Gerrits, and a. F. Otte. Local Control of Single Atom Magnetocrystalline Anisotropy. *Physical Review Letters*, 111(12):127203, Sept. 2013.

[32] K. T. Chan, J. B. Neaton, and M. L. Cohen. First-principles study of metal adatom adsorption on graphene. *Physical Review B - Condensed Matter and Materials Physics*, 77(23):235430, 2008.

[33] D. Chattopadhyay and H. J. Queisser. Electron scattering by ionized impurities in semiconductors. *Reviews of Modern Physics*, 53(4):745–768, 1981.

[34] A. Chudnovskiy, C. Hübner, B. Baxevanis, and D. Pfannkuche. Spin switching: From quantum to quasiclassical approach. *Physica Status Solidi (b)*, 251(9):1764–1776, Sept. 2014.

[35] S. Chutia and A. K. Bhattacharjee. III-V semiconductor quantum dots with a magnetic impurity. *Physica Status Solidi (C)*, 6(10):2101–2106, 2009.

[36] W. T. Coffey and Y. P. Kalmykov. Thermal fluctuations of magnetic nanoparticles: Fifty years after Brown. *Journal of Applied Physics*, 112:121301, 2012.

[37] M. Cohen. On the Schrodinger equation with a Gaussian potential. *Journal of Physics A: Mathematical and General*, 17(3):L101–L104, 1999.

[38] I. C. da Cunha Lima, E. J. R. de Oliveira, E. Dias Cabral, and M. A. Boselli. Roles of extended and localized states in the magnetic and transport properties of GaMnAs alloys. *Journal of Superconductivity and Novel Magnetism*, 26(6):2201–2207, 2013.

[39] M. D. Daybell and W. A. Steyert. Localized magnetic impurity states in metals: Some experimental relationships. *Reviews of Modern Physics*, 40(2):380–389, 1968.

[40] W. de Haas, J. de Boer, and G. van dën Berg. The electrical resistance of gold, copper and lead at low temperatures. *Physica*, 1(7-12):1115–1124, 1934.

[41] P.-M. Déjardin, H. Kachkachi, and Y. P. Kalmykov. Thermal and surface anisotropy effects on the magnetization reversal of a nanocluster. *Journal of Physics D: Applied Physics*, 41(13):134004, July 2008.

[42] F. Delgado and J. Fernández-Rossier. Spin dynamics of current-driven single magnetic adatoms and molecules. *Physical Review B*, 82(13):134414, Oct. 2010.

[43] F. Delgado and J. Fernández-Rossier. Cotunneling theory of atomic spin inelastic electron tunneling spectroscopy. *Physical Review B*, 84(4):045439, July 2011.

[44] F. Delgado, C. Hirjibehedin, and J. Fernández-Rossier. Consequences of Kondo exchange on quantum spins. *arXiv:1401.7272 [cond-mat.mes-hall]*, Dec. 2014.

[45] F. Delgado, S. Loth, M. Zielinski, and J. Fernández-Rossier. The emergence of classical behaviour in magnetic adatoms. *EPL (Europhysics Letters)*, 109(5):57001, Mar. 2015.

[46] F. Delgado, J. J. Palacios, and J. Fernández-Rossier. Spin-Transfer Torque on a Single Magnetic Adatom. *Physical Review Letters*, 104(2):026601, Jan. 2010.

[47] T. Dietl. Zener Model Description of Ferromagnetism in Zinc-Blende Magnetic Semiconductors. *Science*, 287(5455):1019–1022, 2000.

[48] P. A. M. Dirac. The Quantum Theory of the Electron. *Proceedings of the Royal Society A: Mathematical, Physical and Engineering Sciences*, 117(778):610–624, 1928.

[49] F. Donati, Q. Dubout, G. Autès, F. Patthey, F. Calleja, P. Gambardella, O. V. Yazyev, and H. Brune. Magnetic moment and anisotropy of individual Co atoms on graphene. *Physical Review Letters*, 111(23):236801, 2013.

[50] F. Donati, A. Singha, S. Stepanow, C. Wäckerlin, J. Dreiser, P. Gambardella, S. Rusponi, and H. Brune. Magnetism of Ho and Er Atoms on Close-Packed Metal Surfaces. *Physical Review Letters*, 113(23):237201, Dec. 2014.

[51] Q. Dubout, F. Donati, F. Calleja, M. Etzkorn, A. Lehnert, L. Claude, P. Gambardella, and H. Brune. Controlling the Spin of Co Atoms on Pt(111) by Hydrogen Adsorption. *Physical Review Letters*, 114(10):106807, 2015.

[52] A. Ekimov, A. Efros, and A. Onushchenko. Quantum size effect in semiconductor microcrystals. *Solid State Communications*, 56(11):921–924, 1985.

[53] F. Elste and C. Timm. Transport through anisotropic magnetic molecules with partially ferromagnetic leads: Spin-charge conversion and negative differential conductance. *Physical Review B*, 73(23):235305, June 2006.

[54] J. Fernández-Rossier. Theory of Single-Spin Inelastic Tunneling Spectroscopy. *Physical Review Letters*, 102(25):256802, June 2009.

[55] R. P. Feynman. There's plenty of room at the bottom. *Engineering and science*, 23(5):22–36, 1960.

[56] D. Fisher and P. Lee. Relation between conductivity and transmission matrix. *Physical Review B*, 23(12):6851(R), June 1981.

[57] S. Flugge. *Practical Quantum Mechanics*, volume 177. Springer-Verlag Berlin Heidelberg, 1999.

[58] L.-H. Frahm. Dynamics of Quantum Systems in Magnetic Environment. Master's thesis, University Hamburg, 2014.

[59] T. A. Fulton and G. J. Dolan. Observation of single-electron charging effects in small tunnel junctions. *Physical Review Letters*, 59(1):109–112, 1987.

[60] J. K. Furdyna. Diluted magnetic semiconductors: An interface of semiconductor physics and magnetism (invited). *Journal of Applied Physics*, 53:7637–7643, 1982.

[61] P. Gambardella, S. Rusponi, M. Veronese, S. S. Dhesi, C. Grazioli, A. Dallmeyer, I. Cabria, R. Zeller, P. H. Dederichs, K. Kern, C. Carbone, and H. Brune. Giant magnetic anisotropy of single cobalt atoms and nanoparticles. *Science*, 300(5622):1130–1133, 2003.

[62] D. Gatteschi and R. Sessoli. Quantum tunneling of magnetization and related phenomena in molecular materials. *Angewandte Chemie (International ed. in English)*, 42(3):268–297, Jan. 2003.

[63] D. Gatteschi and L. Sorace. Hints for the Control of Magnetic Anisotropy in Molecular Materials. *Journal of Solid State Chemistry*, 159(2):253–261, July 2001.

[64] J. P. Gauyacq and N. Lorente. Magnetic reversal of a quantum nanoferromagnet. *Physical Review B*, 87(19):195402, May 2013.

[65] W. Gerlach and O. Stern. Der experimentelle Nachweis der Richtungsquantelung im Magnetfeld. *Zeitschrift für Physik*, 9(1):349–352, 1922.

[66] A. Gerritsen and J. Linde. The electrical resistances of alloys of a noble metal and a transition metal. *Physica*, 18(11):877–890, 1952.

[67] T. Gilbert. A Phenomenological Theory of Damping in Ferromagnetic Materials. *IEEE Transactions on Magnetics*, 40(6):3443–3449, Nov. 2004.

[68] R. Gilmore and A. J. DeWeerd. Elementary Quantum Mechanics in One Dimension. *American Journal of Physics*, 73:480, 2005.

[69] V. Gudmundsson, G. Gudmundsdottir, J. H. Bardarson, I. Magnusdottir, C. S. Tang, and A. Manolescu. Multi-mode transport through a quantum nanowire with two embedded dots. *European Physical Journal B*, 45(3):339–345, 2005.

[70] V. Gudmundsson, Y.-Y. Lin, C.-S. Tang, V. Moldoveanu, J. Bardarson, and A. Manolescu. Transport through a quantum ring, dot, and barrier embedded in a nanowire in magnetic field. *Physical Review B*, 71(23):235302, June 2005.

[71] V. Gudmundsson and C.-S. Tang. Magnetotransport in a double quantum wire: Modeling using a scattering formalism built on the Lippmann-Schwinger equation. *Physical Review B*, 74(12):125302, Sept. 2006.

[72] E. Gull, A. J. Millis, A. Lichtenstein, A. Rubtsov, M. Troyer, and P. Werner. Continuous-time Monte Carlo methods for quantum impurity models. *Reviews of Modern Physics*, 83(2):349–404, May 2011.

[73] C. Haas. Spin-disorder scattering and magnetoresistance of magnetic semiconductors. *Physical Review*, 168(2):531–538, 1968.

[74] H. han Houten and C. W. J. Beenakker. Comment on Conductance oscillations periodic in the density of a one-dimensional electron gas. *Physical Review Letters*, 63(17):1893, 1989.

[75] P. Hänggi and M. Borkovec. Reaction-rate theory: fifty years after Kramers. *Reviews of Modern Physics*, 62(2):251, Apr. 1990.

[76] B. L. Hazelzet, M. R. Wegewijs, T. H. Stoof, and Y. V. Nazarov. Coherent and incoherent pumping of electrons in double quantum dots. *Physical Review B*, 63(16):165313, Apr. 2001.

[77] A. J. Heinrich, J. A. Gupta, C. P. Lutz, and D. M. Eigler. Single-atom spin-flip spectroscopy. *Science*, 306(5695):466–469, Oct. 2004.

[78] W. Heisenberg. Mehrkörperproblem und Resonanz in der Quantenmechanik. *Zeitschrift für Physik*, 38(6-7):411–426, 1926.

[79] W. Heisenberg. Zur Theorie des Ferromagnetismus. *Zeitschrift Für Physik*, 49(9-10):619–636, 1928.

[80] M. Hilbert and P. López. The world's technological capacity to store, communicate, and compute information. *Science*, 332(6025):60–65, 2011.

[81] C. F. Hirjibehedin, C.-Y. Lin, A. F. Otte, M. Ternes, C. P. Lutz, B. A. Jones, and A. J. Heinrich. Large magnetic anisotropy of a single atomic spin embedded in a surface molecular network. *Science*, 317(5842):1199–203, Aug. 2007.

[82] C. F. Hirjibehedin, C. P. Lutz, and A. J. Heinrich. Spin coupling in engineered atomic structures. *Science*, 312(5776):1021–1024, May 2006.

[83] C. Hübner. Spintransport durch magnetisch dotierte Quantenpunkte. Diplomarbeit, Universität Hamburg, 2010.

[84] C. Hübner, B. Baxevanis, a. a. Khajetoorians, and D. Pfannkuche. Symmetry effects on the spin switching of adatoms. *Physical Review B*, 90(15):155134, Oct. 2014.

[85] A.-P. Jauho. Nonequilibrium Green function modelling of transport in mesoscopic systems. In *Progress in Nonequilibrium Green's Functions II:*, pages 181–197, 2003.

[86] C. Karlewski and M. Marthaler. Time-local master equation connecting the Born and Markov approximations. *Physical Review B*, 90(10):104302, Sept. 2014.

[87] C. Karlewski, M. Marthaler, T. Märkl, T. Balashov, W. Wulfhekel, and G. Schön. Magnetic adatoms as memory bits: A quantum master equation analysis. *Physical Review B*, 91(24):245430, 2015.

[88] L. V. Keldysh. Diagram Technique for Nonequilibrium Processes. *Soviet Physics JETP*, 47(4):1018–1026, 1965.

[89] A. A. Khajetoorians, B. Baxevanis, C. Hübner, T. Schlenk, S. Krause, T. O. Wehling, S. Lounis, A. Lichtenstein, D. Pfannkuche, J. Wiebe, and R. Wiesendanger. Current-driven spin dynamics of artificially constructed quantum magnets. *Science*, 339(6115):55–59, Jan. 2013.

[90] A. A. Khajetoorians, S. Lounis, B. Chilian, A. T. Costa, L. Zhou, D. L. Mills, J. Wiebe, and R. Wiesendanger. Itinerant Nature of Atom-Magnetization Excitation by Tunneling Electrons. *Physical Review Letters*, 106(3):037205, Jan. 2011.

[91] A. A. Khajetoorians, J. Wiebe, B. Chilian, and R. Wiesendanger. Realizing all-spin-based logic operations atom by atom. *Science*, 332(6033):1062–1064, May 2011.

[92] M. J. Klein. On a Degeneracy Theorem of Kramers. *American Journal of Physics*, 20:65, 1952.

[93] S. Koller, M. Grifoni, M. Leijnse, and M. Wegewijs. Density-operator approaches to transport through interacting quantum dots: Simplifications in fourth-order perturbation theory. *Physical Review B*, 82(23):235307, Dec. 2010.

[94] J. Kondo. Resistance Minimum in Dilute Magnetic Alloys. *Progress of Theoretical Physics*, 32(1):37–49, July 1964.

[95] J. König, H. H. Lin, and A. H. MacDonald. Theory of diluted magnetic semiconductor ferromagnetism. *Physical Review Letters*, 84(24):5628–5631, 2000.

[96] L. Kouwenhoven, F. Hekking, B. van Wees, C. Harmans, C. Timmering, and C. Foxon. Transport through a finite one-dimensional crystal. *Physical Review Letters*, 65(3):361–364, 1990.

[97] L. P. Kouwenhoven, D. G. Austing, and S. Tarucha. Few-electron quantum dots. *Reports on Progress in Physics*, 64(6):701–736, 2001.

[98] H. Kramers. Théorie générale de la rotation paramagnétique dans les cristaux. *Proceedings Koninklijke Akademie van Wetenschappen*, (33):959–972, 1930.

[99] U. Larsen. A simple derivation of the s-d exchange interaction. *Journal of Physics C: Solid State Physics*, 4(13):1835–1836, 2001.

[100] A. Lehnert, S. Rusponi, M. Etzkorn, S. Ouazi, P. Thakur, and H. Brune. Magnetic anisotropy of Fe and Co adatoms and Fe clusters magnetically decoupled from Ni_{3}Al(111) by an alumina bilayer. *Physical Review B*, 81(10):104430, Mar. 2010.

[101] M. Leijnse and M. Wegewijs. Kinetic equations for transport through single-molecule transistors. *Physical Review B*, 78(23):235424, Dec. 2008.

[102] Z. Li and S. Zhang. Thermally assisted magnetization reversal in the presence of a spin-transfer torque. *Physical Review B*, 69(13):134416, Apr. 2004.

[103] B. A. Lippmann and J. Schwinger. Variational principles for scattering processes. I. *Physical Review*, 79(3):469, 1950.

[104] R. A. Logan and J. M. Rowell. Conductance anomalies in semiconductor tunnel diodes. *Physical Review Letters*, 13(13):404, 1964.

[105] S. Loth, S. Baumann, C. P. Lutz, D. M. Eigler, and A. J. Heinrich. Bistability in atomic-scale antiferromagnets. *Science*, 335(6065):196–199, Jan. 2012.

[106] S. Loth, M. Etzkorn, C. P. Lutz, D. M. Eigler, and A. J. Heinrich. Measurement of fast electron spin relaxation times with atomic resolution. *Science*, 329(5999):1628–1630, Oct. 2010.

[107] S. Loth, C. P. Lutz, and A. J. Heinrich. Spin-polarized spin excitation spectroscopy. *New Journal of Physics*, 12:125021, Dec. 2010.

[108] S. Loth, K. von Bergmann, M. Ternes, A. F. Otte, C. P. Lutz, and A. J. Heinrich. Controlling the state of quantum spins with electric currents. *Nature Physics*, 6:340–344, 2010.

[109] G. Mackh, W. Ossau, a. Waag, and G. Landwehr. Effect of the reduction of dimensionality on the exchange parameters in semimagnetic semiconductors. *Physical Review B*, 54(8):R5227–R5230, 1996.

[110] N. Majlis. *THE QUANTUM THEORY OF MAGNETISM (2nd Edition)*. Springer-Verlag Berlin Heidelberg, 2007.

[111] M. Mannini, F. Pineider, P. Sainctavit, C. Danieli, E. Otero, C. Sciancalepore, A. M. Talarico, M.-A. Arrio, A. Cornia, D. Gatteschi, and R. Sessoli. Magnetic memory of a single-molecule quantum magnet wired to a gold surface. *Nature materials*, 8:194–197, 2009.

[112] P. C. Martin and J. Schwinger. Theory of many-particle systems. I. *Physical Review*, 115(6):1342–1373, 1959.

[113] F. Meier, L. Zhou, J. Wiebe, and R. Wiesendanger. Revealing magnetic interactions from single-atom magnetization curves. *Science*, 320(5872):82–86, Apr. 2008.

[114] M. Misiorny and J. Barnaś. Quantum tunneling of magnetization in single molecular magnets coupled to ferromagnetic reservoirs. *Europhysics Letters (EPL)*, 78(2):27003, Apr. 2007.

[115] M. Misiorny and J. Barnaś. Effects of Transverse Magnetic Anisotropy on Current-Induced Spin Switching. *Physical Review Letters*, 111(4):046603, July 2013.

[116] M. Misiorny, I. Weymann, and J. Barnaś. Spin effects in transport through single-molecule magnets in the sequential and cotunneling regimes. *Physical Review B*, 79(22):224420, June 2009.

[117] S. K. Misra, C. P. Poole, and H. A. Farach. A review of spin Hamiltonian forms for various point-group site symmetries. *Applied Magnetic Resonance*, 11(1):29–46, May 1996.

[118] T. Miyamachi, T. Schuh, T. Märkl, C. Bresch, T. Balashov, A. Stöhr, C. Karlewski, S. André, M. Marthaler, M. Hoffmann, M. Geilhufe, S. Ostanin, W. Hergert, I. Mertig, G. Schön, A. Ernst, and W. Wulfhekel. Stabilizing the magnetic

moment of single holmium atoms by symmetry. *Nature*, 503:242–246, Nov. 2013.

[119] T. Miyazaki and N. Tezuka. Giant magnetic tunneling effect in Fe/Al2O3/Fe junction. *Journal of Magnetism and Magnetic Materials*, 139(3):L231–L234, 1995.

[120] V. Moldoveanu, A. Manolescu, and V. Gudmundsson. Dynamic correlations induced by Coulomb interactions in coupled quantum dots. *Physical Review B*, 82(8):085311, Aug. 2010.

[121] G. E. Moore. Cramming more components onto integrated circuits. *Proceedings of the IEEE*, 86(1):82–85, 1998.

[122] M. G. Moore. Introduction to scattering theory, 2008.

[123] M. Morgenstern, V. Gudmundsson, R. Dombrowski, C. Wittneven, and R. Wiesendanger. Nonlocality of the exchange interaction probed by scanning tunneling spectroscopy. *Physical Review B*, 63:1–4, 2001.

[124] H. Munekata, H. Ohno, S. Von Molnar, A. Segmüller, L. L. Chang, and L. Esaki. Diluted magnetic III-V semiconductors. *Physical Review Letters*, 63(17):1849–1852, 1989.

[125] J. C. Oberg, M. R. Calvo, F. Delgado, M. Moro-Lagares, D. Serrate, D. Jacob, J. Fernández-Rossier, and C. F. Hirjibehedin. Control of single-spin magnetic anisotropy by exchange coupling. *Nature nanotechnology*, 9:64–8, Jan. 2014.

[126] A. F. Otte, M. Ternes, K. von Bergmann, S. Loth, H. Brune, C. P. Lutz, C. F. Hirjibehedin, and A. J. Heinrich. The role of magnetic anisotropy in the Kondo effect. *Nature Physics*, 4:847–850, Sept. 2008.

[127] B. Ouari and Y. P. Kalmykov. Dynamics of the magnetization of single domain particles having triaxial anisotropy subjected to a uniform dc magnetic field. *Journal of Applied Physics*, 100:123912, 2006.

[128] G. E. Pacchioni, L. Gragnaniello, F. Donati, M. Pivetta, G. Autès, O. V. Yazyev, S. Rusponi, and H. Brune. Multiplet features and magnetic properties of Fe on Cu(111): From single atoms to small clusters. *Physical Review B*, 91(23):235426, 2015.

[129] S. S. P. Parkin, C. Kaiser, A. Panchula, P. M. Rice, B. Hughes, M. Samant, and S.-H. Yang. Giant tunnelling magnetoresistance at room temperature with MgO (100) tunnel barriers. *Nature materials*, 3:862–867, 2004.

[130] W. Pauli. Über den Zusammenhang des Abschlusses der Elektronengruppen im Atom mit der Komplexstruktur der Spektren. *Zeitschrift fuer Physik*, 31(1):765–783, 1925.

[131] W. Pauli. The connection between spin and statistics. *Physical Review*, 58(8):716–722, 1940.

[132] W. Pauli. Nobel Lecture: Exclusion Principle and Quantum Mechanics. *Nobel Lecture*, 1946.

[133] K. S. Pedersen, L. Ungur, M. Sigrist, A. Sundt, M. Schau-Magnussen, V. Vieru, H. Mutka, S. Rols, H. Weihe, O. Waldmann, L. F. Chibotaru, J. Bendix, and J. Dreiser. Modifying the properties of 4f single-ion magnets by peripheral ligand functionalisation. *Chemical Science*, 5(4):1650, 2014.

[134] R. E. Prange. Tunneling from a many-particle point of view. *Physical Review*, 131(3):1083–1086, 1963.

[135] F. Qu and P. Hawrylak. Theory of Electron Mediated Mn-Mn Interactions in Quantum Dots. *Physical Review Letters*, 96(15):157201, Apr. 2006.

[136] I. G. Rau, S. Baumann, S. Rusponi, F. Donati, S. Stepanow, L. Gragnaniello, J. Dreiser, C. Piamonteze, F. Nolting, S. Gangopadhyay, O. R. Albertini, R. M. Macfarlane, C. P. Lutz, B. A. Jones, P. Gambardella, A. J. Heinrich, and H. Brune. Reaching the magnetic anisotropy limit of a 3d metal atom. *Science*, 344(6187):988–992, May 2014.

[137] R. Saptsov and M. Wegewijs. Fermionic superoperators for zero-temperature nonlinear transport: Real-time perturbation theory and renormalization group for Anderson quantum dots. *Physical Review B*, 86(23):235432, Dec. 2012.

[138] R. Schleser, T. Ihn, E. Ruh, K. Ensslin, M. Tews, D. Pfannkuche, D. C. Driscoll, and A. C. Gossard. Cotunneling-mediated transport through excited states in the coulomb-blockade regime. *Physical Review Letters*, 94(20):206805, 2005.

[139] J. Schliemann. Disorder-induced noncollinear ferromagnetism in models for (III,Mn)V semiconductors. *Physical Review B*, 67(4):045202, Jan. 2003.

[140] J. Schliemann, J. König, L. Hsiu-Hau, and A. H. MacDonald. Limits on the curie temperature of (III,Mn)V ferromagnetic semiconductors. *Applied Physics Letters*, 78:1550–1552, 2001.

[141] J. Schliemann, J. König, and A. H. MacDonald. Monte Carlo Study of Ferromagnetism in (III,Mn)V Semiconductors. *Physical Review B*, 64(16):165201, 2001.

[142] J. Schliemann and A. H. MacDonald. Noncollinear ferromagnetism in (III,Mn)V semiconductors. *Physical review letters*, 88(13):137201, 2002.

[143] T. Schmidt, M. Tewordt, R. H. Blick, R. J. Haug, D. Pfannkuche, K. V. Klitzing, A. Förster, and H. Lüth. Quantum-dot ground states in a magnetic field studied by single-electron tunneling spectroscopy on double-barrier heterostructures. *Physical Review B*, 51(8):5570(R), 1995.

[144] H. Schoeller and G. Schön. Mesoscopic quantum transport: Resonant tunneling in the presence of a strong Coulomb interaction. *Physical Review B*, 50(24):18436–18452, 1994.

[145] J. Schrieffer and P. Wolff. Relation between the Anderson and Kondo Hamiltonians. *Physical Review*, 149(2):491–492, Sept. 1966.

[146] D. K. Schweizer and E. K. Eigler. Positioning single atoms with a scanning tunneling microscop. *Nature*, 344:524–525, 1990.

[147] J. E. Short, R. E. Bohn, and C. Baru. How much information? 2010: Report on enterprise server information. *UCSD Global Information Industry Center*, pages 1–38, 2011.

[148] S. D. Silverstein and C. B. Duke. Theory of s-d scattering in dilute magnetic alloys. I. Perturbation theory and the derivation of the low Equation. *Physical Review*, 161(2):456–469, 1967.

[149] R. Skomski. *Simple Models of Magnetism*. Oxford Scholarship Online, 2008.

[150] L. L. Sohn, L. P. Kouwenhoven, and G. Schön. *Mesoscopic Electron Transport*. NATO ASI Series, 1 edition, 1997.

[151] K. W. H. Stevens. Matrix Elements and Operator Equivalents Connected with the Magnetic Properties of Rare Earth Ions. *Proceedings of the Physical Society. Section A*, 65(3):209–215, Mar. 1952.

[152] K. Szalowski and T. Balcerzak. The RKKY coupling of two magnetically doped monolayers in thin films. In *Proc. XXXVII International School of Semiconducting Compounds, Jaszowiec*, volume 114, pages 1375–1382, 2008.

[153] K. Szalowski and T. Balcerzak. Antiferromagnetic interlayer coupling in diluted magnetic thin films with RKKY interaction. *Physical Review B*, 79(21):214430, 2009.

[154] K. Tao, V. Stepanyuk, P. Bruno, D. Bazhanov, V. Maslyuk, M. Brandbyge, and I. Mertig. Manipulating magnetism and conductance of an adatom-molecule junction on a metal surface: An ab initio study. *Physical Review B*, 78(1):014426, July 2008.

[155] J. Tejada, J. M. Hernandez, and E. del Barco. Macroscopic quantum tunneling of the magnetic moment. *Journal of Magnetism and Magnetic Materials*, 196-197:552–557, May 1999.

[156] M. Ternes. Spin Excitations and Correlations in Scanning Tunneling Spectroscopy. *arXiv:1505.04430 [cond–mat.mes–hall]*, 2015.

[157] M. Ternes, A. J. Heinrich, and W.-D. Schneider. Spectroscopic manifestations of the Kondo effect on single adatoms. *Journal of Physics: Condensed matter*, 21:053001, 2009.

[158] G. Thorgilsson, C.-S. Tang, and V. Gudmundsson. Time-dependent magnetotransport of a wave packet in a quantum wire with embedded quantum dots. *Physical Review B*, 76(19):195314, Nov. 2007.

[159] C. Timm. Tunneling through molecules and quantum dots: Master-equation approaches. *Physical Review B*, 77(19):195416, May 2008.

[160] C. Timm. Time-convolutionless master equation for quantum dots: Perturbative expansion to arbitrary order. *Physical Review B*, 83(11):115416, Mar. 2011.

[161] K. Torfason. Quantum Transport in the Presence of a Local Time-Periodic Potential in a Magnetic Field. Master's thesis, University of Iceland, 2009.

[162] K. Torfason, C.-S. Tang, and V. Gudmundsson. Coherent magnetotransport and time-dependent transport through split-gated quantum constrictions. *Physical Review B*, 80(19):195322, Nov. 2009.

[163] S. E. Ulloa and D. Pfannkuche. Electronic Correlations and the Non-Linear Conductance of Quantum Dots. *Superlattices and Microstructures*, 15(3):269, 1994.

[164] A. van Houselt and H. J. W. Zandvliet. Colloquium: Time-resolved scanning tunneling microscopy. *Reviews of Modern Physics*, 82(2):1593, May 2010.

[165] J. H. Van Vleck. Note on the interactions between the spins of magnetic ions or nuclei in metals. *Reviews of Modern Physics*, 34(4):681–686, 1962.

[166] S. von Molnar and S. Methfessel. Giant Negative Magnetoresistance in Ferromagnetic Eu_{1-x}Gd_{x}Se. *Journal of Applied Physics*, 38:959–964, 1967.

[167] P. Wahl, L. Diekhöner, G. Wittich, L. Vitali, M. A. Schneider, and K. Kern. Kondo Effect of Molecular Complexes at Surfaces: Ligand Control of the Local Spin Coupling. *Physical Review Letters*, 95(16):166601, Oct. 2005.

[168] X. Waintal and P. Brouwer. Tunable Magnetic Relaxation Mechanism in Magnetic Nanoparticles. *Physical Review Letters*, 91(24):247201, Dec. 2003.

[169] J. Weber. Fluctuation Dissipation Theorem. *Physical Review*, 101(6):1620–1626, Mar. 1956.

[170] T. O. Wehling, A. I. Lichtenstein, and M. I. Katsnelson. Transition-metal adatoms on graphene: Influence of local Coulomb interactions on chemical bonding and magnetic moments. *Physical Review B - Condensed Matter and Materials Physics*, 84(23):235110, 2011.

[171] D. Weinmann, W. Häusler, and B. Kramer. Spin Blockades in Linear and Nonlinear Transport through Quantum Dots. *Physical Review Letters*, 74(6):984–987, Feb. 1995.

[172] D. Weinmann, W. Häusler, W. Pfaff, B. Kramer, and U. Weiss. Spin Blockade in Non-linear Transport through Quantum Dots. *Europhysics Letters (EPL)*, 26(6):467–472, 1994.

[173] E. W. Weisstein. Legendre-Gauss Quadrature., 2015.

[174] W. Wernsdorfer. Classical and quantum magnetization reversal studied in nanometer-sized particles and clusters. *arXiv:cond–mat/0101104 [cond–mat.mes–hall]*, Jan. 2001.

[175] R. Wiesendanger. Spin mapping at the nanoscale and atomic scale. *Reviews of Modern Physics*, 81(4):1495–1550, Nov. 2009.

[176] R. Wiesendanger, H.-J. Güntherodt, G. Güntherodt, R. Gambino, and R. Ruf. Observation of vacuum tunneling of spin-polarized electrons with the scanning tunneling microscope. *Physical Review Letters*, 65(2):247–250, 1990.

[177] A. F. G. Wyatt. Anomalous densities of states in normal tantalum and niobium. *Physical Review Letters*, 13(13):401–404, 1964.

[178] S. Yan, D.-J. Choi, J. A. J. Burgess, S. Rolf-Pissarczyk, and S. Loth. Control of quantum magnets by atomic exchange bias. *Nature nanotechnology*, 10:40–45, Dec. 2014.

[179] S. Yan, D.-J. Choi, J. A. J. Burgess, S. Rolf-Pissarczyk, and S. Loth. Three-Dimensional Mapping of Single-Atom Magnetic Anisotropy. *Nano Letters*, 15(3):1938–1942, 2015.

[180] S. Yoshida, Y. Aizawa, Z.-H. Wang, R. Oshima, Y. Mera, E. Matsuyama, H. Oigawa, O. Takeuchi, and H. Shigekawa. Probing ultrafast spin dynamics with optical pump-probe scanning tunnelling microscopy. *Nature nanotechnology*, 9:588–593, 2014.

[181] K. Yosida. Anomalous electrical resistivity and magnetoresistance due to an s-d interaction in Cu-Mn alloys. *Physical Review*, 107(2):396, 1957.

[182] A. N. Zaitsev. Exchange interaction between conduction electrons and localized d (f) electrons with allowance for the nonorthogonality of their wave functions. *JETP*, 74(3):1012, 1978.

[183] L. Zhou, J. Wiebe, S. Lounis, E. Vedmedenko, F. Meier, S. Blügel, P. H. Dederichs, and R. Wiesendanger. Strength and directionality of surface Ruderman-Kittel-Kasuya-Yosida interaction mapped on the atomic scale. *Nature Physics*, 6(3):187–191, 2010.